

Data-driven Methods for Characterizing Transportation System Performances

Under Congested Conditions: A Phoenix Study

by

Baloka Belezamo

A Dissertation Presented in Partial Fulfillment
of the Requirements for the Degree
Doctor of Philosophy

Approved October 2020 by the
Graduate Supervisory Committee:

Xuesong Zhou, Chair
Ram Pendyala
Yingyan Lou

ARIZONA STATE UNIVERSITY

December 2020

©2020 Baloka Belezamo

All Rights Reserved

ABSTRACT

Travel time is the main transportation system performance measure used by the planning community to evaluate the impacts of traffic congestion on infrastructure investment projects and policy development plans. Planners rely on the travel demand model tool estimates for the selection and prioritization of critical and sensitive projects to meet the fiscally constraint requirements imposed by the Federal Highway Administration (FHWA) on their transportation improvement programs (TIP). While travel demand model estimates have been successfully implemented in the evaluation of project scenarios or alternatives, the application of the methods used in the travel demand model to generate these estimates continues to present a critical challenge, particularly to modelers who have to produce a validated model upon which traffic predictions can be made. The various volume-delay functions (VDFs) including the Bureau of Public Roads (BPR) function, used in the travel demand model to relate traffic volume to travel time, are developed based on system-wide attributes. BPR function in its polynomial form is computationally efficient and simple for implementation in a transport planning software. The planning community has long recognized that the BPR function cannot capture traffic flow dynamics and queue evolution processes. Besides, it has difficulties in using the average travel time measure to describe an oversaturated bottleneck with high density but low throughput.

This dissertation aims to propose a simplified and yet effective point-queue based modeling approach built on the cumulative vehicle arrival concept, and the polynomial equation formula, based on Newell's method, to estimate travel time at a corridor level using real world speed and count measurements. A traffic state estimation (TSE) method is also

proposed to characterize data into various states, such as congested state and uncongested state, using Markov Chain to capture current traffic pattern and Bayesian Classifier to infer congestion effects. As the test bed for the case study, the research selects the Phoenix freeway corridor with year-round traffic data collected from embedded traffic loop detectors. The results and effectiveness of the proposed methods are discussed to shed light on the calibration of link performance function, which is an analytical building block for system-wide performance evaluation.

DEDICATION

To my dear dad, Mr. Belezamo,

You have trusted me with your name.

I am honored and proud to promote your name from

Mr. Belezamo to Dr. Belezamo.

Mission accomplie!

To my children Odelya Belezamo and Benjamin Belezamo

Thank you for all the sacrifices you have endured.

This dissertation is for you two from Papa.

Je vous aime profondément!

ACKNOWLEDGMENTS

The wonderful journey of my doctoral degree started in Africa, then continued in Turkey and Canada, for the final destination here in Arizona. The fantastic people whose advice, guidance, and sacrifices helped me to successfully complete the journey deserve my sincere gratitude.

At an early age, my brother Rombaut Belezamo and my high-school principal Malenso Nnodila instilled in me the importance of an education. My commitment to education constituted the roots that would support me when I left Africa to go to study Engineering in Turkey. Professors Ugur Ersoy from Middle East Technical University, Semih Tezcan, Mustafa Erdik, Nuray Aydinoglu, and Ozal from Bosphorus University would shape and strengthen my interest in Engineering. My Turkish family Zulfikar (Can, Candan, Handan and their parents), my friends Volkan Sahin and Mehmet Emre Ozcanli, my first true companion Suay Cankaya, my boss Faruk Tuncel, and my colleagues Neslihan and Hale provided me with the much needed family support away from home. I will always be grateful to you all. Leading engineering companies such as STFA (Sezai Turkes Feyzi Akkaya), ENKA holding, and Tuncel Engineering, where I worked as a Civil Engineer, offered me a solid engineering experience.

Moving to Montreal, Canada, and working for INRO Consultant as analyst for several unforgettable years, opened up career opportunities I am still benefitting from to date. Linda Lefebvre, Mr. Ptak, Serge Gauthier, Kim, Michel, Frederic, Nicolas, Michael Mahut, Zvi Levi, Gina, Diane, Nicole, Sylvie, Isabelle (la force tranquille), Mike Florian,

and Heinz Spiess impressed me with their professionalism, commitment to excellence, and friendship. INRO also introduced me to skiing. While at INRO, I completed part-time my Master's in Transportation from Concordia University under the supervision of Professor Bala Ashtakala. Viviane Nguessan N'dri also deserves my dearest gratitude.

I moved from Montreal, Canada, to Phoenix, Arizona, to accept a job offer from Maricopa Association of Governments (MAG). I first worked under Marc Schlappi, the best manager I ever had, then with Vladimir Livshits (we knew each other back in Canada). I was privileged to work with Haidong Zhu, one of the best colleagues. Then, I moved to Arizona Department of Transportation (ADOT) to work with Deng Bang Lee and Keith Killough. This move was one of the best decisions I ever made in my career. Working with Anson Gock, Daniel Gabiou, Ashim Garg, Veronica Green, and training interns like Ardeshir, made me appreciate my profession even more. I became a Professional Engineer, member of a Transportation Research Board (TRB) committee, and completed my Doctoral Program in Transportation from Arizona State University (ASU).

Many thanks to my Doctoral committee members, Dr. Ram Pendyala and Dr. Yingyan Lou. My dissertation supervisor, Dr. Xuesong Zhou, deserves special thanks for being the best advisor I could have possibly hoped for. I had a great academic and personal experience with his fantastic team composed of Dr. Jiangton, Dr. Monireh, Dr. Avci, Dr. Taylor Li, and Dr. Xin Wu.

Finally, my deepest thanks to Viviane and to my two wonderful children, Odelya Belezamo and Benjamin Belezamo, for their love and support. Papa vous aime énormément.

TABLE OF CONTENTS

| | Page |
|--|------|
| LIST OF TABLES | xi |
| LIST OF FIGURES | xiii |
| CHAPTER | |
| CHAPTER 1 INTRODUCTION..... | 1 |
| 1.1 Motivation..... | 1 |
| 1.2 Goal and Objectives..... | 5 |
| 1.3 Contributions | 10 |
| 1.4 Organization of the Dissertation | 11 |
| CHAPTER 2 LITERATURE REVIEW..... | 14 |
| 2.1. Introduction..... | 14 |
| 2.2. Travel Demand Model..... | 16 |
| 2.2.1. Importance of Travel Demand model in Planning Process | 16 |
| 2.2.2. Travel Demand Model Components | 17 |
| 2.2.3. Trip Assignment Step and Its Practical Role..... | 18 |
| 2.3. Travel Time | 19 |
| 2.3.1. Definition and Importance of Travel Time | 19 |
| 2.4. Congestion | 19 |
| 2.4.1 Definition Traffic Congestion | 19 |
| 2.4.2. Main Cause of Traffic Congestion | 19 |
| 2.4.3. Congestion Mitigation Measures..... | 20 |

| CHAPTER | Page |
|---|------|
| 2.5. Volume-Delay Function | 20 |
| 2.5.1. Definition and Categories of Volume-delay Function | 20 |
| 2.5.2. Predetermined Traffic Variables | 21 |
| 2.6. Traffic Loop Detectors | 22 |
| 2.6.1. Introduction | 22 |
| 2.6.2. Flow and Speed Estimation Formulas..... | 22 |
| 2.6.3. Traffic Detector and Traffic Data Issues | 23 |
| 2.7. Steady-state Flow Analysis..... | 23 |
| 2.7.1. Introduction | 23 |
| 2.7.2. Formulas for Estimating Steady-state Traffic Flow | 25 |
| 2.7.3. Sparse Traffic Data Impact on Steady-state Flow Analysis..... | 27 |
| 2.8. Traffic State Estimation (TSE)..... | 27 |
| 2.8.1. Introduction | 27 |
| 2.8.2. Definition of Traffic State Estimation (TSE)..... | 27 |
| 2.8.3. Background | 28 |
| 2.8.4. Summary | 29 |
| 2.9. Capacity Estimation..... | 30 |
| 2.10. Free-flow Speed Estimation | 32 |
| 2.11. Estimation of Optimum Speed at Capacity | 33 |
| 2.12. Traffic Flow Conditions and Types Used in Volume-delay Function | 35 |
| 2.12.1. Introduction | 35 |
| 2.12.2. Definitions of Uncongested State and Congested Conditions..... | 35 |

| CHAPTER | Page |
|---|------|
| 2.12.3. Definitions of Traffic Flow Types..... | 35 |
| 2.12.4. Impact of Capacity on Traffic Flow Types | 36 |
| 2.12.5. Traffic Flow Types and Congestion Index..... | 36 |
| 2.13. Alternatives to Volume over Capacity Ratio as Congestion Index | 37 |
| 2.13.1. Estimations of Demand Beyond Capacity..... | 37 |
| 2.13.2. Density over Optimum Density Ratio as Congestion Index | 39 |
| 2.13.3. Summary | 39 |
| 2.14. Parameters Used in Volume-Delay Function | 40 |
| 2.14.1. Introduction | 40 |
| 2.14.2. Meaning of BPR Parameters | 40 |
| 2.14.3. BPR Parameter Values and Ranges..... | 41 |
| 2.14.4. Summary | 42 |
| 2.15. Summary..... | 42 |
| 2.16. Limitations | 43 |
| CHAPTER 3 TRAFFIC STATE ESTIMATION USING STATE TRANSITION | |
| PROCESSES | 45 |
| 3.1. Introduction..... | 45 |
| 3.2. Problem Statement and Overall Framework..... | 46 |
| 3.3. Describing Traffic Shockwave Using Newell’s Three-Detector Problem | 51 |
| 3.4. Describing State Transition on the Space-Time Probabilistic Graph..... | 54 |
| 3.5. Summary..... | 59 |

| CHAPTER | Page |
|---|------|
| CHAPTER 4 TRAVEL TIME DERIVATION FROM QUEUEING AND POLYNOMIAL MODELS | 60 |
| 4.1. Introduction..... | 60 |
| 4.2. Bottleneck Identification Using Integrated Heat Map Space-Time Speed Profile | 63 |
| 4.3. Computation of Key Queue System Parameters | 66 |
| 4.4. Key Assumption of Quadratic Polynomial Function Using Queue Parameters..... | 71 |
| 4.5 Examining Queue-Based Average Delay and Average Travel Time Functions During Congestion Period | 75 |
| 4.6 Summary | 77 |
| CHAPTER 5 EXPERIMENTS | 78 |
| 5.1. Introduction..... | 78 |
| 5.2. Raw Data Description and Data Processing | 82 |
| 5.3. Quality Control of Collected Data and General Discussion on Data Aggregation | 86 |
| 5.4. Traffic State Estimation (TSE) Method..... | 87 |
| 5.4.1. Definition of States Using Clustering | 87 |
| 5.4.2. Calibration | 88 |
| 5.4.3. State Prediction..... | 88 |
| 5.5. Average Travel Time Estimation Approach..... | 94 |
| 5.5.1. Data Visualization Techniques..... | 94 |

| CHAPTER | Page |
|--|------|
| 5.5.2. Maximum Observed Value Method | 98 |
| 5.5.3. Cumulative Vehicle Count Method..... | 104 |
| 5.5.4. Calibration of Polynomial Equation Parameters | 109 |
| 5.5.5. Travel Time Calibration and Validation | 110 |
| 5.6. Discussions of the Results | 114 |
| CHAPTER 6 CONCLUSIONS | 117 |
| REFERENCES..... | 120 |

LIST OF TABLES

| Table | Page |
|---|------|
| 2-1 Four-Step Model Components and Descriptions..... | 18 |
| 2-2 BPR Parameter Values for Freeway Used in Research and in Practice | 42 |
| 3-1 Notations and Input Data..... | 47 |
| 3-2 Traffic Flow Model Parameters..... | 52 |
| 3-3 Emission Function Interpretation from Typical Models | 55 |
| 4.1 Variables and Their Definitions..... | 63 |
| 5-1 Summary of Traffic Detector Characteristics and Traffic Data Collected and Time Interval Period..... | 81 |
| 5-2 Freeway Segment Lane Configuration | 81 |
| 5-3 Summary of Data Checking | 86 |
| 5-4 RMSE of Estimates Obtained Using M1 and M2 under Different Number of States..... | 90 |
| 5-5 RMSE Obtained Using M1, M2, and M2 (W=0)..... | 91 |
| 5-6 Traffic Data for Detector 78 | 103 |
| 5-7 Cumulative Count, N, and Queue Length, Q | 105 |
| (5-minute Time Interval)..... | 105 |
| 5-8 Cumulative Count, N, and Queue Length, Q | 108 |
| (1-hour Time Interval) | 108 |
| 5-9 Calibration Summary Spreadsheet of ϕ Parameter Using Link Specific Traffic Data from Detector 84 During Congested Period | 111 |

| Table | Page |
|--|------|
| 5-10 ϕ Parameters for Detectors 78, 84, 137, and 139..... | 111 |
| 5-11 Travel Time Summary Spreadsheet of the New Method Using Calibrated ϕ Parameters and Traffic Data from Detector 84 During Congested Period | 112 |
| 5-12 Statistical Results (R-Squared) of the New Method and BPR Validation with Field Data..... | 114 |

LIST OF FIGURES

| Figure | Page |
|---|------|
| 1-1 Illustration of Model Structure with Chapters and Sections as Individual Modules. Numbers and Letters Represent Chapter and Section Numbers, Respectively | 13 |
| 2-1 Travel Time-Flow Relationships for Several Sampling Time-Interval Durations, by Rothrock and Keefer, 1957 | 24 |
| 2-2 Flowchart for Estimating “Steady-state” Volume (from 5-minute Time Interval) ... | 26 |
| 2-3 Flow Chart for Capacity Estimation (Based on Collected Data from Detectors) | 31 |
| 2-4 Flow Chart for Free-flow Speed Estimation (Based on Collected Data from Detectors) | 33 |
| 2-5 Flow Chart for Optimum Speed Estimation (Based on Collected Data from Detectors) | 34 |
| 3-1 Triangular Flow-density Fundamental Diagram | 49 |
| 3-2 An illustration Describing a Deterministic Three-detector Model Adapted from Deng et al. (2013) | 49 |
| 3-3 Overall TSE and Prediction Framework | 51 |
| 3-4 Forward and Backward Propagation on Cumulative Curves Adapted from Hurdle and Son (2000) | 54 |
| 3-5 An Illustrative Example of STPG | 57 |
| 4-1 Common Causes of Congestion | 60 |
| 4-2 Module Descriptions and Representations of Sections from Chapter 4 | 62 |

| Figure | Page |
|---|------|
| 4-3 Illustration of a Roadway Configuration with Loop Detectors and Vehicle Trajectories on a Space-time Diagram and the Queue Extent Along a Single Bottleneck | 64 |
| 4-4 Bottleneck Location (from Speed Heat Map of a Freeway Corridor over One Day)..... | 65 |
| 4-5 Bottleneck Location (from Speed Profile of a Freeway Corridor over One Day) | 66 |
| 4-6 A Typical Cumulative Flow Curve (in Blue Line) Representing Cumulative Vehicle Count Within Congested Period | 67 |
| 4-7 Illustration of Queue Parameters Within the Cumulative Curve Concept | 68 |
| 4-8 Queue Length Curve (b) Derived from Cumulative Curve (a). The Maximum Queue Length Occurs at Time t_2 | 70 |
| 4-9 Quadratic Polynomial Approximation of Queue Length | 71 |
| 5-1 Freeway Corridor Lane Configuration, Loop Detector Identifications and Locations, and Traffic Direction..... | 80 |
| 5-2 Raw Data File with Volume Data from All Detectors Collected Every 5 Minute Interval | 82 |
| 5-3 Traffic Data File with Speed Data from All Detectors Collected Every 5 Minute Interval | 83 |
| 5-4 Traffic Data File with Volume Data Aggregated to 1 Hour Interval | 84 |
| 5-5 Traffic Data File with Speed Data Averaged over 1 Hour Interval..... | 85 |
| 5-6 Clustering Representation of 8 States..... | 89 |
| 5-7 Calibration of Basic Parameters Using Collected Data..... | 89 |

| Figure | Page |
|---|------|
| 5-8 Comparison Between State Estimation (Using M2 with 30 States) and Historically Continuous Mean Values | 92 |
| 5-9 Historical, Real-time Observations, and Estimates of Section 84 Updated by Real-time Data (Using M2 with 30 States) | 93 |
| 5-10 Speed Heat Map Showing Bottleneck Location, Congested Segments and Congested Period on a Typical Day..... | 95 |
| 5-11 Speed Profile Showing Bottleneck and Congested Period at the Lane Level (a) and at the Link Level (b) on a Typical Day..... | 96 |
| 5-12 Speed-Density Profile Showing Bottleneck and Congested Period at The Link Level on a Typical Day..... | 97 |
| 5-13 Maximum Flow and Critical Speed for All Lanes (a) and for the Link (b) from the Flow-Speed Diagram of Detector 78 | 99 |
| 5-14 Maximum Flow and Critical Density for all Lanes (a) and for the Link (b) from the Flow-Speed Diagram of Detector 78 | 99 |
| 5-15 Flow-Density Relationship for all Lanes (a) and for the Link (b) of Detector 78. | 100 |
| 5-16 Detector 78 Fundamental Diagrams: Link Maximum Flow and Critical Speed (a), Link Maximum Flow and Critical Density (b), and Speed-Density (c) | 102 |
| 5-17 Cumulative Flow Curve (in Blue Line) Representing Cumulative Vehicle Count and Discharge Rate (in Orange) within Congested Period for 5-minute Time Interval . | 106 |
| 5-18 Queue Length Curve Derived from Cumulative Curve During Congested Period for 5-minute Time Interval | 107 |

| Figure | Page |
|---|------|
| 5-19 Cumulative Flow Curve (in Blue Line) Representing Cumulative Vehicle Count and Discharge Rate (in Orange) within Congested Period for 1-hour Time Interval | 108 |
| 5-20 Queue Length Curve Derived from Cumulative Curve During Congested Period for 1-hour Time Interval | 109 |
| 5-21 Link/Field, BPR, and New Method Travel Time Curves from Detector 84 | 113 |
| All Curves Display an Increase in Steepness after the Congestion Occurs at $K/K_c=1.0$ | 113 |
| 6-1 General Graphical Illustration of Queue Evolution for a Single Oversaturated Bottleneck | 118 |

CHAPTER 1

INTRODUCTION

1.1 Motivation

Transportation agencies rely on transportation planning to address the transportation problems of the state, region, or communities they serve and to satisfy federal requirements.

Transportation planning process involves the development of performance measures, the collection of data to be used in the analysis methods, the evaluation of the impacts and benefits of project alternatives, identification of projects, identification of studies such as corridor studies, and the development of federally mandated plans and policies.

Transportation problems faced by communities can be grouped into different major categories that include economic development, land use, accessibility, and congestion. Clearly, all these issues are directly connected to transportation system that is impacted by continuous population growth, evolving economic markets, and changing travel patterns.

Travel demand models aim to provide an analytical tool to support the transportation planning process. Among the many performance measures produced by the travel demand model, travel time can be considered as the most significant output. In particular, travel time and other correlated performance measures such as vehicle mile traveled (VMT) and vehicle hour traveled (VHT) are used in planning and decision-making process to evaluate traffic conditions such as mobility, accessibility, and congestion in transportation systems, and the economic benefits and environmental impacts of improvement projects as freeway expansion projects.

Various methods exist to perform the travel demand modeling. They consist of a series of mathematical formulations that use such variables as population, land use, employment, and transportation networks to perform specific tasks. Transportation networks represent the supply side and population, land use, and employment constitute the demand side of the model. The widely used travel demand model is called the four-step model. This designation is the result of the model that considerably reduces the convoluted operation of data requirement and processing by aggregating these formulations into four sequential steps that are referred to as trip generation, trip distribution, mode choice, and trip assignment.

The trip assignment step is most computationally involving building block of the travel demand model. In the trip assignment step, the relationship between the demand side and the supply side of the model is established as the performance measure function that computes travel time on the transportation system from the assigned demand. The performance measure function is referred to as volume-delay function (VDF) and satisfies certain conditions. One important condition, which is referred to as the equilibrium assignment, is that all the routes from an origin to a destination must have the same travel time. This property is Wardrop's first principle of equilibrium (Wardrop, 1952). Another important condition is that congestion occurs when an assigned demand to the network exceeds the capacity of the network.

The planning community has long recognized that the static BPR function cannot capture traffic flow dynamics and queue evolution processes, particularly related to the queue formation, propagation, and dissipation. Besides, it has difficulties in using the average travel time measure to describe an oversaturated bottleneck with high density but low throughput. Compared to the STA model, the dynamic traffic assignment (DTA) model aims to embed a queueing model or other types of dynamic traffic flow models to capture the evolution processes of traffic congestion. With discretized time and space dimensions (such as the cell transmission model and link transmission model), DTA models have to address many computational challenges due to the introduced finer resolution

In practice, the VDF function tends to underestimate the congested link travel time. Some possible reasons could be stated below:

- (1) VDF function considers each link individually and the link congested travel time is estimated without considering the possible impact of congestion from a downstream link. Any bottleneck on the downstream link can result in queue propagation from downstream link to the current link further increasing any congestion duration,
- (2) Inconsistency in scale between VDF parameters and variables. Parameters are estimated at the area type and facility type level whereas the speed and capacity are estimated at the link level,
- (3) VDF parameters are not sensitive to time of day traffic conditions.

Related to system performance functions, many practitioners have the following specific important questions: 1) where are those coefficients of alpha and beta in the VDF function coming from? 2) how to use observed traffic dynamics data to calibrate these coefficients? In addition, from a traffic state estimation perspective, there are a number of pressing questions to be addressed:

1. How to derive traffic flow characteristics from collected traffic data?
2. How to develop a new traffic state estimation method that infers traffic propagation impacts between connected traffic locations?

How to determine bottleneck conditions from collected traffic data?

3. How to estimate queue evolution process (formation, propagation, and dissipation) and its parameters?
4. How to compute congested traffic demand used in VDF from collected traffic data?

To develop a new generation of travel time performance model, we also need to have the following considerations for system-wide performance evaluation.

- 1) What mathematical function/curve best fits traffic flow distribution/theory?
- 2) How to derive relationships between queue characteristics and mathematical function?
- 3) How to express the mathematical function in a format standard to a volume-delay function (VDF)?
- 4) Does the proposed mathematical function satisfy all the requirements of a VDF to be used in the trip assignment step of the travel demand model to compute the link travel time?

The focus of this dissertation is how to find a new form of VDF in the traffic assignment of the travel demand model, and how to estimate waiting times under congestion conditions using link-level data such as traffic data collected from freeway detectors. The broader impact of this research could lead to an improved and reliable analytical tool, which allows planners and decision-makers to evaluate the financial magnitudes of their decisions on infrastructure development projects. This is particularly important for solving their community problems including the changing demand patterns and increasing congestion.

1.2 Goal and Objectives

The main goal of the dissertation is to propose a new method of estimating the travel time at the link level under congestion conditions that can be incorporated in the trip assignment step of the travel demand model. The new method presents an important research improvement over the existing link performance measure functions or volume-delay functions (VDFs). Its parameters are estimated directly from the link collected data and, hence, make its travel time estimation more reliable.

The development of the new method requires an integration of traffic flow theory knowledge and a solid background in applied mathematics to achieve the goal's objectives listed below. Objectives 1 through 5 involves traffic flow characteristics analysis whereas objectives 6 through 8 include derivation and integral operations in calculus.

This study can be viewed as a combination of two research approaches:

- The first approach is the traffic state estimation method focusing on objectives 1-5 that estimates the link congested traffic state variables using the link observed traffic data.

- The second approach is the derived mathematical function related objectives 6-8 that estimates the congested travel time at the link level using the observed traffic data.

1. Calibrate **traffic flow characteristics** from collected traffic data using Newell's kinematic wave method.
2. Perform **traffic state estimation** (TSE) using the proposed method to determine congestion conditions
3. Identify the **bottleneck location** using speed profile or heat map diagram
4. Calibrate parameters for **queue evolution process** (formation, propagation, and dissipation)
5. Compute **congested traffic demand** from collected traffic data
6. Select the mathematical function for **queue-based traffic flow function** and determine its parameters
7. Derive **polynomial relationships** between queue characteristics and travel time function parameters
8. **Validate** that the proposed mathematical function satisfies all the requirements of a VDF.

A detailed discussion of the above objectives is given below.

In detail, the first objective is to calibrate **traffic flow parameters** from collected traffic data using Newell's kinematic wave method. There are several methods that can calibrate traffic flow parameters. These methods are mathematical expressions that combine traffic

variables based on predefined assumptions. These relationships between traffic variables including speed, density, and flow, are represented in the fundamental diagram (FD), which constitutes the foundation of traffic flow theory.

In addition to inherent limitations, these single-regime models developed over the past decades also represent the flow-density ($q-k$) relationship as a non-linear curve. This assumption makes the traffic data variable estimation challenging. Because of the non-linear relationship, there can be many different speeds on the $q-k$ curve. Newell's kinematic wave method is a representative method that simplifies the calculation of speeds into uncongested speed and congested speed that are referred to as forward speed and backward speed. These speeds are used as input data in the second objective for the traffic state estimation process.

The second objective is to develop a new method that performs **traffic state estimation** (TSE) on one location and update the estimation with congested speed waves from upstream and downstream locations. A traffic state is composed of flow and density. The traffic data can be grouped into many different numbers of clusters that represent different numbers of states. One important characteristics of a cluster is that all traffic data within that cluster have the same speed, thanks to Newell's simplified method mentioned in the objective 1. The traffic state is estimated at one location using the Markov Chain (MC) Model and then the forward and backward waves from the upstream and downstream locations are transferred to the current location using the Bayesian Classifier (BC) approach. Given that every traffic record represents a traffic state, the new method can be used to simplify the various number of states by grouping them, for analysis purpose, into

two states: uncongested state and congested state. The change from uncongested state to congested state, caused by capacity reductions at freeway on-ramp merges, lane drop, or weaving sections, may result in the propagation of congestion upstream from a traffic bottleneck in a form of a shock wave.

Since traffic flow restricted by a downstream bottleneck may cause congestion, the third objective consists in identifying possible recurring **bottleneck locations** from the traffic data. Two methods considered in this study to identify bottleneck are based on speed profile and heat map diagram developed from the traffic data. The speed profile method is straightforward in that it consists in very simple steps of traffic data processing. Using traffic data, the speed-flow diagram is plotted to illustrate the relationship between speed and flow. The speed-flow curve is important in that it sets up the boundary conditions that define traffic flow parameters such as free-flow speed, capacity, and critical speed that represents the limit between uncongested state and congested state. The next step is to draw the speed time series, also called the speed profile, and identify the critical speed. There is evidence of a bottleneck when the speed profile first drops below the critical speed and then rises up above the critical speed. Heat map is another method of visually identifying the location of a bottleneck.

Once the congestion has been located, the next objective, which is the objective four, is then to define the **formation, the propagation, and the dissipation of the resulting queue**. The speed data is plotted against time to produce the speed profile which will be used to identify the duration of the queue. The time that corresponds to the speed profile falling below the critical speed constitutes the start time of the queue. It is the beginning of

the queue formation. The time when the speed profile exceeds the critical speed profile indicates the end time of the queue. The difference between the end time and the start time represents the queue duration. A similar procedure can be followed to estimate the queue intensity. The density data is plotted against time to produce the density profile plot. The density on the plot that corresponds to the start time of the queue represents the queue length. It is important to note that the same density would have been obtained if the end time of the queue had been used instead of the start time of the queue. This is the consequence of the linear relationship between the speed and the density.

The same procedure above that has been used on the speed and on the density to determine the queue duration and the queue extension, respectively, does not apply to determine the queue intensity. Objective No 5 is to use the traffic volume data and the queue start time and queue end time to compute **congested traffic demand**. Traffic volumes are accumulated from the queue start time until the queue end time. Otherwise stated, arriving vehicles to the queue from the beginning of the queue to the end of the queue are counted and the total count represents the cumulated congested demand.

The objective six is to select an **analytic polynomial model** that represents the traffic condition where the congestion is caused by a bottleneck (objective three) and the congested demand represents the number of vehicles arriving on the link during the congested time (objective five). One such a model will include the Poisson distribution which can be used to predict the probability of the arrival flow rate at bottleneck. To predict travel time during a congestion period, the arrival flow rate can be approximated by a polynomial function.

After the selection of the polynomial function, the objective seven is to substitute the function variables with the corresponding queue characteristics and their boundary conditions. The substitution process mainly involves the application of mathematical calculus properties. Certain terms in the polynomial function that refer to the slope of the curve or the area under the curve are substituted by corresponding values from derivatives or integrals, respectively.

The objective eight is to express the variables and parameters of the final derived queueing-theoretic function in a structure similar to a volume-delay function (VDF), namely BPR function.

The final objective is to **validate** that the proposed mathematical function satisfies all the requirements of a VDF and hence can potentially be used in the trip assignment step of the travel demand model.

1.3 Contributions

The main contributions of these approaches can be summarized as follows:

The modified traffic state method can comprehensively update the current link state estimation with the upstream link and downstream link congestion propagation effects by combining two methods, Markov Chain (MC) model and Bayesian Classifier (BC) method. MC model is used to capture current traffic state and BC serves to transfer forward congestion wave from upstream location/link and backward congestion wave from downstream location/link to the current location/link.

Based on **continuous and polynomial-based approximation**, the proposed model explicitly establishes a coherent connection between the average performance relationship and the deterministic dynamic queuing model during a single oversaturated period.

The derived polynomial function combines the principles of fluid dynamics, traffic flow theory, and queue evolution process to estimate link congested travel time. Traffic flow characteristics and queue formation, propagation, and dissipation characteristics equivalent to fluid dynamics characteristics are substituted in the quadratic polynomial equation to result in a function that computes travel time. Because this derived function satisfies all the requirements of a volume-delay function (VDF), it can potentially be incorporated in the trip assignment step of the travel demand model and produce travel time estimates that are more reliable and more consistent than those produced by the existing VDF functions.

1.4 Organization of the Dissertation

There are three main tasks covered in the dissertation:

The first task involves the development of an innovative approach that updates traffic state estimation (TSE) at local location based on captured traffic deviation from regular traffic state patterns at both local and nonlocal (upstream and downstream) locations caused by congested conditions. Chapter 3, which starts by mentioning the notations used to describe traffic variables followed by the definition of a traffic state, elaborates on the main parts of the new method that include the prediction process and the updating process.

The prediction process, performed at the upstream, local, and downstream locations, includes the following steps: Calibrate traffic parameters (using Newell's method), identify traffic states (using K-state clustering), development of transition matrices from historical

data (using space-time probabilistic graph (STPG), and estimation of regular traffic state patterns using the transition matrices (using Markov Chain Model).

The updating process, mainly performed at local location, consists of the following steps: Capturing of traffic deviation from regular traffic state pattern at both upstream and downstream locations, and update estimation at local location (using Bayesian Classifier method).

The final output results are produced by weighing both regular and updating traffic state patterns.

The new method, therefore, updates the intensity, the extension, and the duration of the congested state at the local location based on the captured deviation from the upstream and downstream locations.

The second task consists of deriving a novel formula that estimates congested traffic flow pattern caused by bottleneck conditions on highway network links equipped with loop detectors. Chapter 4 analyzes the characteristics and impacts of traffic queue caused by congestion resulting from the existence of a bottleneck. Traffic variables including speed and density are used to establish the boundary conditions of the queue. The congested demand is obtained by accumulating the traffic flows arriving in the queue until the queue dissipates. The traffic flow arrival rate is expressed as a quadratic polynomial mathematical equation. Using the derivation and integral properties combined with the queue boundary conditions, the quadratic polynomial expression is transformed into the final mathematical model that can estimate travel time as a volume-delay function (VDF). The innovation

from the model is that the variables and the parameters of the model are estimated from the link traffic data.

The last task consists of applying the Phoenix freeway loop detector dataset to the proposed TSE model and the proposed VDF model. The results and conclusions of these Phoenix case studies are discussed and summarized in Chapter 5. Figure 1-1 shows the graphic representation of the chapters and their respective sections.

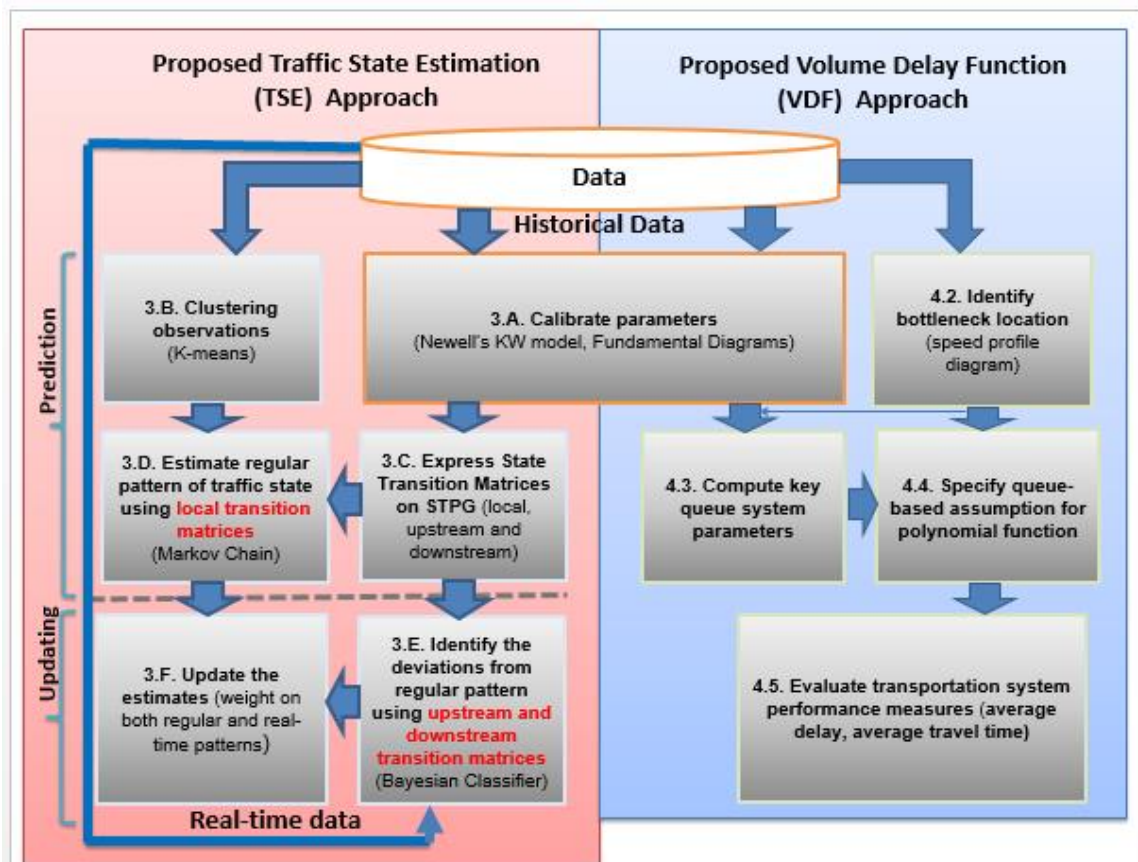


Figure 1-1 Illustration of Model Structure with Chapters and Sections as Individual Modules. Numbers and Letters Represent Chapter and Section Numbers, Respectively

CHAPTER 2

LITERATURE REVIEW

2.1. Introduction

In this chapter, the evaluation stage of the transportation planning process that includes using travel demand model tool to analyze a transportation issue, i.e., congestion caused by bottleneck, is reviewed in detail.

The review starts with a general overview of the travel demand model in Section 2.2. In the planning process, the travel demand model is an important analytical tool designed to evaluate traffic conditions such as travel time and level of service. Since travel demand model uses four submodels in sequence to estimate traffic conditions, it is referred to as the four-step model. Among these submodels, the traffic assignment is the true model driver in that it converts the demand to the travel time on the roadway segments or links. Section 2.3 and Section 2.4 define and explain the relationship between travel time and traffic congestion, the causes and mitigation measures for traffic congestion. In order to estimate the link travel time, the traffic assignment utilizes the link performance measure called the volume-delay function (VDF). Section 2.5 presents all the major VDFs used in practice. The VDF variables that include speed and volume are considered as prior variables and can be collected in real time by traffic detectors. Section 2.6 introduces the traffic detectors which are loops embedded in the pavement of the roadway to record vehicle movements, especially vehicle counts and speeds. The problems related to the correct functioning of the detectors and to the data collection are also covered. Typically, loop detectors collect traffic data every 30 seconds for a duration sampling time interval of 5 minutes. This data needs to be aggregated to a 60-minute time interval to represent a steady-state traffic flow where dynamic fluctuations are defused in order

to be used in the travel demand model. The formulas for steady-state and impacts of sparse traffic data on steady-state are included in Section 2.7. Models such as Markov Chain that estimate traffic states including flow, density, and speed are important for data-driven methods such as the travel demand model. Section 2.8 reviews traffic state estimation (TSE) approach and possible limitations. Prior variables to VDF are free-flow speed, capacity and corresponding speed referred here as optimum speed. The optimum speed represents the speed limit below which the congestion starts. Section 2.9, Section 2.10, and Section 2.11 cover in detail the formulas, the algorithms, and the flowcharts required to estimate free-flow speed, capacity, and optimum speed from the traffic data (volume and speed) collected by traffic detectors. The volume and speed estimated from the traffic detector data can be used as input in the VDF formula only in the speed-flow region called hypocritical region. This is the region where volume is less than capacity, i.e., the region where there is no congestion. Since volume cannot be greater than capacity in real life, the volume and speed estimated from the traffic detector data that are in the hypercritical region, where there is congestion, cannot be used “verbatim” as input in the VDF formula. One important assumption of the traffic assignment process is that, under congestion, the volume can exceed capacity. This is expressed in VDF as volume over capacity greater than or equal to 1. Section 2.12 provides a comprehensive review of traffic flow conditions and traffic flow types used in VDF formula, the impact of the capacity on traffic flow types, the definitions of uncongested and congested conditions, and the congestion index. Section 2.13 reviews the methods that compute a new congested volume by offsetting/adding the drop in the volume to the capacity so that the new volume is greater than the capacity and can be used in the VDF formula. Also, another method that does not need to compute the new volume is reviewed. This method stipulates that while there is no one-to-one correspondence in the speed-flow fundamental diagram, the one-to-one correspondence exists

in the speed-density fundamental diagram. Therefore, instead of volume over capacity, density over critical density can be used in the VDF formula for both uncongested and congested conditions. In addition to capacity and speed variables, VDF formula such as BPR includes parameters that must be calibrated to reflect the local conditions. In Section 2.14, the meaning and values of BPR parameters are reviewed. Finally, Section 2.15 discusses the limitations of VDF with respect to the traffic data. The VDF parameters cannot be derived directly from the collected data. VDF parameters are estimated using statistical methods such as Excel Solver. In practice, these parameters are calibrated using area type and facility type data.

2.2. Travel Demand Model

2.2.1. Importance of Travel Demand model in Planning Process

Travel demand models are computer-based analytical programs used to estimate and forecast traffic conditions on the transportation systems. It is designed to assist policy makers in general and transportation planners in particular in evaluating the impacts and benefits of various projects, plans, and policies.

Typically, travel demand models use a series of mathematical formulations to perform regional transportation planning. In these formulations, data from demographic, travel survey, and transportation networks are used as input data; household characteristics, trip purpose, and transportation system characteristics are used to develop model parameters. To reduce the complexity and the data requirements of these formulations, they are grouped into a sequential process with four basic steps, where each step becomes inputs to the next step. This is known as the four-step model.

2.2.2. Travel Demand Model Components

Transportation planning divides a study area into several zones that typically represent census tracts and geographic limits. The trip generation step/model predicts the total trips based on household characteristics of each zone within the study area and trip purposes. The trip distribution model distributes the generated trips into trip productions and trip attractions. The mode choice model predicts the total trips that use available modes. Finally the trip assignment model predicts the total trips that use various routes of the transportation system (Ben Akkiva, 1973).

Based on transportation planning, a trip is made by a household, which represents a house and its occupants regarded as a unit. Also, a trip is characterized by its purpose, origin and destination, time of day, mode, and route. Finally, trips in general are made during the peak hours. These peak hour trips affect the transportation system performance by the resulting congestion (Ben Akkiva, 1973).

The components of the four-step model and the corresponding questions they address are summarized in the table below (VDOT, 2014).

Table 2-1 Four-Step Model Components and Descriptions

| Step | Description |
|----------------------|--|
| 1. Trip Generation | How many trips will be made? |
| 2. Trip Distribution | Where will the trips go? |
| 3. Mode Choice | What modes of transportation will the trips use? |
| 4. Trip Assignment | What routes will the trips take? |

Further detailed information on these steps can be found in any classical book on transportation planning and in some research papers. Papacostas and Prevedouros (2001) provide an extensive coverage of demand modeling and forecasting that includes major components of travel behavior. Ortuzar and Willumsen (2001) present transportation modeling and its practical applications in an informative manner easily understandable to engineers and practitioners alike. Boyce (2004) covers in detail the history of travel demand modeling developments in both research and practice including the origins and development of the sequential procedure of travel demand models.

2.2.3. Trip Assignment Step and Its Practical Role

Among all the steps of travel demand model, the trip assignment step is of particular interest to planners because it predicts the quantity or volume of trips from an origin to a destination during a specific time using a specific mode and a specific route (composed of several links) of a transportation system. The predicted volume is then used as an input data in estimating the travel time on the roadway network.

2.3. Travel Time

2.3.1. Definition and Importance of Travel Time

Generally speaking, travel time refers to the time required to complete a trip or traverse a roadway segment. Travel time may be measured directly using field studies or can be estimated using empirical relationships with traffic volume and roadway characteristics, or computer network models.

Travel time in planning is an important variable used in the evaluation of the transportation system. The speed that indicates the congestion state is derived from the travel time.

2.4. Congestion

2.4.1 Definition Traffic Congestion

FHWA (2005) states that highway congestion happens when there are more vehicles than available space on the road. In other words, congestion occurs when traffic demand approaches or exceeds the available capacity of the highway system. Congestion is recognized as a national issue that affects the economy, environment, and equity.

2.4.2. Main Cause of Traffic Congestion

The planning community recognizes that traffic congestion on urban road networks has been increasing for the past decades. According to FHWA (2005), the vehicle of miles traveled (VMT) grew by 76 percent between 1980 and 1999 while the amount of new roads or lanes increased only by 1.5 percent. Among the many reasons causing congestion, traffic bottleneck alone counts for almost half of all the causes to 40%.

2.4.3. Congestion Mitigation Measures

Planners realize that effective new strategies to mitigate congestion are needed. In the past, the primary focus of congestion responses was oriented to adding more physical capacity: changing highway alignment, adding more lanes (including turning lanes at signals), and improving merging and weaving areas at interchanges. In other words, congestion can be reduced by either increasing road capacity (supply), or by reducing traffic (demand).

In the travel demand modeling, congestion occurs when the assigned volume on a link exceeds the link capacity. This crucial link performance measure is computed during the trip assignment stage of the travel demand modeling process using the function called volume-delay function.

2.5. Volume-Delay Function

2.5.1. Definition and Categories of Volume-delay Function

The volume-delay function (VDF) is used in the highway assignment stage of the travel demand model to estimate link average travel time. In the trip assignment of the travel demand model process, travel times are estimated as a function of traffic demand/volume. Such a function is called volume-delay function (VDF). Several such functions are found in the technical literature and the three most common volume-delay functions used in highway assignment are BPR, Conical, and Akcelik functions. This study only considers the BPR function because of its advantages over the other functions. BPR function has the following form:

$$t = t_0 / \left(1 + \alpha \left(\frac{q}{q_{max}} \right)^\beta \right) \quad (2.1)$$

where t is average link travel time, t_0 is the free-flow link travel time, q is the volume (or demand), q_{max} is the capacity, α and β are parameters to be determined.

The chronology of these volume-delay functions can be found in the literature section of most of publications on travel time. From planning perspective, it does not make any difference which model is used in the trip assignment process. However, the selection of the model to use should be determined on the basis of computational efficiency and convenience considerations (Ben Akkiva, 1973).

2.5.2. Predetermined Traffic Variables

The volume-delay function (VDF) is used in the highway assignment stage of the travel demand model to estimate link average travel time. Among the input variables used in VDF, there are some that need to be known a priori (Kucharski and Drabicki, 2017). These variables include flow capacity and free-flow speed. In practice, a correspondence table is developed that includes speed and capacity values for each link type and area type. In the link-specific approach, these variables can be derived directly from the collected traffic data. The next sections cover procedures, formulas, and flowcharts that explain how capacity, free-flow speed, and optimum speed are identified from collected traffic data. A rudimentary approach has been preferred to a complex one to ensure that these procedures can be reproduced easily using any computer language.

2.6. Traffic Loop Detectors

2.6.1. Introduction

In order to study the growing traffic congestion problem, transportation agencies need to collect traffic data on transportation systems to perform such operations as traffic analysis, management, and pavement design. One device that is commonly used for this purpose is traffic loop detector. Traffic detectors are magnetic induction loops (sensors) that are embedded in the roadway pavement to detect and relay, within a specified time interval, vehicle movements to a nearby station and permit transportation agencies to determine traffic counts, density and vehicle speed (Transportation Defined: Loops, 2019). The traffic data are used by traffic planners and engineers to make better and informed decisions.

2.6.2. Flow and Speed Estimation Formulas

State transportation agencies, responsible of managing traffic on freeways, install traffic loop detectors on a freeway to collect and report the vehicle counts and speeds at a specific time interval ranging from 30 seconds to 5 minutes. Flow or volume, q , which represents the vehicle count, N , recorded in a given sampling time interval, t , and the vehicle speed, v , are computed using the following formulas (Bickel et al., 2007, p. 587).

$$q(t) = \frac{N(t)}{T} \quad (2.2)$$

$$v(t) = \frac{1}{N(t)} \sum_{j \in J(t)} v_j \quad (2.3)$$

2.6.3. Traffic Detector and Traffic Data Issues

Traffic detectors and collected traffic data are known to have issues that need to be considered in the data analysis. Jacobson et al. (1990) recognize that many detector failures and data errors remain undetected. De Laski et al. (1985) on the other hand list some causes of these detector failures that affect the data accuracy. Bickel et al. (2007) find that loop detectors are not easy to calibrate accurately and that the data will be biased if the calibration is not properly done. They also warn that bad and missing data present a challenge for any algorithm that uses data for analysis. Their proposed solution is simply to detect and discard bad data.

2.7. Steady-state Flow Analysis

2.7.1. Introduction

As already mentioned in the previous section, traffic volume (or flow) and speed data collected by traffic detectors are recorded and reported at time interval ranging from 30 seconds to 5 minutes. Based on Branston's (1976) observations, 5-minute sampling time interval can be sufficient to capture almost any immediate change in flow and speed. Such a small sampling is therefore appropriate for dynamic traffic analysis.

For the static assignment procedure, the variations of any time dependent effects on speed and flow on a link are smoothed over. This implies measuring speeds during periods when flow on a link is almost balanced or "steady".

A steady-state flow can be approximated by having a long sampling time interval, as experiments conducted by Rothrock and Keefer (1957) revealed. They conducted experiments to predict the shape of the speed-flow curve under different sampling time intervals. They have observed that the apex of the curve becomes smaller as the sampling time interval increases, almost disappearing completely with the 60 minute sampling (Figure 2-1). In other words, a “steady-state” is achieved by increasing the sampling time interval to 60-minutes.

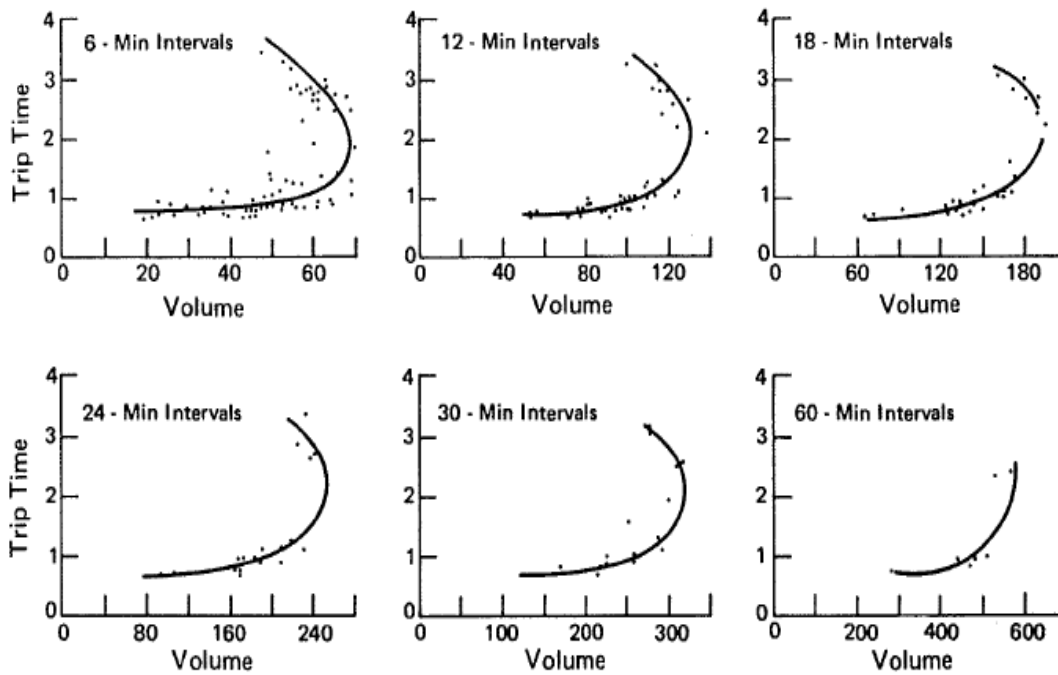


Figure 2-1 Travel Time-Flow Relationships for Several Sampling Time-Interval Durations, by Rothrock and Keefer, 1957

Since the mathematical formulation of the assignment procedure only applies to steady-state conditions, it is important to develop simple methods that aggregate traffic data from 5-minute time interval to 60-minute time interval. The next section presents the proposed formula, flowchart, and pseudocode developed to perform these aggregation operations.

2.7.2. Formulas for Estimating Steady-state Traffic Flow

Equation 2.9 represents the general formula for estimating volume for different sampling time intervals, including steady-state conditions.

$$q_{ij} = \sum_{\varphi j - (\varphi - 1)}^{\varphi j} \bar{q}_{ij} \quad \forall i = 1, 2, \dots, N \quad \forall j = 1, 2, \dots, T/\varphi \quad \forall t = 1, 2, \dots, T \quad (2.4)$$

where φ is the ratio of the new time interval to 5-minute interval. For example, $\varphi = 3$ for 15-minute time interval, and $\varphi = 12$ for 60-minute time interval.

Figure 2-2 depicts the necessary steps involved in the procedure.

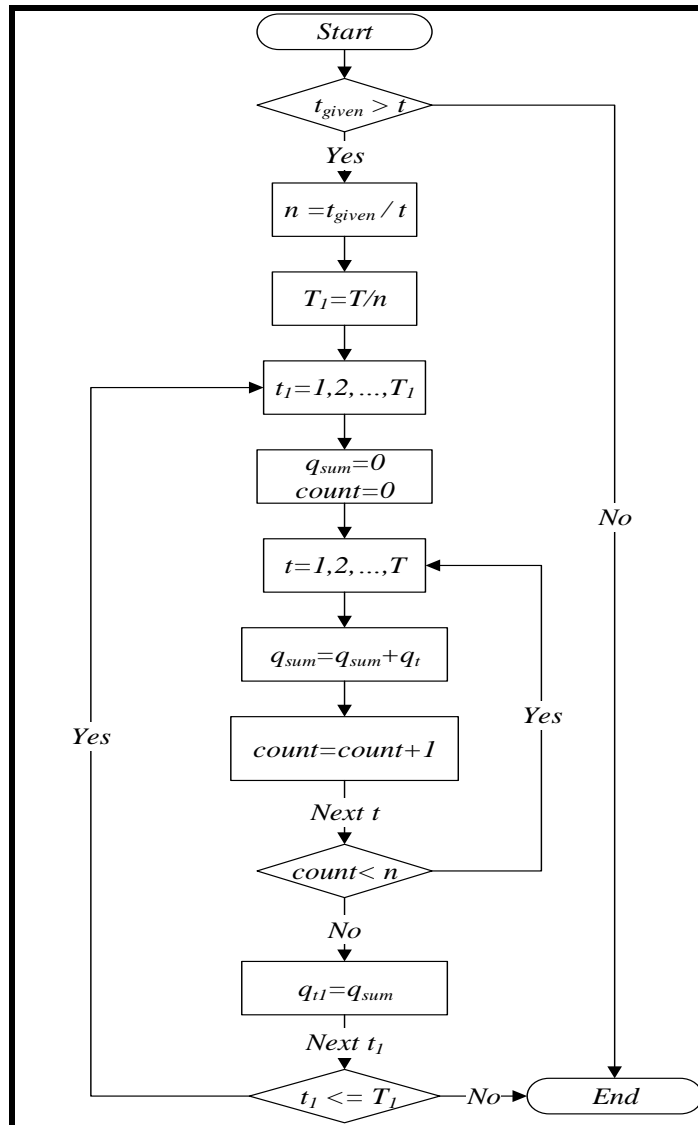


Figure 2-2 Flowchart for Estimating “Steady-state” Volume (from 5-minute Time Interval)

2.7.3. Sparse Traffic Data Impact on Steady-state Flow Analysis

The impact analysis for an actual link of sampling time intervals on speed-flow curve has revealed that steady flow conditions are achieved with the 60-minute sampling interval (Rothrock and Keefer, 1957). Given 5-minute traffic database, steady-state flow is obtained by aggregating 5-minute flows to

60-minute ones. Steady flow database has therefore fewer data than the original database. This makes the speed-flow curve-fitting challenging for steady flow analysis, especially given that the database will most likely be further reduced because of inherent problems with traffic detectors.

2.8. Traffic State Estimation (TSE)

2.8.1. Introduction

Based on traffic detector issues mentioned above, it can be expected to have missing or bad data in the collected traffic data. The proposed solution of deleting bad data will further reduce the database size. A method that would estimate traffic data for missing or bad data will prevent the situation where the traffic data is so sparse that performing steady-flow traffic analysis become a challenge.

2.8.2. Definition of Traffic State Estimation (TSE)

Typically, traffic state estimation (TSE) is defined as the process of estimating and predicting the spatiotemporal evolution of three state variables, individually: flow $q(x, t)$ (veh/h), density $k(x, t)$ (veh/mile), and speed $v(x, t)$ (mile/h) on location x and time t , according to observed traffic data.

2.8.3. Background

Substantial research efforts have been devoted to the TSE problems. The classic kinematic wave (KW) model developed by Lighthill, Whitham and Richards, uses a partial differential equation (PDE) to express traffic states. Fundamental diagrams (FDs) are used to capture the relationship among the traffic state variables. FDs also contain important info about traffic characteristics, e.g. free-flow speed, backward wave, capacity, and jam density (Immers and Logghe, 2002). Moreover, the Cell Transmission Model (CTM) is developed as a numerical method to solve the PDE (Daganzo, 1994). Recently, many TSE approaches are derived based on the KW model or CTM model using different state representations (Muñoz et al., 2003). Newell G.F. (1993) proposed a KW model based on the simplified triangular flow-density FDs. The model provides a solution for the three-detector problem that is an important TSE problem to estimate the traffic states at intermediate locations, provided vehicle counts of upstream and downstream detectors. The method selects cumulative flow counts as the representation of traffic states. One can simply get the cumulative flow curve of any intermediate location by forward/backward propagating the upstream/downstream cumulative counts. Despite that, the Newell's approach highly depends on deterministic boundary inputs. Although Deng et al. (2013) developed the model under stochastic boundary conditions, it is founded on the assumption of following Gaussian distribution.

In the existing literature, data-driven models become more important with the widespread traffic sensor technologies (Lv, Y. et al. 2015). This kind of models rely more on statistical and machine learning technologies, instead of traffic flow theories. The methods usually

extract probabilistic dependence between observable/latent variables from historical data and predict the future traffic state based on the updated streaming data (Seo et al. 2017). For example, the Markov Chain (MC) models are applied to accomplish data-driven estimation and prediction on freeways (Yeon et al. 2008; Ramezani and Geroliminis, 2012; Antoniou et al. 2013).

2.8.4. Summary

Several models used in traffic state estimation (TSE) have been reviewed. The kinematic wave (KW) model, proposed by Newell and based on the simplified triangular flow-density fundamental diagrams (FDs), is the most important one because it estimates the traffic states (speed and flow) at an intermediate detector location, based on vehicle counts of upstream and downstream detectors.

One challenge in data-driven approaches is how to develop an explainable framework to reflect the underlying phenomenon in traffic flow dynamics.

2.9. Capacity Estimation

HCM (2010) defines capacity as the maximum possible expected throughput of the facility type under consideration. There are several methods and guidelines for estimating capacity of various facility types, including the breakdown method, which is used in traffic operation applications. However, only the two most commonly used methods in planning applications are considered in this study.

In the fundamental diagram curve fitting approach, the observed speed data are plotted against observed flow or volume data, and a curve is then fitted to these data points. The volume at the apex of this curve is considered as the capacity, which represents the maximum throughput of the facility under consideration.

The second method, called the maximum observed value method, is based on the fact that the capacity of a facility at a given location can be easily identified as the maximum volume from the observed data measured over a given time interval (Li and Laurence, 2015). The maximum observed value method is the easier method, from a computational perspective, for estimating capacity from empirical data. Based on this approach, the proposed mathematical formulation for identifying capacity can be generalized as:

$$q_c^i = \max \bar{q}_t^i \quad \forall t = 1, 2, \dots, T \quad \forall i = 1, 2, \dots, N \quad (2.5)$$

where q_c^i , \bar{q}_t^i , i , t , N , and T denote capacity, observed volume, detector number, sampling time interval, number of detectors that collect traffic data, and number of sampling time intervals in a given period, respectively. As an example, for time interval t of 5 minutes,

15 minutes, or 1 hour, the number of sampling time intervals T is 288, 96, or 24, respectively. Figure 2-3 depicts the proposed flow chart that underlines this approach.

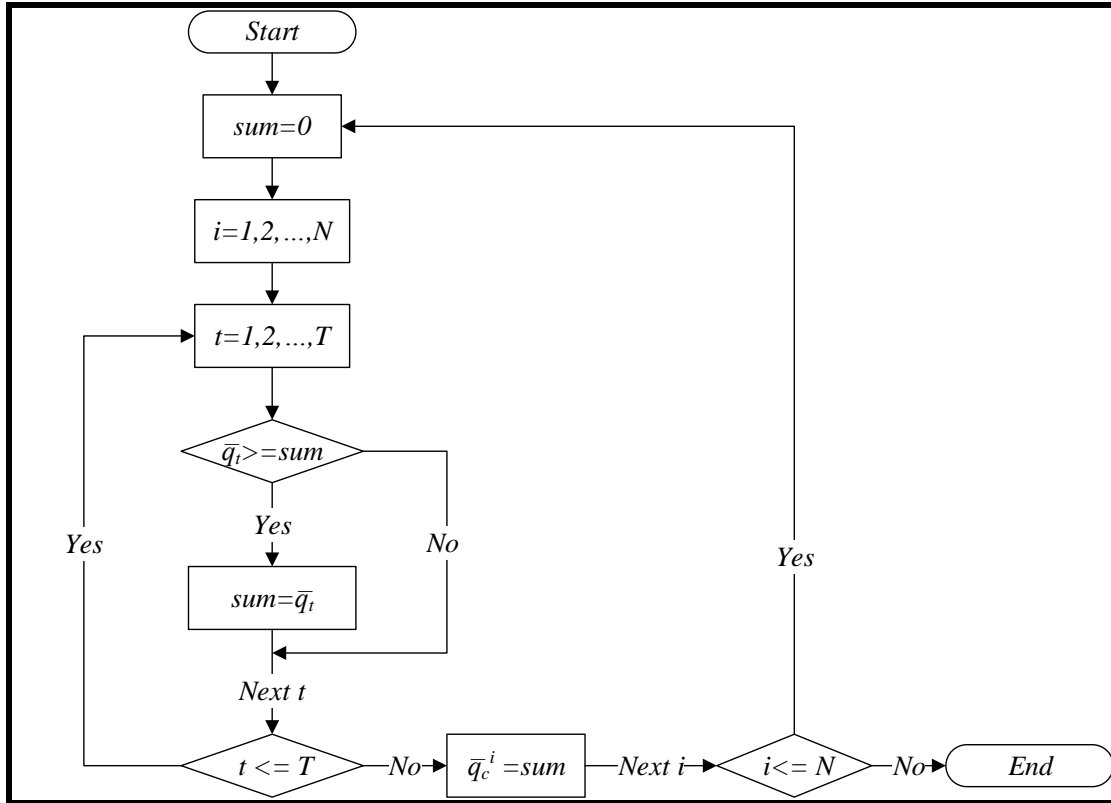


Figure 2-3 Flow Chart for Capacity Estimation (Based on Collected Data from Detectors)

It is worth stressing, as Boyles et al. (2019) have recently published, that capacities are measured with respect to the entire time interval. A 60-minute interval capacity, for example, is the sum of all the 5-minute interval capacities included in that 60-minute interval. In practice where capacity is generally given per hour, a three-hour peak period capacity can be computed as one-hour capacity times 3.

2.10. Free-flow Speed Estimation

The HCM (2010) manual defines free-flow speed as the theoretical speed when density and flow rates on a facility are both zero. Similar to capacity mentioned in the previous section, free-flow speed can also be obtained from the same two planning applications methods used to estimate capacity.

For the fundamental diagram curve fitting approach, the observed speed data are plotted against observed flow or volume data, and a curve is then fitted to these data points. The speed at the upper base/end of the curve represents the free-flow speed.

For the maximum observed value method, the free-flow speed can simply be considered as the maximum speed recorded for the facility. Figure 2-4 illustrates the steps involved in the procedure. The proposed mathematical formulation can simply be expressed as:

$$v_f^i = \max \bar{v}_t^i \quad \forall t = 1, 2, \dots, T \quad \forall i = 1, 2, \dots, N \quad (2.6)$$

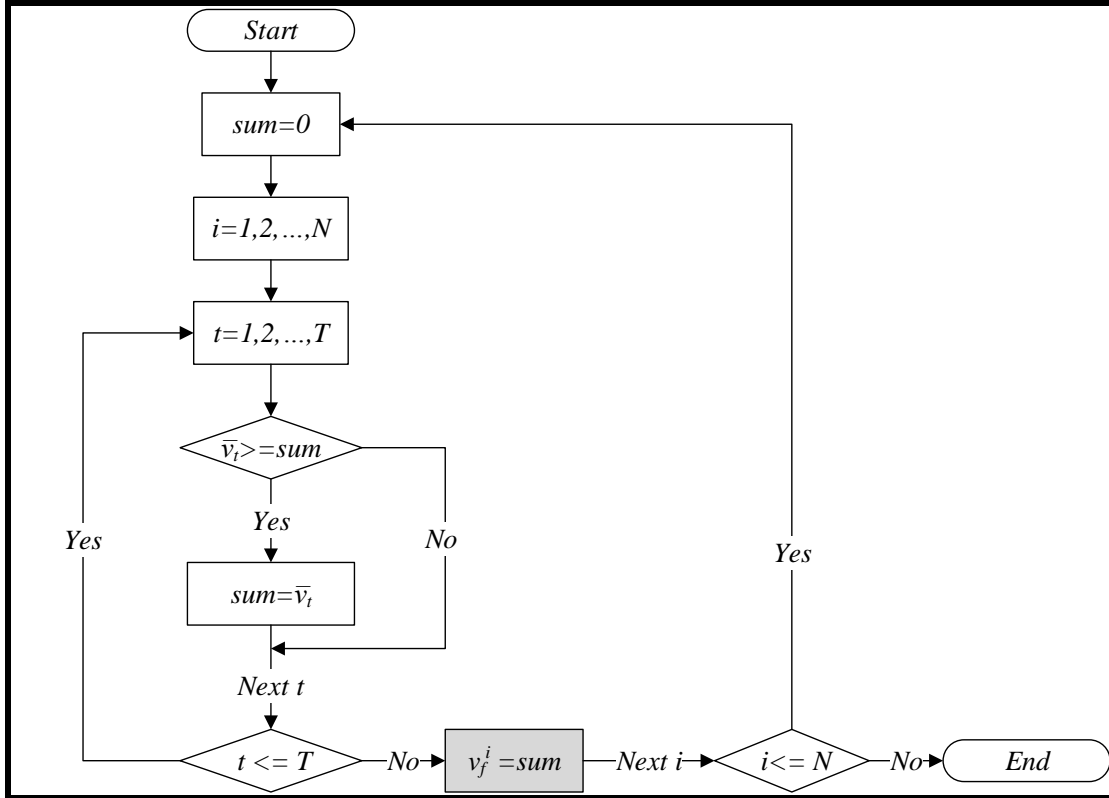


Figure 2-4 Flow Chart for Free-flow Speed Estimation (Based on Collected Data from Detectors)

2.11. Estimation of Optimum Speed at Capacity

It is important to clearly identify the speed that corresponds to the maximum flow or capacity. Mtoi et al. (2013) refer to such as speed as optimum speed at capacity. Optimum speed can be easily identified from the collected data by using either the curve-fitting method or the maximum value method. The proposed formula for optimum speed or cutoff speed is expressed as:

$$v_c^i = \bar{v}_t^i \text{ such that } q_c^i = \max \bar{q}_t^i \quad \forall t = 1, 2, \dots, T \quad \forall i = 1, 2, \dots, N \quad (2.7)$$

The algorithm involved in identifying the optimum speed is illustrated in the Figure 2-5 below.

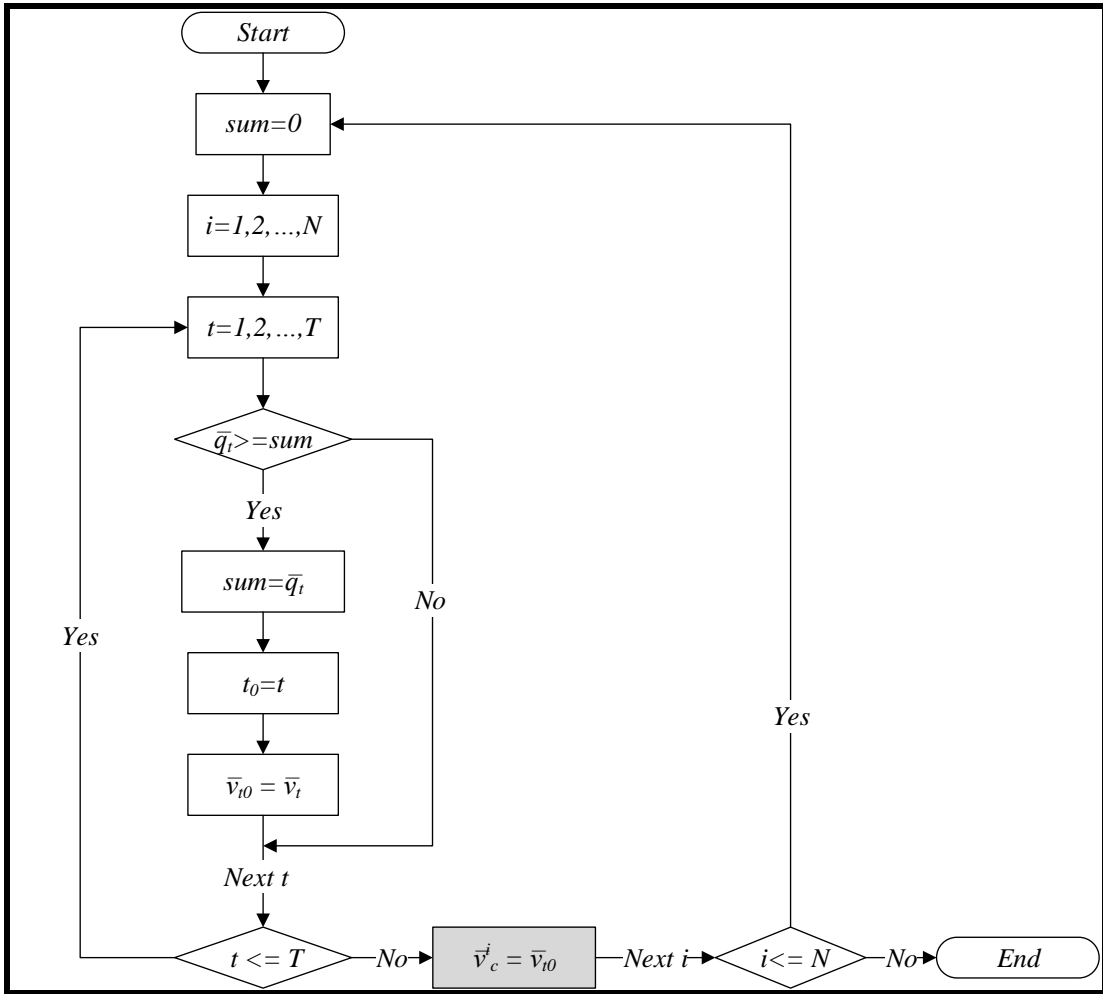


Figure 2-5 Flow Chart for Optimum Speed Estimation (Based on Collected Data from Detectors)

2.12. Traffic Flow Conditions and Types Used in Volume-delay Function

2.12.1. Introduction

Determining the fundamental traffic data variables provides the framework for the analysis of collected traffic data before they can be used in the volume-delay function (VDF). The next sections explain how these variables are used to perform such operations as classifying traffic conditions and flow types.

2.12.2. Definitions of Uncongested State and Congested Conditions

The optimum speed previously defined mainly serves as a borderline to classify the traffic conditions. Traffic data set with speeds less than optimum speed constitutes congested state, whereas traffic data set with speeds above optimum speed forms uncongested set (Elefteriadou and Lertworawanich, 2003).

2.12.3. Definitions of Traffic Flow Types

There are several types of traffic flow depending on the flow sources and conditions.

A demand flow in the basic traffic assignment problem is the total flow that has been allowed (or authorized) to the link and there are no explicit upper bounds imposed on link flows (Boyles et al., 2019). A flow greater than the capacity can simply be interpreted as the demand for travel on the link exceeds the capacity, and this results in queue formation.

A macroscopic (or assigned) flow represents the demand flow that has been supplied to the network, whereas a measured (or physical) flow is the actual flow that has been collected by a traffic detector device. As mentioned in several travel demand modeling courses

including the NHI training course (2012), assigned flows are compared to measured flows (or ground counts) for model validation.

2.12.4. Impact of Capacity on Traffic Flow Types

Kucharski and Drabicki (2017) mentioned the distinction between the macroscopic assigned flow and measured flow. Both of these flows are different and have different physical interpretations with respect to demand and capacity.

The assigned flow continuously grows with the demand (i.e., the higher the demand is, the greater the assigned flow is) and, therefore, may exceed the capacity. The assigned flow can get severely delayed but in general is allowed.

Measured flow, on the other hand, grows with the demand too but drops down when the demand flow exceeds the capacity limit. This corresponds to reality of the actual flow pattern.

2.12.5. Traffic Flow Types and Congestion Index

As mentioned in the previous section, the main difference between measured flow and assigned flow with respect to the demand flow is that measured flow drops when it reaches capacity, whereas the assigned flow exceeds the capacity limit. Therefore, since capacity is the borderline between uncongested state and congested state (Mtoi et al., 2013), it can be expected that measured flows and assigned flows will display the same pattern under uncongested state, but that they will present a different behavior under congested state. For example, the volume (or flow) over capacity (v/c) ratio is used in the volume-delay function to account for the effects of congestion on highway network (Huntsinger and Roupail,

2011). A v/c ratio greater than one indicates congestion has occurred. Under assigned flows, this congestion index can have values greater than one as assigned flows continue to grow with demand past capacity. However, under measured flows, this congestion index never gets greater than one as measured flow does not exceed capacity. This does not mean congestion does not occur under measured flows. The challenge, therefore, remains which index to use that will reflect correctly congestion both under measured flows and under assigned flows in the volume-delay function.

2.13. Alternatives to Volume over Capacity Ratio as Congestion Index

Conceptually, the congestion notion is the same under measured flows as well as under assigned flows. These two flows actually experience the same speeds. The challenges reside in the understanding and interpretations of traffic data with respect to the demand in computing the congestion index. There are several solutions proposed in the literature that can be divided into two groups based on variables used in congestion index. In the first group, only the volume in the congestion index (v/c) is replaced by the demand. However, in the second group, both the volume and the capacity are replaced by density and optimum density, respectively; optimum density represents the density that corresponds to capacity. The formulas for these two groups are provided in the next sections.

2.13.1. Estimations of Demand Beyond Capacity

In reality, an assigned volume on a roadway cannot exceed its capacity. This explains why the v/c ratio of the HCM speed-flow curve does not exceed 1. However, for planning purpose, the assigned volume must exceed the capacity to accommodate the demand. There

exists a couple of methods based on queueing analysis that can estimate speeds for v/c that exceeds 1.

Huntsinger and Roupail (2011) show that the demand beyond capacity can be estimated by performing bottleneck and queue analysis using collected traffic data. At the end of their research, they proposed the following equation:

$$demand = capacity + queue\ length \quad (2-8)$$

The obvious problem with this approach is that the queue length computation requires additional exogenous information such as the area of influence for detector under consideration.

Moses and Mtoi (2013), on the other hand, propose a straight-forward method of computing the demand above capacity with the simple formula:

$$demand = capacity + (capacity - measured\ flow) \quad (2-9)$$

This method simply means that the demand is equal to the capacity plus the drop that the measured flow experiences after reaching the capacity limit. The convenience of this method is that all the required data are readily available.

Dowling et al. (2016) refer to the extra demand as carry-over demand, which indicates the presence of a queue at a specific location.

2.13.2. Density over Optimum Density Ratio as Congestion Index

Kucharski and Drabicki (2017) propose a completely different approach that consists in estimating the volume-delay function by using density instead of flow. As mentioned previously, measured flow grows with the demand and then decreases after capacity is reached. This results in a speed-flow relationship where, for a given flow, there are two different speed values: one speed in the uncongested state and another speed in the congested state. This is an evidence that there is no unique functional relation between speed and flow.

One observation made by the authors is that density behaves the same way as the macroscopic (assigned) flow. Density grows with the demand past capacity limit until it reaches its maximum value. The density at capacity and the maximum density are denoted as critical density and jam density, respectively.

This one-to-one relationship between density and macroscopic (assigned) flow has led the authors to reformulate the volume-delay function. Instead of the volume over capacity ratio, the authors use density over critical density ratio. This formula can be used for both uncongested and congested conditions to compute travel times from observed data.

2.13.3. Summary

Traffic data collected by detectors include such variables as traffic volume (or traffic flow) and speed. Capacity represents the maximum flow and is used to determine the optimum speed. Uncongested and congested traffic conditions are defined relative to the optimum speed. Different types of flow definitions are presented and the relationships between these flows and capacity limit with respect to the demand are considered. Demand formulas

based on different interpretations of overcapacity demand are presented. And a proposed new congestion index that represents the density over critical density ratio rather than volume over capacity ratio is also discussed.

2.14. Parameters Used in Volume-Delay Function

2.14.1. Introduction

Like all functions, VDFs are composed of variables and parameters. The input variables common to all VDFs have been covered in the above sections. It has been shown that variables such as free-flow speed, optimum speed, and capacity can be derived from collected traffic data. Parameters differ from function to function. Since Arizona Travel Demand model (AZTDM) results will be used in the case study and this model uses BPR function as VDF, the discussions in the next sections will be based on BPR parameters only. However, the final conclusions will be valid for parameters from other VDFs as well. The next sections cover the practical meanings of BPR parameters, their values and ranges.

2.14.2. Meaning of BPR Parameters

The original BPR function was based on the relationships found in the 1965 Highway Capacity Manual (HCM) (Papacostas and Prevedouros, 2001). The general meaning of BPR parameters, according to the NCHRP Report 387 (1997), can be summarized as follows. The parameter α determines the ratio of free-flow speed to the speed at capacity. The parameter β , on the other hand, determines how abruptly the BPR curve drops from the free-flow speed. The higher the value of β , the more abrupt the speed drops after reaching capacity.

2.14.3. BPR Parameter Values and Ranges

Actually, the formula for α parameter can be derived directly from the BPR formula below

$$v = v_f / (1 + \alpha \left(\frac{q}{q_{max}} \right)^\beta) \quad (2.10)$$

In the maximum observed value method, the capacity, q_{max} , corresponds to the optimum speed, v_c . After substituting these values in the above equation, the expression becomes

$$v_c = v_f / (1 + \alpha \left(\frac{q_{max}}{q_{max}} \right)^\beta) \quad (2.11)$$

After rearranging, α parameter can be estimated as

$$\alpha = v_f / v_c - 1 \quad (2.12)$$

Regarding β parameter, there is no such substitution mechanism. In other words, unlike α , the parameter β cannot be estimated from the collected traffic data.

However, the original values for BPR parameters α and β are 0.15 and 4, respectively, but the data from which they were obtained were not shown in the original report (Branston, 1976). These parameters have since been modified by researchers and transportation agencies to be consistent with more recent data. Researchers suggest different values based on their studies, whereas transportation agencies prefer to propose range of values to use on different facility types.

Zhao and Kockelman (2001) suggests values of 0.84 and 5.5 for α and β , respectively, which have originally been reported by NCHRP Report 365 (Martin 1998).

VDOT (2014) proposes values that range between 0 and 2 for α and between 2 and 10 for β . Hansen (2011), referring to the Danish road system, suggests a broader range of values between 0.5 and 2 for α , 1.4 and 11 for β . Table (2-1) summarizes different α and β values as proposed by researchers and transportation agencies.

Table 2-2 BPR Parameter Values for Freeway Used in Research and in Practice

| Parameter | Standard value | Zhao | Danish Road System | Virginia DOT | Arizona DOT | SCAG California |
|------------------|-----------------------|-------------|---------------------------|---------------------|--------------------|------------------------|
| α | 0.15 | 0.84 | 0.5-2 | 0-2 | 0.1-0.8 | 0.60 |
| β | 4.00 | 5.5 | 1.4-11 | 2-10 | 2-5 | 8.0 |

2.14.4. Summary

Fitting a function curve into traffic data is not a straight-forward procedure. It requires adjusting the function curve parameters to match the traffic data. In the above sections, the meanings of BPR parameters and the ranges of their values have been discussed.

2.15. Summary

In order to estimate travel time from collected traffic data, fundamental variables used in the volume-delay function (VDF) must be determined a priori. Speed and volume data are collected from detectors in 5-minute time interval. Since by definition static models do not consider temporal variations in traffic conditions and consequently assume a steady-state condition, these data have been aggregated to 60-minute time interval that has been proven to correspond to the traffic steady-state condition. The concept and importance of steady-state flow in static assignment procedure have been explained. Then formulas, flowcharts,

and algorithms needed to derive steady-state flow and fundamental variables such as capacity, free-flow speed, and optimum speed have been presented.

2.16. Limitations

It has been demonstrated, in the above sections, that not all of the BPR function components can be estimated using the collected traffic data. Variables such as free-flow speed, capacity, optimum speed, and congestion index can be estimated by using simple or simplified formulas or algorithms derived from data collected by detectors at the link level. On the other hand, BPR parameters α and β required advanced methods and exogenous data to calibrate their values to better fit the shape of speed-flow curve to the data making the process challenging.

The following compiled citations from the literature clearly indicate the limitations of volume-delay function in general and of BPR function in particular.

- Although the standard BPR curve was developed in the late 1960s by BPR (predecessor to the Federal Highway Administration (FHWA)) by fitting a polynomial equation to the freeway speed-flow curves in the 1965 HCM, its parameters were not link-specific.
- In practice, these parameters are estimated as a function of both area type and facility type.
- In addition to other limitations of static assignment models in their paper, Saw et al. (2015) mention the difficulty in determining the efficient values of BPR parameters α and β .

- Establishing proper values for the function parameters, which vary from region to region, is critical.
- Practitioners have noted that the BPR function leads to an overestimation of speeds for V/C ratios of greater than 1.0 and an underestimation of volumes for V/C ratios of less than 1.
- Another inherent drawback is that early assignment iterations by use of the BPR function can lead to extreme values for the link travel time that can slow the convergence process.
- Whereas Montezo et al. (2013) indicate that, even though the values for the BPR parameters are pre-defined based on assumptions and practice, they have inherent uncertainty which originates partly from the stochastic behavior of the parameters.
- The BPR curve does not account for the effects of queueing on travel speeds and demand. Planning models consequently will significantly overestimate speeds of facilities near, at, or over capacity.
- In the conclusion from his popular paper on VDF, Spiess (1989) provides the best possible recommendation regarding the estimation of these parameters. He recognizes that “further research would be needed to develop statistical methods for directly estimating the parameters of the conical functions, using observed speeds and volumes”.

CHAPTER 3

TRAFFIC STATE ESTIMATION USING STATE TRANSITION PROCESSES

3.1. Introduction

Chapter 3 uses the state transition process to capture the traffic deviation patterns and to update the evolution of traffic states by integrating traffic flow fundamentals and local traffic data.

In Section 3.2, the notations and indexes for traffic variables used in this chapter are clearly described, traffic flow variables used to define a traffic state are specified, traffic state variables are represented as discretized states on fundamental diagrams, and traffic parameters are calibrated using triangular flow-density fundamental diagram from Newell's method.

Section 3.3 describes shock wave process using the Newell's three-detector model approach where upstream, local, and downstream locations are represented in space-time graph. The shock wave boundary divides the graph into two distinct areas composed of free-flow/uncongested area and congested area. The free-flow area includes forward wave that originates from the upstream location to the local location. The congested area, on the other hand, encompasses the backward wave that propagates from the downstream location to the local location. Also represented on the graph are the cumulative traffic flow counts at the upstream, local, and downstream locations.

Section 3.4 covers functions and probability concepts as they apply to state transitions at all locations and kinematic wave impacts from upstream and downstream locations. Emission function is used to determine the state representations of the observed traffic data

by using the aggregated technique K-cluster approach. This technique groups flow-density pairs with similar characteristics that can be represented by centroids into states on the fundamental diagram (FD). Since a state sequence at a location satisfies the condition that the current state is independent of all other states but the previous one, Markov Chain (MC) is used as the transition function. This dependence structure is described using the probabilistic graph (PG). To describe the impacts of kinematic waves in a corridor, PG is extended to the space-time probabilistic graph (STPG). The conditional probabilities from upstream and downstream locations are estimated using the Bayesian Classifier (BC). The state update is performed by applying the weight average model to the combination of the MC model and the BC model.

3.2. Problem Statement and Overall Framework

Table 3-1 lists the notations used to represent all the variables in the traffic state (TSE) estimation formulation. Consider a traffic database that can provide every-5-minutes speed profiles and flow counts on several locations in a traffic network over any time period of days. Furthermore, real-time traffic information is also frequently updated to enable on-line traffic analyses. The framework proposed in this study attempts to undertake the following four tasks:

Table 3-1 Notations and Input Data

| Indexes and sets | |
|-------------------------|--|
| x, x' | Indexes of locations |
| x_d | Downstream sections of location x |
| x_u | Upstream sections of location x |
| $1, 2, \dots, T, t, t'$ | Indexes of timestamps |
| s | Indexes of samples |
| (x, t) | Space-time vertexes |
| M | Set of discrete states |
| N | Set of sections |
| Observations | |
| $\bar{q}(x, t)$ | Observed flow at location x time t |
| $\bar{k}(x, t)$ | Observed density at location x time t |
| $\bar{v}(x, t)$ | Observed speed at location x time t |
| $\bar{o}_{x,t}$ | Observed density-flow pair $(\bar{k}(x, t), \bar{q}(x, t))$ |
| Variables | |
| $q(x, t)$ | Estimated flow at location x time t |
| $k(x, t)$ | Estimated density at location x time t |
| $v(x, t)$ | Estimated speed at location x time t |
| $m_{x,t}$ | Estimated state at location x time t |
| $n(x, t)$ | Cumulative counts at location x time t |
| v_f | Free-flow speed |
| v_c | Congested/critical speed |
| $BWTT(x, x_d)$ | Travel time from a downstream location x_d to x with speed w_b |
| $FFTT(x_u, x)$ | Travel time from an upstream location x_u to x with speed v_f |
| $L(x, x')$ | Distance from location x to x' |

(i) define traffic states considering the coupling of different types of state variables on FDs (see Figure 3-1); (ii) develop the transition matrices considering how the traffic states of local, upstream, and downstream locations change and interact from one time to another (see Figure 3-2); (iii) estimate regular pattern of traffic states of each location using the historical data; (iv) update the estimates using real-time observations, and developed transition matrices.

The fundamental diagram relationship states that the flow q is proportional to both the density k and the speed v , as expressed in the equation below.

$$q = k v \tag{3-1}$$

Figure 3-1 and the above equation show that a traffic state, $m_{x,t}$, can be defined using a pair of flow and density.

$$m_{x,t} = (q(x, t), k(x, t)) = \left(q(x, t), \frac{q(x,t)}{v(x,t)} \right) \tag{3-2}$$

And traffic state variable at location x is $\begin{bmatrix} (q(x,1),k(x,1)) \\ (q(x,2),k(x,2)) \\ \dots \\ (q(x,T),k(x,T)) \end{bmatrix}$

The proposed framework is a two-step process including predicting and updating, similar to Kalman Filter (KF) (Wang et al. 2007). During the predicting step, historical data (e.g. flow and speed) are used to (A) calibrate the coefficients of Newell's KW model, as shown in Figure 3-2 and (B) identify discretize traffic states using clustering analyses on FDs. (C) The state transition matrices are then constructed to represent the spatiotemporal correlations based on a space-time probabilistic graph (STPG). The spatiotemporal correlations underlined in the forward and backward waves of the three-detector problem are expressed in the STPG (See Figure 3.2). (D) An MC model is used to estimate the historical patterns of the evolution of traffic states. During the updating step, (E) real-time observations are applied to update the estimates based on Bayesian Classifier (Friedman et al. 1997). (F) The final outputs are produced by weighing both regular state patterns and real-time updating. The overall framework and tasks achieved by the 6 modules are shown in Figure 3-3.

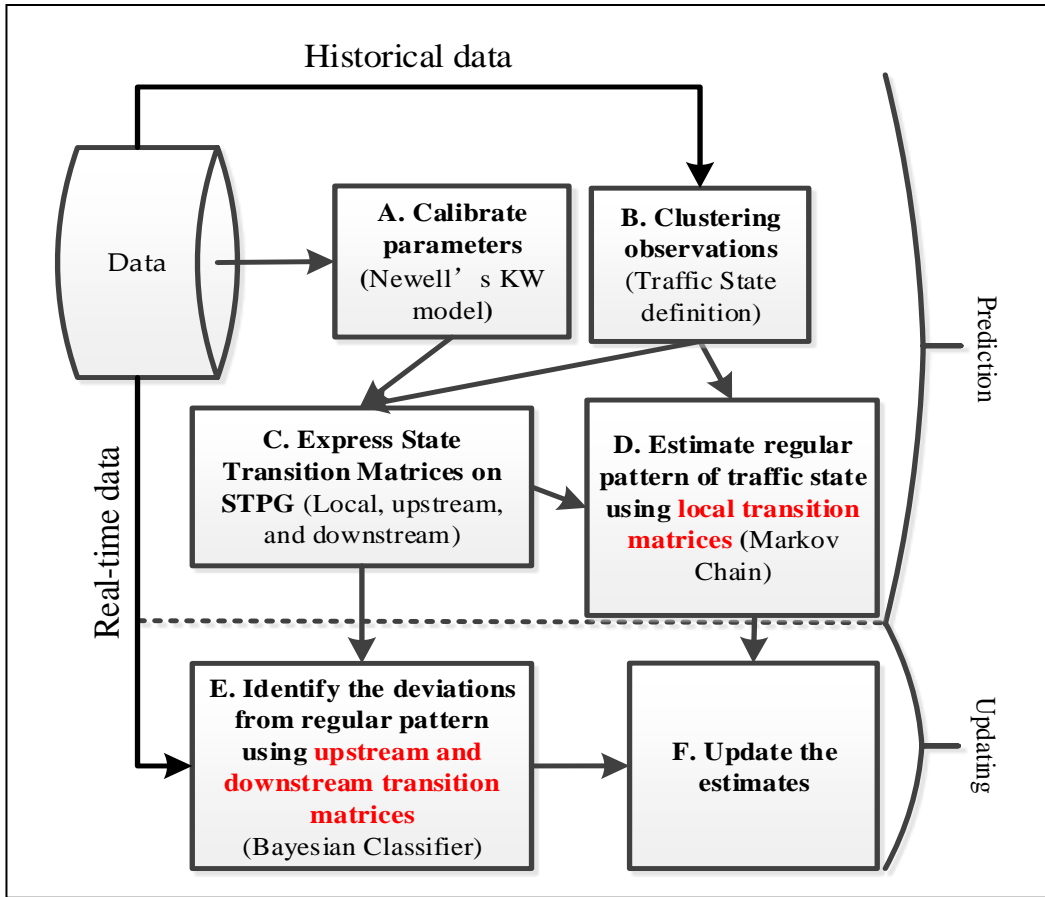


Figure 3-3 Overall TSE and Prediction Framework

3.3. Describing Traffic Shockwave Using Newell's Three-Detector Problem

A simplifying assumption of Newell's KW model is that the derivatives of the FD are discontinuous and correspond to the pacing of two types of kinematic waves. By using the linear regression, we calibrate the parameters of the FDs in Figure 3-1, and Table 3-2 (Module A in Figure 3-3). For densities $k < k_c$, the wave speed is free-flow speed v_f . For densities $k > k_c$, the wave speed is backward wave speed w_b . The traffic flow equation can then be expressed as

$$q = \begin{cases} v_f k & \text{if } k < k_c \\ q_c - \frac{k-k_c}{k_j-k_c} q_c & \text{if } k \geq k_c \end{cases} \quad (3-3)$$

Since the wave characteristics changes only at boundaries between uncongested and congested states, the cumulative flow counts $n(x, t)$ of any intermediate point can be derived from the cumulative flow counts at the upstream and downstream.

Table 3-2 Traffic Flow Model Parameters

| | |
|-------|---|
| v_f | Free-flow speed in the free-flow state |
| w_b | Backward wave speed in the congestion state |
| q_c | Capacity of a road or the maximum flow rate |
| k_c | Density associated with the maximum flow rate |
| k_j | Jam density where the flow rate reduces to zero |

As illustrated in Figure 3-2, the space-time domain is divided into two sub-areas by the shock wave boundary. In the area of the uncongested state, $n(x, t)$ can be determined by $n(x_u, t - FFTT(x_u, x))$. Figure 3-4 illustrates the relationship between $n(x_u, t)$ and $n(x, t)$. It is that a vehicle v passes location x_u at time $t_0 - FFTT(x_u, x)$, and arrives at location x at t_0 .

$$n(x, t_0) = n(x_u, t_0 - FFTT(x_u, x)) \quad (3-4)$$

In the subarea of congested states, the traffic flow is restricted by a downstream bottleneck.

Figure 3-4 displays the relationship between $n(x_d, t)$ and $n(x, t)$. As the total number of vehicles that can be stored between $L(x, x_d)$ is $k_j \times L(x, x_d)$, then

$$n(x, t_2) = n(x_d, t_2 - BWTT(x, x_d)) + k_j \times L(x, x_d) \quad (3-5)$$

Newell's method uses the smaller value of the above two values to determine the shock wave boundary. As shown in Figure 3-4, at location x , the characteristics is changed at time t_0 which divides the curve $n(x, t)$ into two parts. Except for the discontinuous point at time t_1 , the left part of curve $n(x, t)$ is translated from the green curve $n(x_u, t)$. The right part of curve $n(x, t)$ is translated from the curve $n(x_d, t)$ (i.e. "moving coordinate" (Newell, 1993)). Newell's method provides a simple way to describe the state transitions on freeways. From the function $n(x, t)$, the flow, density, and speed can be calculated directly from the derivatives of $n(x, t)$. It implies that the traffic states at location x equal to the traffic states of the upstream location along the forward wave, when $t < t_1$. Location x has the same traffic state to the downstream location along the backward wave, when $t > t_1$ until the state of congestion ends (Hurdle and Son, 2000).

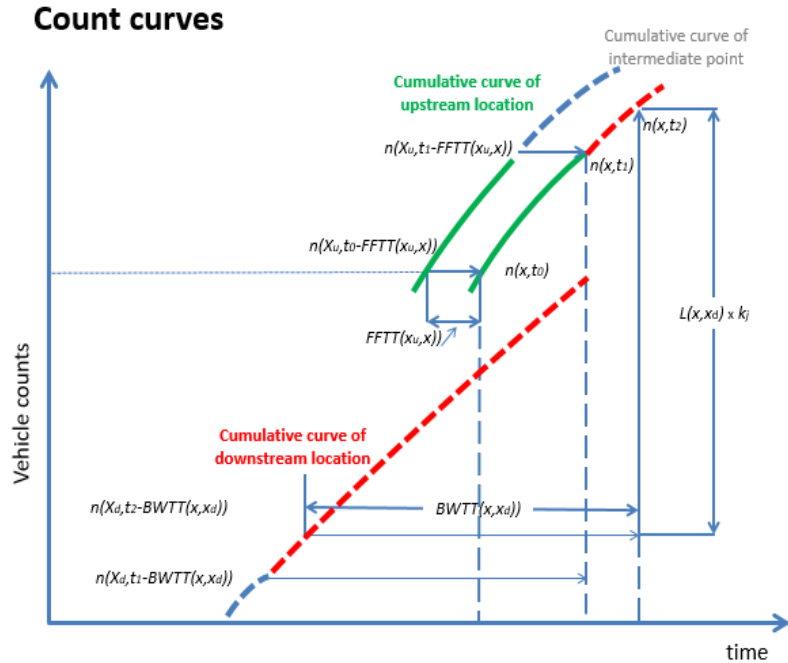


Figure 3-4 Forward and Backward Propagation on Cumulative Curves Adapted from Hurdle and Son (2000)

3.4. Describing State Transition on the Space-Time Probabilistic Graph

A probabilistic graph (PG) describes dependence structures between random variables. It can be also viewed as a generalized expression of MCs or linear state-space model (usually solved by standard KF).

- **State Representation Assignment**

Denoting the observation vector as $\{\bar{o}_{x,1}, \dots, \bar{o}_{x,T}\}$, each $\bar{o}_{x,t}$ is generated by an emission function whose input is state $m_{x,t}$ at location x time t :

$$\bar{o}_{x,t} = g(m_{x,t}) \quad \forall t = 1, 2, \dots, T \quad (3.6)$$

The emission function, g , determines the state representation of the observation $\bar{o}_{x,t}$. In a Hidden Markov Chain (HMC) model, g is a probability density function. In a Kalman

Filter (KF) model, g is a linear function with Gaussian noises. In travel demand model, g is a volume-delay function (VDF).

Table 3-3 Emission Function Interpretation from Typical Models

| Model | Emission function, g |
|---------------------|--------------------------------------|
| Hidden Markov Chain | Probability density function (PDF) |
| Kalman Filter | Linear function with Gaussian noises |
| Travel Demand | Volume-delay function (VDF) |

In this research, the emission function is assumed by directly clustering the flow-density pairs on the FDs. K-means clustering is applied to classify the observation $\bar{o}_{x,t}$ into traffic states with similar characteristics (Module B in Figure 3.3). Readers can refer to Antoniou et al. (2013) to learn more on other clustering algorithms applied in TSE problems.

- **Local State Transitions**

For each location x , $\{m_{x,1}, \dots, m_{x,T}\}$ is defined as a state sequence satisfying the first order Markov property, which implies that current state $m_{x,t}$ is independent of all other states except $m_{x,t-1}$. Then, the MC model, Eq. (4), means that the joint distribution $P(m_{x,1}, \dots, m_{x,t})$ is calculated by:

$$P(m_{x,1}) \prod_{t=2}^{t=T} P(m_{x,t} | m_{x,t-1}) \quad \forall t' = 2 \dots T \quad (3-7)$$

The MC model becomes a state-space model when the transition probability $P(m_{x,t} | m_{x,t-1})$ is expressed by:

$$m_{x,t} = f_t(m_{x,t-1}) \quad \forall t = 1, 2, \dots T \quad (3-8)$$

If the transition function f_t is a linear function with Gaussian noises, then the equation expresses the predicting process in KF.

Figure 3-5 (A) illustrates a PG to express the MC model. The vertexes represent random variables. The directed edge from a vertex to vertex indicates that the head vertex is conditioned by the tail vertex. For each edge, the corresponding conditional probability is labeled (Ghahramani, 2001). The MC model (Eq. 4) is utilized to estimate the historical sequence of traffic states from vertex $(x, 1)$ to (x, T) for the following model (Module C and D in Figure 3.3).

Given $m_{x,1}, m_{x,2}, \dots, m_{x,t-1}$, the regular state $m_{x,t}$ can be estimated as

$$\mathbf{M1:} \operatorname{argmax}_{m_{x,t}} \{P(m_{x,t}|m_{x,t-1})P(m_{x,1}, m_{x,2}, \dots, m_{x,t-1})\} \quad (3-9)$$

- **Upstream and Downstream State Transitions**

To describe the impact of kinematic waves in a corridor, we extend the PG to an STPG. The spatiotemporal correlations are expressed by space-time edges in the STPG. As illustrated in Figure 3-5 (B), the traffic state of vertex $(x, 3)$ is conditioned by two parent vertexes labeled by two conditional probabilities:

- a) Backward wave state transition: $P(m_{x,3}|m_{x_d,1})$
- b) Forward wave state transition $P(m_{x,3}|m_{x_u,2})$

- **Bayesian Classifier**

Now considering the case of the real-time data input. For example, the traffic states (evidence) of two vertexes (as shown in Figure 3-5 (B)) are already know: $m_{x_d,1} = \bar{o}_{x_d,1}$ and $m_{x_u,2} = \bar{o}_{x_u,2}$. Then, the conditional probabilities can be calculated using a (naïve) Bayesian classifier (Friedman et al. 1997) (Module E in Figure 3-3) based on forwarding and backward waves in the figure:

a) $P(m_{x,3}|m_{d,1}) = P(m_{x,3}|\bar{o}_{x_d,1}) \propto P(m_{x,3})P(\bar{o}_{x_d,1}|m_{x,3})$

b) $P(m_{x,3}|m_{x_u,2}) = P(m_{x,3}|\bar{o}_{x_u,2}) \propto P(m_{x,3})P(\bar{o}_{x_u,2}|m_{x,3})$

Generally, we have

$$P(m_{x,t}|\bar{o}_{x_d,t-BWTT(x,x_d)}) \propto P(m_{x,t})P(\bar{o}_{x_d,t-BWTT(x,x_d)}|m_{x,t})$$

$$P(m_{x,t}|\bar{o}_{x_u,t-FFTT(x_u,x)}) \propto P(m_{x,t})P(\bar{o}_{x_u,t-FFTT(x_u,x)}|m_{x,t})$$

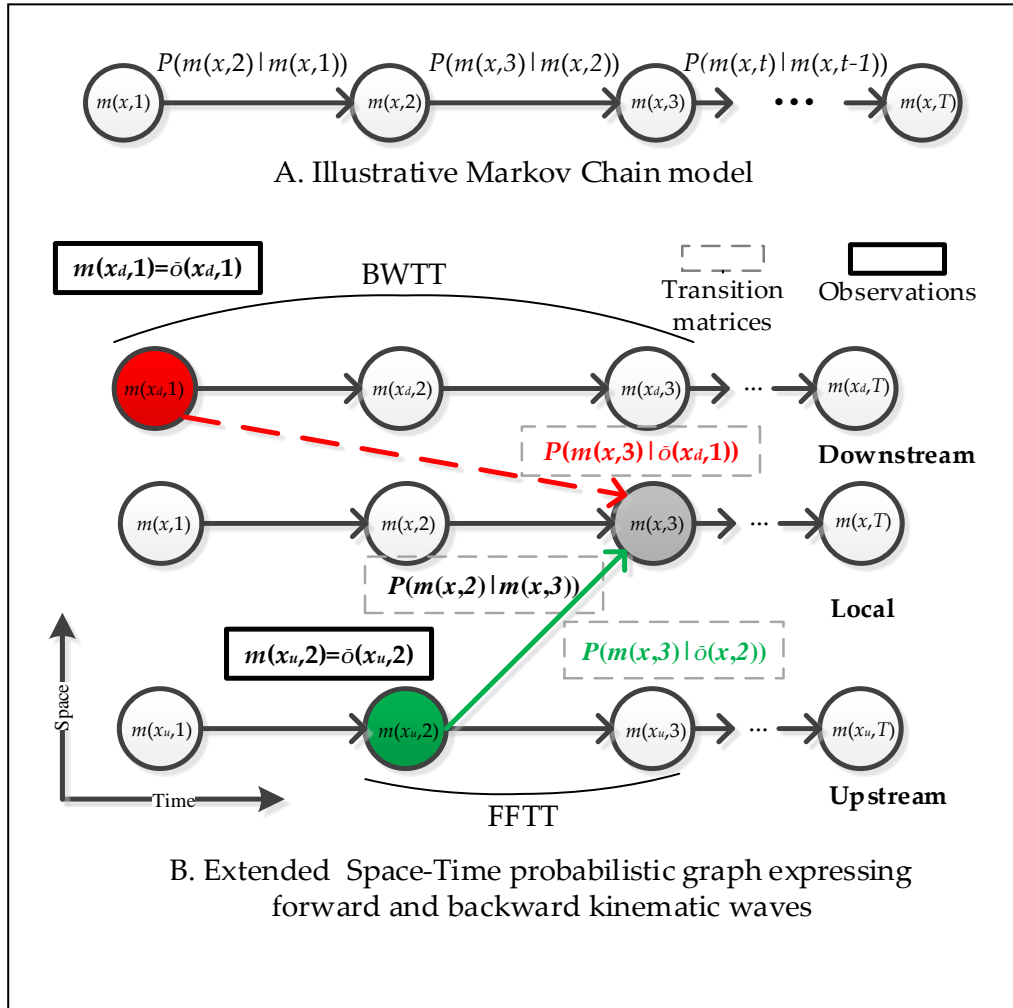


Figure 3-5 An Illustrative Example of STPG

- **Update the Prediction**

In this study, real-time data is introduced to update the regular pattern of traffic states (Module F in Figure 3-3). If the state $m_{x,t}$ is updated using observations from the upstream and downstream locations, the weight average model to combine Bayesian Classifier and the MC model will be applied to estimate $m_{x,t}$ for each $x \in N$ and $t = 1, 2, \dots, T$:

$$\mathbf{M2}: \operatorname{argmax}_{m_{x,t} \in \mathbf{M}} \{W_u \times P(m_{x,t} | \bar{o}_{x_u, t - FFTT(x_u, x)}) + W_d \times P(m_{x,t} | \bar{o}_{x_d, t - BWTT(x_d, x)}) + W \times P(m_{x,t} | m_{x, t-1}) P(m_{x,1}, m_{x,2}, \dots, m_{x, t-1})\} \quad (3-10)$$

W_u : Weight of the impact from upstream locations

W_d : Weight of the impact from downstream locations

W : Weight of the historical pattern (set to $W=1$)

The three conditional probabilities in Eq. (3.10) (M2) are shown in Figure 3-5 (B). In the basis of the Newell's method for the three-detector problem, the weights of the transition matrices in M2 can be determined (See Appendix for details). After the states at each vertex are estimated, the density, speed, and flow at the vertex (x, t) can be estimated using the centroids generated by the K-means clustering algorithm. It should be noted that, to avoid fluctuation of the estimates and prediction, any digital filter can be used for smoothing the data.

3.5. Summary

Traffic data collected from detectors can be plotted and calibrated on a fundamental diagram (FD). However, in order to analyze the traffic impacts of these data on a corridor, they must undergo a series of mathematical procedures. This chapter has provided the necessary framework for observed traffic to be used to predict and update traffic states at a location using kinematic waves from upstream and downstream locations. In the prediction stage, emission function K-clustering has been used to group flow-density pairs with similar characteristics and determine their state estimation. Markov Chain (MC) model and the probability graph (PG) have been used to capture the state dependences and transitions. PG has been extended to spatiotemporal probability graph (STPG) to infer the impacts of the kinematic waves in a corridor using Bayesian Classifier (BC) method. The updating stage included the application of weight average model to the combined MC and BC models for the updated state estimation at the current location.

CHAPTER 4

TRAVEL TIME DERIVATION FROM QUEUEING AND POLYNOMIAL MODELS

4.1. Introduction

Among the many other causes of congestion, a physical bottleneck is with capacity constraints considered in this research because it happens fairly regularly and results in the formation of a queue while other factors such as traffic incidents vary in occurrence and characteristics. The research report from FHWA (2005) estimates that 40 percent of all congestion nationwide can be attributed to road bottlenecks, as shown in the pie chart below.

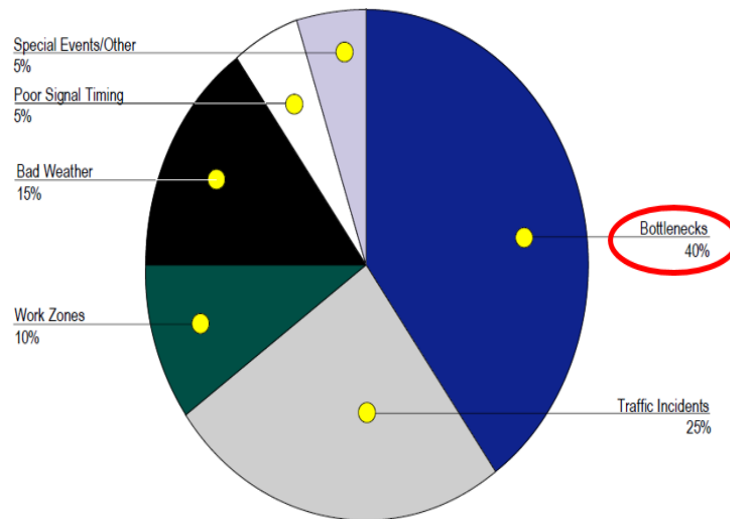


Figure 4-1 Common Causes of Congestion
Source:<http://www.ops.fhwa.dot.gov/aboutus/opstory.htm>

Chapter 4 aims to analyze the analytical computing procedures involved in the various factors involved in a queue caused by the existence of a bottleneck, ranging from congestion location and overall demand supply relationships.

Section 4.2 presents a method of identifying (1) spatial bottleneck locations based on integrated speed heat map and speed profile diagrams, and (2) the temporal congested period during the analysis horizon. In section 4.3, the cumulated vehicle arrival counts are integrated along the congested period to estimate the time-dependent queue length. Other queue characteristics, such as time-dependent queue waiting time and total waiting time, are also derived. Section 4.4 demonstrates that the fluid dynamic equation can be used to approximate the traffic queue length formation and dissipation (with physical queue length) since the traffic flow patterns can be viewed as similar to those of a fluid with specific characteristics. This section adopts and extends the fluid approximation approach by Newell (1993) to a spatially distributed queue model. It specifically discusses the selection and estimation of parameters of a polynomial equation that represents the complex spatial queue profile. Finally, Section 4.5 examines the derivation steps to convert the final mathematical expression to a BPR-like formula that computes the spatial queue-based transportation system performance measures. The flow chart in Figure 4-2 shows the descriptions and relationships of individual modules representing sections of Chapter 4.

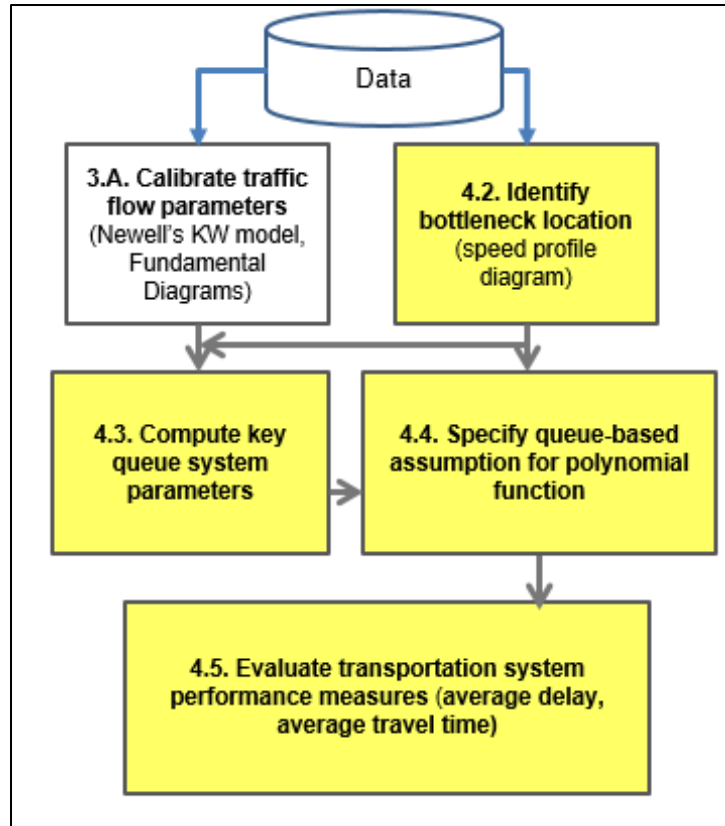


Figure 4-2 Module Descriptions and Representations of Sections from Chapter 4

The variables used in this chapter are summarized in Table 4-1 below.

Table 4.1 Variables and Their Definitions

| Variables | Description |
|------------------|--|
| v_f | Free-flow speed |
| v_c | Critical speed |
| t_0 | Start time of congestion period |
| t_1 | Time index with maximum inflow rate |
| t_2 | Time index with maximum queue length |
| t_3 | End time of congestion period |
| $\lambda(t)$ | Arrival rate function at time t |
| μ | Capacity (or discharge rate, assumed constant) |
| D | Total demand during congested period |
| P | Congestion period, $P=t_3-t_0$ |
| \bar{w} | Average delay during congested period |
| W | Total delay during congested period |
| $Q(t)$ | Queue length at time t |
| $A(t)$ | Cumulative arrival curve at time t |
| $D(t)$ | Cumulative departure curve at time t |
| ρ | Parameter for the quadratic form of inflow rates |
| t_t | Average travel time during congested period |

4.2. Bottleneck Identification Using Integrated Heat Map Space-Time Speed Profile

The cumulative traffic count at the shockwave boundary created by the downstream bottleneck has been described in section 3 of Chapter 3. This section presents the methods used to identify the downstream bottleneck based on heat map technique or space-time speed profile.

Figure 4-3 depicts a configuration of vehicles traveling on a roadway network link equipped with loop detector that experience a bottleneck at a downstream location and vehicle trajectories on a space-time diagram. The space-time vehicle trajectory domain is divided into two sub-areas by the shock wave boundary that represents the physical queue boundary caused by a bottleneck at a downstream location.

A typical vehicle trajectory, shown in green line, indicates a vehicle traveling the free-flow sub-area at the free-flow speed of v_f until it reaches the back of the queue caused by the downstream bottleneck. The vehicle then enters the queue in the congested sub-area and reduces its speed to the congested speed of v_c .

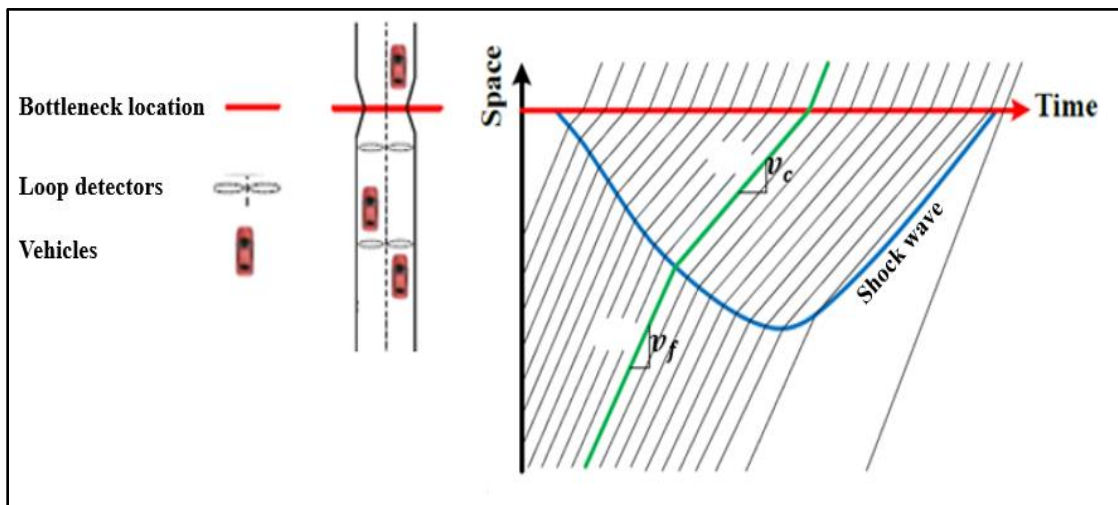


Figure 4-3 Illustration of a Roadway Configuration with Loop Detectors and Vehicle Trajectories on a Space-time Diagram and the Queue Extent Along a Single Bottleneck

It is clear from the figure that a bottleneck can be identified by analyzing speed data in a space-time plane. The heat map is a technique that can represent speed data values as different colors with color intensity varying with speed value magnitude. This technique can therefore be used to visually represent the change in speed data of a vehicle trajectory.

Figure 4-4 below clearly illustrates the presence of a bottleneck along a freeway corridor and the congested period.

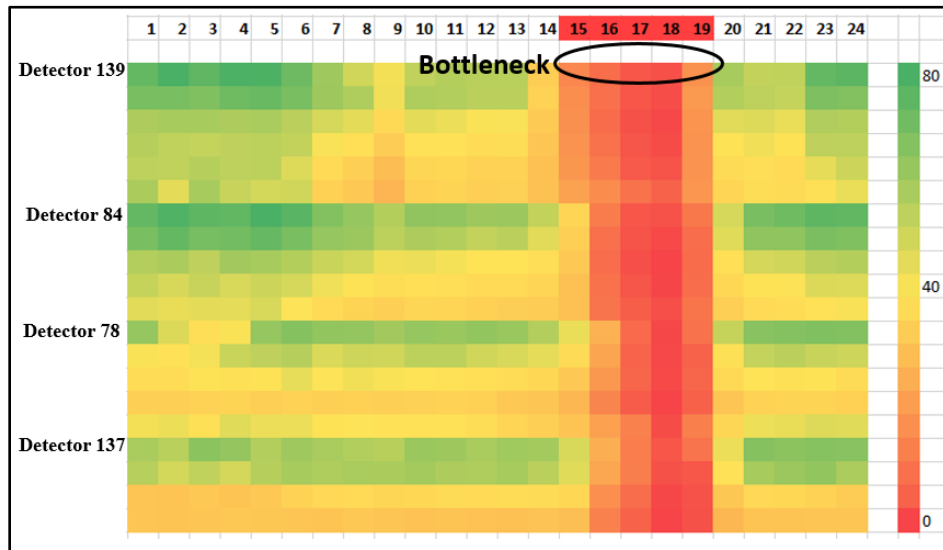


Figure 4-4 Bottleneck Location (from Speed Heat Map of a Freeway Corridor over One Day)

The bottleneck occurs at detector 137 from 3 PM to 7 PM where the speed is below 45. Any region with red color is in congested state. The bottleneck has, therefore, created a physical queue that extends from detector 137 (downstream) to detector 139 (upstream). A speed-time plot showing the same information is also plotted in Figure 4-5 below.

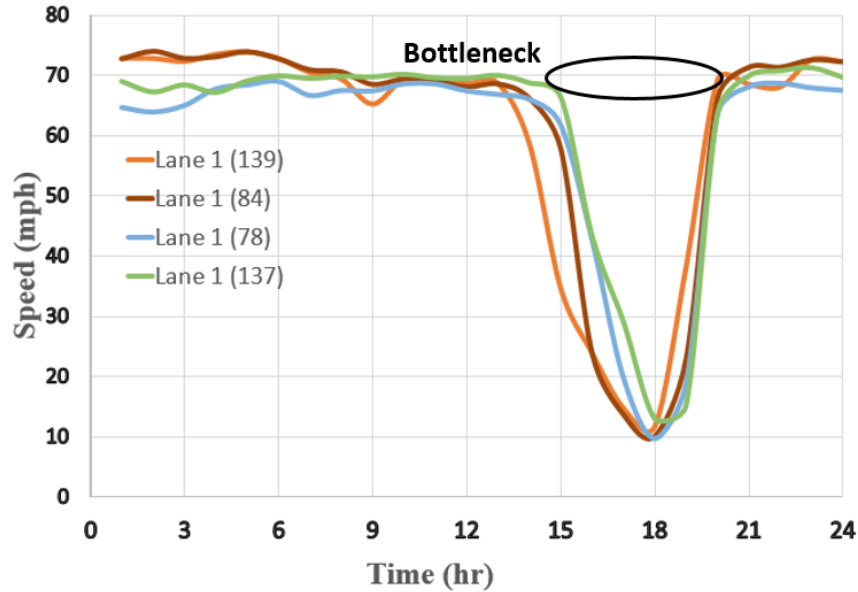


Figure 4-5 Bottleneck Location (from Speed Profile of a Freeway Corridor over One Day)

4.3. Computation of Key Queue System Parameters

(1) Traffic Demand During Congestion Period

The integrated heat map and speed profile technique can be used to visually show the location of the bottleneck and the beginning and the end of the congestion duration. An additional technique that uses critical density check can also be used. Once the congested period and the densities are identified, the cumulative vehicle counts within the congested period can be easily computed by using the formula:

$$N(t) = N(t - 1) + q(t) \quad \text{for } t_0 \leq t \leq t_3 \quad (4-1)$$

A typical curve for cumulative vehicle count, N , within congested period, P , is shown in Figure 4-6. For simplicity, no vehicle count is shown outside of the congested period.

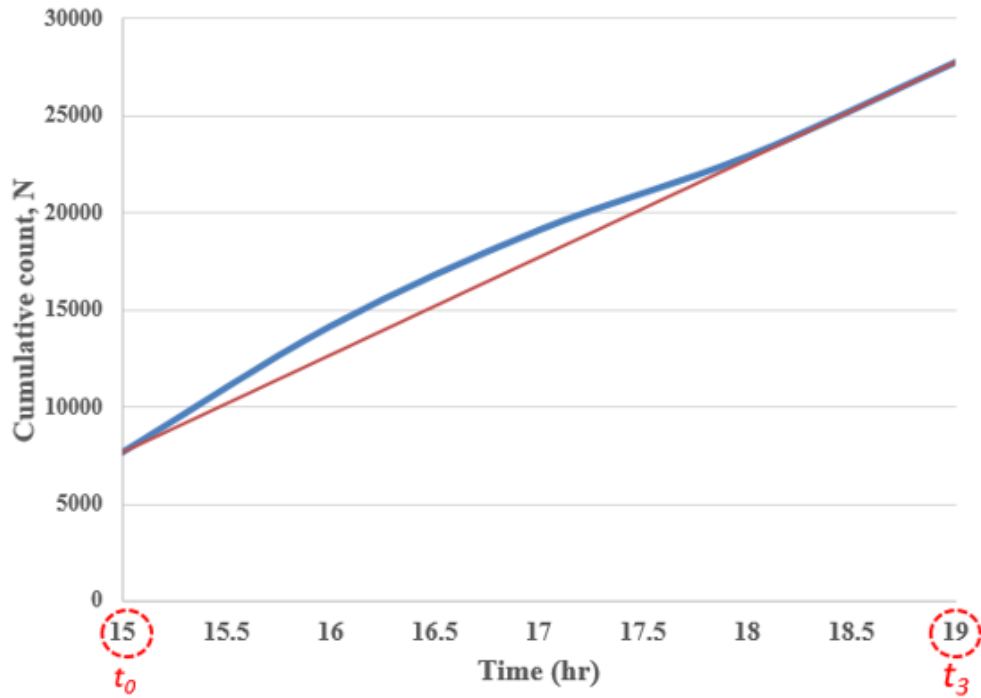


Figure 4-6 A Typical Cumulative Flow Curve (in Blue Line) Representing Cumulative Vehicle Count Within Congested Period

To derive the overall demand-supply analytical form, the total congested demand, D , during congested period, P , can be computed as the difference between the cumulative vehicle count at the end of congestion, t_3 , and the cumulative vehicle count at the beginning of congestion, t_0 , as

$$D = N(t_3) - N(t_0) \quad (4-2)$$

Accordingly, the assumed constant discharge rate, μ , is computed as the ratio of the total demand, D , and the congested period, P , as expressed in Equation 4.3 below. It is represented in Figure 4-6 by the red line beneath the blue cumulative curve. The red line is actually drawn tangent to the blue curve.

$$\mu = D/P \tag{4-3}$$

The cumulative flow curve, the discharge rate line, N , D , and P create the boundary conditions of a cumulative vehicle count process. These variables constitute the prerequisite variables for calibration of the spatial queue parameters.

(2) Cumulative Flow Curves for Total Demand and Assumed Constant Discharge Rates

Figure 4-7 indicates the total demand, D , from the cumulative curve, and the queue parameters that can be derived from the cumulative vehicle count parameters. Using the spatial queue theory terminology, the cumulative input and output vehicle curves are referred to as the cumulative arrival curve, $A(t)$, and the discharge rate line with the assumed constant slope μ is denoted as the cumulative departure curve, $D(t)$.

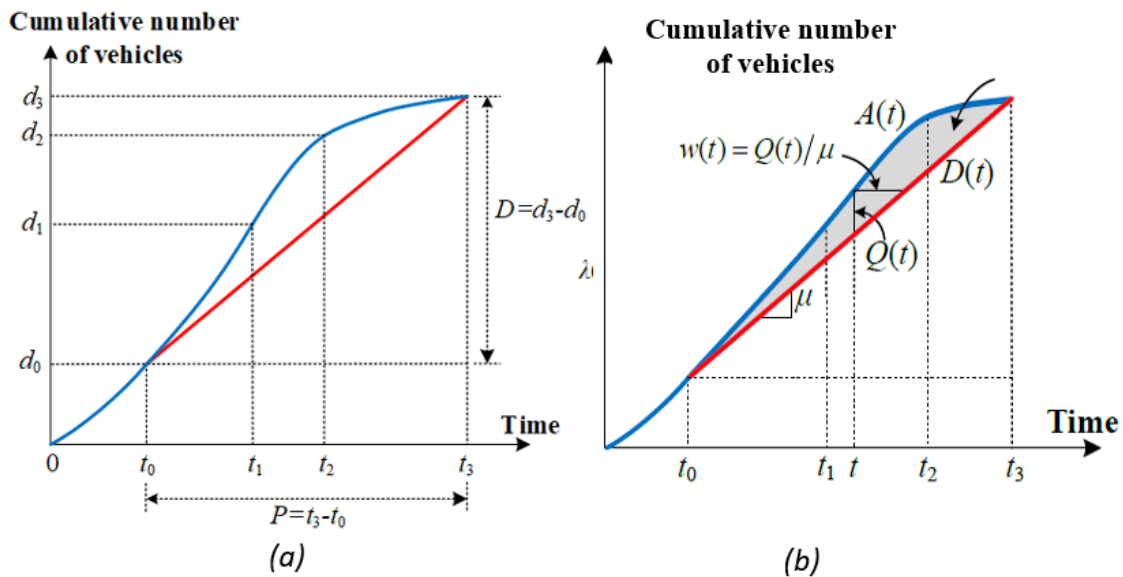


Figure 4-7 Illustration of Queue Parameters Within the Cumulative Curve Concept

The queue length at time t , $Q(t)$, in the congested period, P , is equal to the vertical difference between the cumulative arrival curve, $A(t)$, and the cumulative departure curve, $D(t)$. It can be computed as the difference between the cumulative vehicle arrival count, $N(t)$, and , $A(t)$, and the cumulative vehicle departure count, $N'(t)$, expressed as

$$Q(t) = N(t) - N'(t) \quad (4.4)$$

The waiting time at time t , $w(t)$, can easily be estimated as the ratio of the queue length and the constant slope μ , as

$$w(t) = Q(t)/\mu \quad (4-5)$$

The total waiting time in the queue, W , is the ratio of total queue length, Q , over the congested period, P , as

$$W = Q/P \quad (4.6)$$

These queue parameters can also be expressed mathematically using the cumulative arrival curve $A(t)$ and the cumulative departure curve $D(t)$. The tilted area inside $A(t)$ and $D(t)$ (Figure 4-8 (a)) can be aligned horizontally, as shown in Figure 4-8 (b).

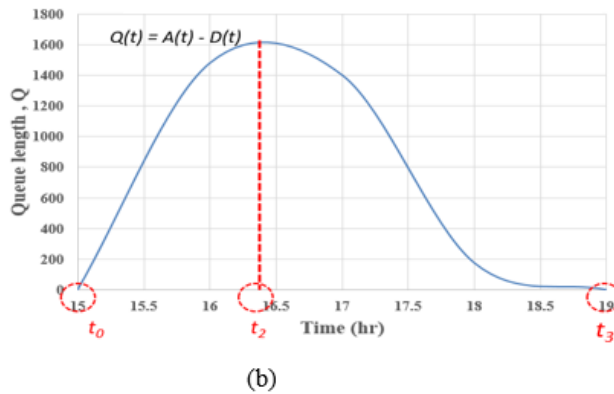
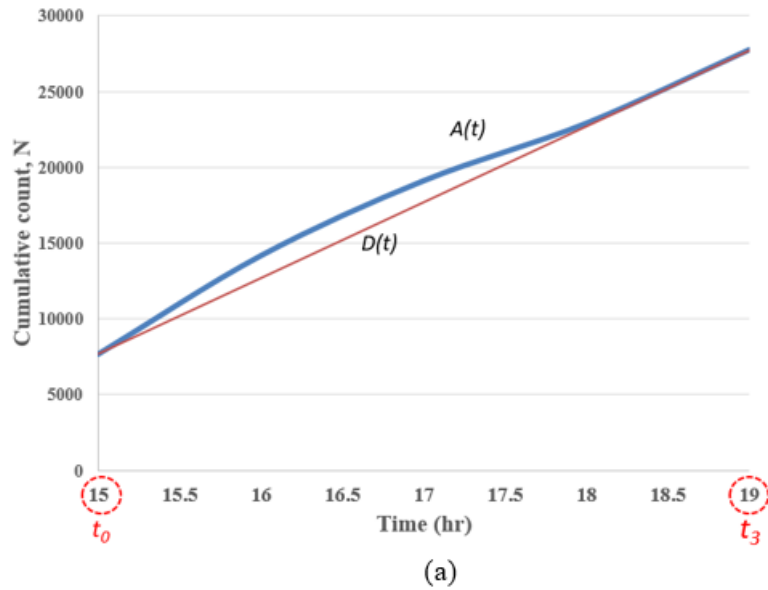


Figure 4-8 Queue Length Curve (b) Derived from Cumulative Curve (a). The Maximum Queue Length Occurs at Time t_2

Figure 4-8 clearly shows that the queue length evolution curve, $Q(t)$, follows a quadratic distribution. There are a few important boundary conditions to be highlighted along the time horizon. The queue formation process starts at time t_0 and grows exponentially to reach the maximum at time t_2 . Then the queue dissipation process follows from time t_2 to time t_3 where the queue decreases gradually until it disappears at time t_3 .

4.4. Key Assumption of Quadratic Polynomial Function Using Queue Parameters

The key assumption is that the queue length evolution pattern can be reasonably approximated by the general polynomial function shown in Figure 4-9 below.

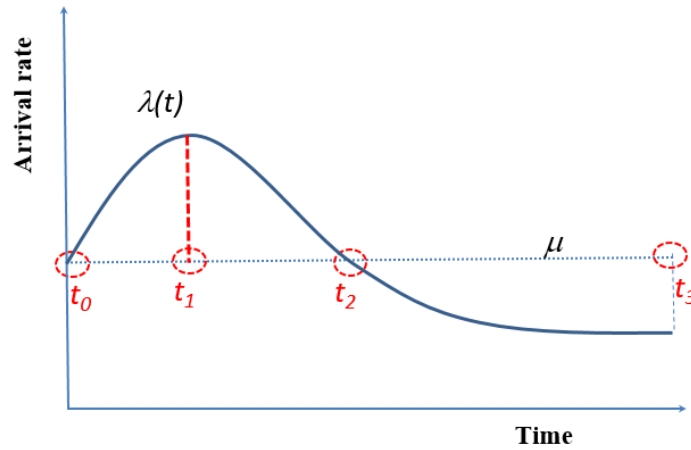


Figure 4-9 Quadratic Polynomial Approximation of Queue Length

The queue length at time t , $Q(t)$, corresponds to the area under the curve $\lambda(t)$. The queue length starts to build up as the area under the curve $\lambda(t)$ increases gradually from time t_0 and the queue reaches its maximum length, $Q(t_2)$, at time t_2 when $\lambda(t)=\mu$. The queue then starts to decrease until time t_3 when the area between $\lambda(t)$ and μ from time t_2 to time t_3 is equal to the area from time t_0 to time t_2 .

Mathematically, the queue length at time t can be expressed as

$$Q(t) = A(t) - D(t) = \int_{t_0}^t [\lambda(t) - \mu] dt \quad (4.7)$$

It is also noted that, various scholars such as William Vickrey, Arnott, De Palma, Lindsey, Kenneth Small have used constant or linear arrival rates in the classical bottleneck model and a recent survey paper on the bottleneck model is offered by Li, Huang and Yang (2020).

Newell (1982) assumes that virtual arrival flow $\lambda(t)$ can be approximated by a quadratic function as

$$\lambda(t) = \lambda(t_1) + \lambda'(t_1)(t - t_1) + \frac{1}{2}\lambda''(t_1)(t - t_1)^2 \quad (4.8)$$

The quadratic polynomial curve presents some important characteristics that can reduce its expression and also the expressions of its two roots, t_0 and t_2 . If a corridor is covered with detectors, then the virtual arrival rate $\lambda(t)$ can be directly estimated based on the proposed three-detector model presented in Chapter 3. If sensor data are only available for individual locations that cover part of the congested corridor, observed speed or density from the loop detector needs to be used to first estimate the waiting time/queue length along the corridor. The quality of waiting time estimate can be improved if third party data providers such as HERE or INRIX also have speed measures on the same segment, but the actual end-to-end travel time and queue length should be observed from very detailed trajectory data. At the second step of TSE in this chapter, we will use the estimated waiting time or queue length to further estimate the (unobserved virtual arrival rates $\lambda(t)$), while the flow rates at a single location are used directly to derive the constant departure rate μ . It is important to recognize the complexity of the traffic state estimation for the proposed analytical formula, as only a subset of queue system parameters are observable under the current sensor technology. On the other hand, this analysis also indicates our proposed parsimonious model with has its own advantages in TSE compared to numerically complex models with finite difference form.

First, the inflow rate is at its maximum at time t_1 . Hence, $\lambda'(t_1) = 0$.

Second, the concave form of the polynomial curve means that the inflow rate will start to decrease after time t_1 . Hence, the shape parameter $\rho = -\frac{1}{2}\lambda''(t_1)$. Eq. (4.8) would then be reduced to

$$\lambda(t) = \lambda(t_1) - \rho(t - t_1)^2 \quad (4-9)$$

Third, the inflow rate and the discharge rate are equal at time t_0 and time t_2 , i.e.,

$$\lambda(t_0) = \mu = \lambda(t_1) - \rho(t_1 - t_0)^2 \quad (4-10)$$

$$\lambda(t_2) = \mu = \lambda(t_1) - \rho(t_2 - t_1)^2 \quad (4-11)$$

The two roots t_0 and t_2 can then be expressed as follows:

$$t_0 = t_1 - \left[\frac{\lambda(t_1) - \mu}{\rho} \right]^{\frac{1}{2}} \quad (4-12)$$

$$t_2 = t_1 + \left[\frac{\lambda(t_1) - \mu}{\rho} \right]^{\frac{1}{2}} \quad (4-13)$$

Since the queue length, $Q(t)$, is zero at these two roots t_0 and t_2 , the expression $\lambda(t) - \mu$ can be written in a factored form that includes both roots, as follows:

$$\lambda(t) - \mu = \rho(t - t_0)(t_2 - t) \quad (4-14)$$

After substituting Eq. (4-14) into Eq. (4-7), $Q(t)$ can be expressed in terms of t_0 , t_2 and ρ

$$Q(t) = \int_{t_0}^t [\lambda(t) - \mu] dt = \int_{t_0}^t [\rho(t - t_0)(t_2 - t)] dt \quad (4-15)$$

Setting $u = t - t_0$ into the equation yields the general expression of $Q(t)$ as

$$\begin{aligned}
 Q(t) &= \int_{t_0}^t [\rho(t - t_0)(t_2 - t)] dt \\
 &= \int_0^{t-t_0} [\rho u(t_2 - t_0 - u)] du \\
 &= \rho \left[-\frac{1}{3}u^3 + \frac{1}{2}(t_2 - t_0)u^2 \right] \Big|_{u=0}^{u=t-t_0} \\
 Q(t) &= \rho(t - t_0)^2 \left[\frac{t_2 - t_0}{2} - \frac{t - t_0}{3} \right] \tag{4-16}
 \end{aligned}$$

When the queue reaches its maximum length at time t_2 , the expression becomes

$$Q(t_2) = \frac{\rho}{6}(t_2 - t_0)^3 \tag{4-17}$$

The shape parameter, ρ , can then be derived as

$$\rho = \frac{6Q(t_2)}{(t_2 - t_0)^3} \tag{4-18}$$

Since the queue dissipates at time t_3 , i.e., $Q(t_3) = 0$, t_3 can be expressed as:

$$t_3 = t_0 + \frac{3}{2}(t_2 - t_0) \tag{4-19}$$

Eq. (4-19) can be rearranged as follows

$$\frac{1}{3}(t_3 - t_0) = \frac{1}{2}(t_2 - t_0) \tag{4-20}$$

Substituting Eq. (4-20) into Eq. (4-16) further reduces the queue length to

$$\begin{aligned}
 Q(t) &= \rho(t - t_0)^2 \left[\frac{t_3 - t_0}{3} - \frac{t - t_0}{3} \right] \\
 Q(t) &= \frac{\rho}{3}(t - t_0)^2(t_3 - t) \tag{4-21}
 \end{aligned}$$

4.5 Examining Queue-Based Average Delay and Average Travel Time Functions During Congestion Period

The waiting time, $w(t)$, can be computed as

$$w(t) = Q(t)/\mu = \frac{\rho}{3\mu} (t - t_0)^2 (t_3 - t) \quad (4-22)$$

The total delay between time t_0 and t_3 , W , can be calculated by integration of Eq. (4-21) as follows:

$$W = \int_{t_0}^{t_3} Q(t) dt$$

$$W = \int_{t_0}^{t_3} \left[\frac{\rho}{3} (t - t_0)^2 (t_3 - t) \right] dt$$

Setting $u = t - t_0$, the above equation becomes

$$W = \frac{\rho}{3} \int_0^{t_3-t_0} u^2 (t_3 - t_0 - u) du$$

$$= \frac{\rho}{3} \left[\frac{t_3 - t_0}{3} u^3 - \frac{u^4}{4} \right] \Bigg|_{u=0}^{u=t_3-t_0}$$

$$W = \frac{\rho}{36} (t_3 - t_0)^4 \quad (4-23)$$

Given the total delay, W , and the total congested demand, D , the average delay during the congestion period t_0 to t_3 can be computed as follows:

$$\bar{w} = \frac{W}{D} = \frac{\rho}{36} \cdot \frac{(t_3-t_0)^4}{D} = \frac{\rho}{36} \cdot \frac{(P)^4}{D} \quad (4-24)$$

The discharge rate (or capacity) can be calculated as the ratio of the total congested demand, D , over the congested period, P , as

$$\mu = \frac{D}{P} \quad (4-25)$$

After substitution of Eq. (4-24) into Eq. (4-23), the average delay can now be expressed in terms of congested demand and capacity, as

$$\bar{w} = \frac{\rho}{36\mu} \cdot \left(\frac{D}{\mu}\right)^3 \quad (4-26)$$

By definition, the average travel time is equal to the sum of free-flow travel time and the average delay and it is expressed as

$$t_t = t_f + \bar{w} \quad (4-27)$$

After substitution and rearranging some terms, the equation becomes

$$t_t = t_f + \frac{\rho}{36\mu} \cdot \left(\frac{D}{\mu}\right)^3 = t_f \cdot \left[1 + \frac{\rho}{36\mu t_f} \cdot \left(\frac{D}{\mu}\right)^3\right] \quad (4-28)$$

As a conclusion, Eq. (4-27) is derived from a quadratic polynomial equation and estimates the average travel time based only on queue parameters. Most importantly, it is similar to BPR function $t_t = t_f \cdot \left[1 + \alpha \cdot \left(\frac{V}{C}\right)^\beta\right]$ where

$$\alpha = \frac{\rho}{36\mu t_f}, V = D, C = \mu, \text{ and } \beta = 3$$

The proposed average travel time formula has possibilities of being used in the trip assignment step of a travel demand model. It satisfies the necessary requirements of a volume-delay function. The most important condition is that the function must be monotonically increasing for the highway assignment to converge to a unique solution.

4.6 Summary

This chapter analyzes the congestion caused by bottleneck conditions and suggests a few methods using integrated heatmap and space-time speed diagram to visually identify the bottleneck and the critical density to mark the congested data values. Once the congested period and data identify, the cumulative vehicle count method has been used to develop the cumulative count curve over the congested period, and to estimate the congested demand and the discharge rate. Using the area under the cumulative curve and the discharge rate line, the queue variables such as queue length, waiting time, and total delay, have been derived. Since the queue length distribution can be approximated by a set of polynomial equations, a quadratic function has been selected as a representative illustration to further analyze the queue characteristics.

By extending Newell's approach and the boundary conditions from the fluid based point queue theory, the quadratic function is used to approximate incoming flow rates. Further, real-world flow parameters are used to establish some relationships or correspondences between the root solutions of the quadratic function and the queue length variables. By substituting the demand and the discharge rate from the cumulative curve to the processed quadratic function, this chapter has examined the average delay estimation and the average travel time function development. The proposed point-queue based travel time function satisfies major requirements to be used as a volume-delay function in the trip assignment stage of a travel demand model to estimate the travel time based solely on congested traffic data.

CHAPTER 5

EXPERIMENTS

5.1. Introduction

Traffic data are collected for several purposes and this chapter will focus on how to use different sources of measurements to study how transportation system performs. In urban areas in general and in central business district (CBD) in particular, where congestion is a major concern, loop detectors are located on major freeways to collect vehicle counts and speeds at time interval of 5 minutes or less. These data, that are collected all year round by state transportation agencies, contain important traffic information that need to be analyzed to understand the impacts of congestion and develop mitigation measures and plans. Finding a simple, easy, and direct method to interpret these big data to answer questions on congestion such as the formation, duration, intensity, and extend of the traffic queue, becomes a theoretically complex and practically important challenge.

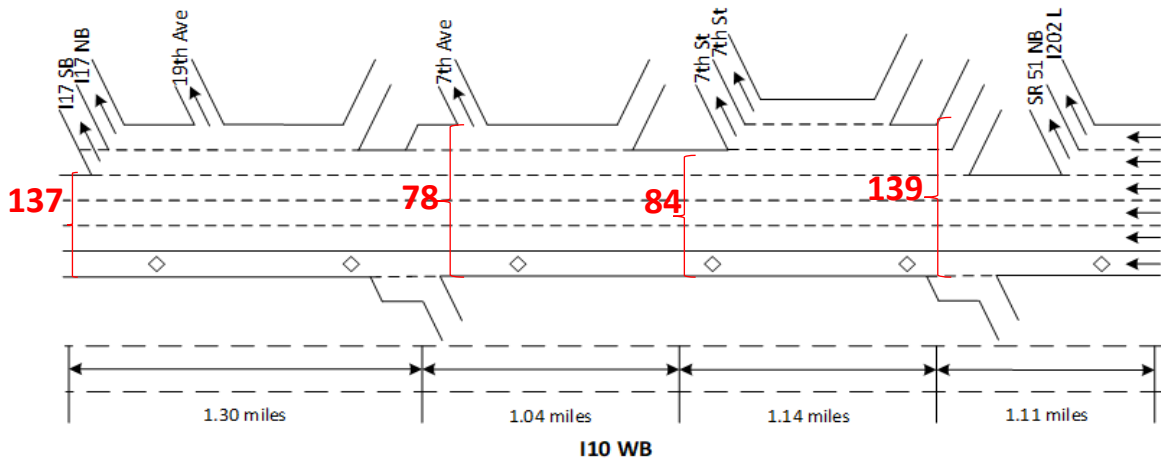
In this data analysis process, a visualization approach will be used to detect traffic patterns and characterize such data problems as outliers or missing data. Since traffic data can be saved in Excel spreadsheet, they can be transformed into a bar graph, pie chart, or table to create a data visualization. On the other hand, considering the traffic congestion characteristics, the most effective visualization method tends to be the heat map based on a space-time modeling approach. As it will be demonstrated in this chapter, the heat map has been very effective in quality control of data.

This section presents a freeway corridor equipped with loop detectors that continuously collect traffic volume and speed data that can be used in research studies such as traffic estimation and travel time estimation.

Figure 5-1 illustrates the detector numbers and locations. The freeway corridor is a 4.59-mile section on interstate 10 (I-10) with a combination of ramps (both entrance and exit), high-occupancy vehicle (HOV) lanes, and general purpose (GP) lanes located in Phoenix, Arizona. In this simplified case study, we only consider the HOV and GP lanes at location 137, 84, 78 and 139 and neglect the impact of ramps. The loop detectors, installed by the Arizona Department of Transportation (ADOT) in this downtown corridor, recorded both traffic counts ($\bar{q}(x, t)$) and speeds ($\bar{v}(x, t)$) every five minutes, each week day and weekend from January to December 2016.



(a)



(b)

Figure 5-1 Freeway Corridor Lane Configuration, Loop Detector Identifications and Locations, and Traffic Direction

Information on loop detector identification numbers and locations, types of traffic data collected, and traffic data collection year, months, and time interval are summarized in Table 5.1 and Table 5-2.

Table 5-1 Summary of Traffic Detector Characteristics and Traffic Data Collected and Time Interval Period

| | |
|--------------------------------|--|
| Detector | Description |
| Loop detector IDs | 78, 84, 137, 139 |
| Locations | I-10 freeway corridor, Westbound direction |
| Traffic data collected | Speed (mph) and volume (vph) in 5 minutes |
| Traffic data collection | Year: 2016 |

Table 5-2 Freeway Segment Lane Configuration

| Order | 4 | 3 | 2 | 1 |
|--------------------|------------|-------------------------|------------------|-------------------|
| Detector ID | 137 | 78 | 84 | 139 |
| Records | 1449 | 2897 | 2173 | 2346 |
| Length | 1.3 | 1.04 | 1.14 | 1.11 |
| Ramp | - | entr from 3rd ave hov | - | - |
| Ramp | - | entr from 7th ave lane1 | - | - |
| Ramp | - | entr from 7th ave lane2 | entr from 7th st | entr from 16th st |
| HOV | Yes | Yes | Yes | Yes |
| Lane1 | Yes | Yes | Yes | Yes |
| Lane2 | Yes | Yes | Yes | Yes |
| Lane3 | Yes | Yes | Yes | Yes |
| Lane4 | No* | Yes | Yes | Yes |
| Lane5 | No* | | | Yes |
| * = Lane drop | | | | |

5.2. Raw Data Description and Data Processing

In practice, vehicle count and speed data are not typically recorded in one single file system. Figure 5-2 and Figure 5-3 show the file format of the vehicle count data and speed data, respectively, collected every 5-minutes by the loop detectors. Every row in the count data file includes every day of the year 2016 with the 5 minute interval vehicle counts entered in columns from 00:00 until 23:55 for every lane of every detector in a typical freeway corridor, as shown in Figure 5-2.

| | A | B | C | D | E | F | G | H | I | J | K | L | M | N | |
|----|---------|----------|----------|-----------------------|-------|-------|-------|-------|-------|-------|--------------------------|--------|-----------|----------|------|
| 1 | | | | | 1 | 2 | 3 | 4 | 5 | 6 | 7 | 8 | 9 | 10 | |
| 2 | det_num | date | sum_type | lane_descr | H0000 | H0005 | H0010 | H0015 | H0020 | H0025 | H0030 | H0035 | H0040 | H0045 | |
| 3 | 78 | 1/1/2016 | vol | entr from 3rd ave hov | 1 | 0 | 4 | 6 | 0 | 2 | 6 | 3 | 0 | 3 | |
| 4 | 78 | 1/2/2016 | vol | entr from 3rd ave hov | 3 | 1 | 6 | 1 | 3 | 6 | 5 | 4 | 2 | 2 | |
| 5 | 78 | 1/3/2016 | vol | entr from 3rd ave hov | 11 | 11 | 11 | 4 | 7 | 7 | 6 | 4 | 5 | 6 | |
| 6 | 78 | | JY | JZ | KA | KB | KC | KD | KE | KF | KG | KH | KI | KJ | KK |
| 7 | 78 | 1 | 281 | 282 | 283 | 284 | 285 | 286 | 287 | 288 | | | | | |
| 8 | 78 | 2 | H2320 | H2325 | H2330 | H2335 | H2340 | H2345 | H2350 | H2355 | location | route | direction | milepost | year |
| 9 | 78 | 3 | 2 | 1 | 3 | 5 | 1 | 1 | 0 | 1 | I-10__WB 144.641 7TH AVE | I-10__ | WB | 144.641 | 2016 |
| 10 | 78 | 4 | 5 | 3 | 0 | 8 | 3 | 4 | 10 | 7 | I-10__WB 144.641 7TH AVE | I-10__ | WB | 144.641 | 2016 |
| 11 | 78 | 5 | 2 | 1 | 0 | 2 | 0 | 1 | 0 | 0 | I-10__WB 144.641 7TH AVE | I-10__ | WB | 144.641 | 2016 |
| 12 | 78 | 6 | 2 | 2 | 1 | 1 | 5 | 3 | 1 | 0 | I-10__WB 144.641 7TH AVE | I-10__ | WB | 144.641 | 2016 |
| 13 | 78 | 7 | 1 | 0 | 4 | 3 | 3 | 1 | 1 | 0 | I-10__WB 144.641 7TH AVE | I-10__ | WB | 144.641 | 2016 |
| 14 | 78 | 8 | 1 | 3 | 7 | 4 | 3 | 1 | 3 | 1 | I-10__WB 144.641 7TH AVE | I-10__ | WB | 144.641 | 2016 |
| 15 | 78 | 9 | 3 | 1 | 3 | 2 | 4 | 1 | 2 | 5 | I-10__WB 144.641 7TH AVE | I-10__ | WB | 144.641 | 2016 |
| | | 10 | 8 | 3 | 9 | 4 | 3 | 4 | 3 | 4 | I-10__WB 144.641 7TH AVE | I-10__ | WB | 144.641 | 2016 |
| | | 11 | 6 | 1 | 5 | 1 | 5 | 5 | 2 | 6 | I-10__WB 144.641 7TH AVE | I-10__ | WB | 144.641 | 2016 |
| | | 12 | 3 | 2 | 4 | 5 | 1 | 1 | 1 | 4 | I-10__WB 144.641 7TH AVE | I-10__ | WB | 144.641 | 2016 |
| | | 13 | 2 | 5 | 2 | 4 | 3 | 4 | 1 | 2 | I-10__WB 144.641 7TH AVE | I-10__ | WB | 144.641 | 2016 |
| | | 14 | 1 | 0 | 4 | 0 | 1 | 8 | 3 | 1 | I-10__WB 144.641 7TH AVE | I-10__ | WB | 144.641 | 2016 |
| | | 15 | 1 | 2 | 1 | 1 | 1 | 1 | 0 | 1 | I-10__WB 144.641 7TH AVE | I-10__ | WB | 144.641 | 2016 |

Figure 5-2 Raw Data File with Volume Data from All Detectors Collected Every 5 Minute Interval

Every row in the speed data file includes every day of the year 2016 with the 5 minute interval vehicle speed data entered in columns from 00:00 until 23:55 for every lane of every detector in a typical freeway corridor, as depicted in Figure 5-3.

| | A | B | C | D | E | F | G | H | I | J | K | L | M | N | | | | |
|----|---------|----------|----------|-----------|-------|-------|-------|-------|-------|-------|-------|-------|-------|----------|--------|-----------|----------|------|
| 1 | | | | | 1 | 2 | 3 | 4 | 5 | 6 | 7 | 8 | 9 | 10 | | | | |
| 2 | det_num | date | sum_type | lane_desc | H0000 | H0005 | H0010 | H0015 | H0020 | H0025 | H0030 | H0035 | H0040 | H0045 | | | | |
| 3 | 78 | 1/1/2016 | mph | entr from | 69 | 0 | 74 | 76 | 0 | 74 | 76 | 76 | 0 | 74 | | | | |
| 4 | 78 | 1/2/2016 | mph | entr from | 70 | 73 | 72 | 73 | 76 | 76 | 75 | 73 | 71 | 71 | | | | |
| 5 | 78 | 1/3/2016 | mph | entr from | 75 | 75 | 73 | 67 | 66 | 71 | 75 | 75 | 72 | 74 | | | | |
| 6 | 78 | JV | JW | JX | JY | JZ | KA | KB | KC | KD | KE | KE | KG | KH | KI | KJ | KK | |
| 7 | 78 | 1 | 278 | 279 | 280 | 281 | 282 | 283 | 284 | 285 | 286 | 287 | 288 | | | | | |
| 8 | 78 | 2 | H2305 | H2310 | H2315 | H2320 | H2325 | H2330 | H2335 | H2340 | H2345 | H2350 | H2355 | location | route | direction | milepost | year |
| 9 | 78 | 3 | 76 | 74 | 76 | 76 | 76 | 76 | 76 | 73 | 76 | 0 | 69 | I-10 | W/I-10 | WB | 144.641 | 2016 |
| 10 | 78 | 4 | 74 | 74 | 73 | 75 | 75 | 0 | 73 | 76 | 74 | 73 | 74 | I-10 | W/I-10 | WB | 144.641 | 2016 |
| 11 | 78 | 5 | 70 | 69 | 72 | 76 | 76 | 0 | 76 | 0 | 76 | 0 | 0 | I-10 | W/I-10 | WB | 144.641 | 2016 |
| 12 | 78 | 6 | 75 | 73 | 73 | 74 | 70 | 66 | 69 | 71 | 70 | 73 | 0 | I-10 | W/I-10 | WB | 144.641 | 2016 |
| 13 | 78 | 7 | 75 | 0 | 0 | 69 | 0 | 66 | 72 | 76 | 76 | 73 | 0 | I-10 | W/I-10 | WB | 144.641 | 2016 |
| 14 | 78 | 8 | 75 | 74 | 70 | 69 | 67 | 74 | 71 | 68 | 73 | 68 | 69 | I-10 | W/I-10 | WB | 144.641 | 2016 |
| 15 | 78 | 9 | 74 | 76 | 71 | 74 | 76 | 76 | 76 | 76 | 76 | 76 | 74 | I-10 | W/I-10 | WB | 144.641 | 2016 |
| | | 10 | 71 | 73 | 73 | 76 | 73 | 70 | 74 | 76 | 74 | 68 | 69 | I-10 | W/I-10 | WB | 144.641 | 2016 |
| | | 11 | 75 | 73 | 76 | 76 | 76 | 72 | 73 | 71 | 75 | 76 | 76 | I-10 | W/I-10 | WB | 144.641 | 2016 |
| | | 12 | 76 | 76 | 76 | 75 | 74 | 75 | 75 | 73 | 76 | 69 | 69 | I-10 | W/I-10 | WB | 144.641 | 2016 |
| | | 13 | 75 | 73 | 76 | 76 | 76 | 76 | 73 | 74 | 76 | 76 | 73 | I-10 | W/I-10 | WB | 144.641 | 2016 |
| | | 14 | 70 | 73 | 74 | 73 | 0 | 73 | 0 | 73 | 72 | 72 | 73 | I-10 | W/I-10 | WB | 144.641 | 2016 |
| | | 15 | 75 | 75 | 75 | 73 | 73 | 73 | 76 | 0 | 73 | 0 | 69 | I-10 | W/I-10 | WB | 144.641 | 2016 |

Figure 5-3 Traffic Data File with Speed Data from All Detectors Collected Every 5 Minute Interval

For the purpose of the steady-state analysis, these 5-minute interval data need to be extended to 1-hour interval data. This condition requires that the volume data be aggregated and the speed data be averaged. Figure 5-4 further shows an example of volume data aggregated to 1-hour interval.

| | A | B | C | D | E | F | G | H | I | J | K | L | M | | | | | |
|----|---------|----------|----------|-----------------------|-------|-------|-------|-------|-------|-------|-------|-------|-------|----------|-------|-----------|----------|------|
| 1 | | | | | 1 | 2 | 3 | 4 | 5 | 6 | 7 | 8 | 9 | | | | | |
| 2 | det_num | date | sum_type | lane_descr | H0100 | H0200 | H0300 | H0400 | H0500 | H0600 | H070 | H080 | H090 | | | | | |
| 3 | 78 | 1/1/2015 | vol | entr from 3rd ave hov | 78 | 22 | 23 | 10 | 16 | 7 | 14 | 22 | 28 | | | | | |
| 4 | 78 | 1/2/2015 | vol | entr from 3rd ave hov | 41 | 18 | 17 | 15 | 7 | 6 | 20 | 20 | 20 | | | | | |
| 5 | 78 | 1/3/2015 | vol | entr from 3rd ave hov | 107 | 117 | 39 | 21 | 12 | 5 | 13 | 17 | 26 | | | | | |
| 6 | 78 | R | S | T | U | V | W | X | Y | Z | AA | AB | AC | AD | AE | AF | AG | |
| 7 | 78 | 1 | 14 | 15 | 16 | 17 | 18 | 19 | 20 | 21 | 22 | 23 | 24 | | | | | |
| 8 | 78 | 2 | H1400 | H1500 | H1600 | H1700 | H1800 | H1900 | H2000 | H2100 | H2200 | H2300 | H2400 | location | route | direction | milepost | year |
| 9 | 78 | 3 | 39 | 64 | 52 | 41 | 58 | 47 | 43 | 58 | 47 | 74 | 32 | 1-10 | W1-10 | WB | 144.641 | 2016 |
| 10 | 78 | 4 | 72 | 81 | 81 | 71 | 57 | 44 | 54 | 47 | 61 | 83 | 60 | 1-10 | W1-10 | WB | 144.641 | 2016 |
| 11 | 78 | 5 | 67 | 70 | 73 | 60 | 72 | 60 | 47 | 35 | 35 | 25 | 16 | 1-10 | W1-10 | WB | 144.641 | 2016 |
| 12 | 78 | 6 | 110 | 187 | 207 | 247 | 172 | 63 | 47 | 38 | 42 | 34 | 28 | 1-10 | W1-10 | WB | 144.641 | 2016 |
| 13 | 78 | 7 | 154 | 195 | 166 | 196 | 191 | 70 | 93 | 73 | 45 | 49 | 24 | 1-10 | W1-10 | WB | 144.641 | 2016 |
| 14 | 78 | 8 | 176 | 241 | 233 | 211 | 222 | 97 | 89 | 74 | 114 | 62 | 38 | 1-10 | W1-10 | WB | 144.641 | 2016 |
| 15 | 78 | 9 | 133 | 237 | 240 | 268 | 268 | 88 | 112 | 62 | 64 | 52 | 35 | 1-10 | W1-10 | WB | 144.641 | 2016 |
| | 78 | 10 | 176 | 267 | 231 | 223 | 207 | 103 | 91 | 97 | 94 | 149 | 77 | 1-10 | W1-10 | WB | 144.641 | 2016 |
| | | 11 | 93 | 121 | 119 | 111 | 93 | 62 | 69 | 71 | 90 | 94 | 51 | 1-10 | W1-10 | WB | 144.641 | 2016 |
| | | 12 | 70 | 88 | 91 | 110 | 75 | 58 | 72 | 58 | 63 | 50 | 29 | 1-10 | W1-10 | WB | 144.641 | 2016 |
| | | 13 | 167 | 142 | 65 | 252 | 207 | 116 | 106 | 67 | 43 | 31 | 36 | 1-10 | W1-10 | WB | 144.641 | 2016 |
| | | 14 | 147 | 253 | 218 | 242 | 225 | 113 | 105 | 85 | 61 | 35 | 31 | 1-10 | W1-10 | WB | 144.641 | 2016 |
| | | 15 | 172 | 203 | 209 | 253 | 216 | 116 | 121 | 109 | 110 | 54 | 32 | 1-10 | W1-10 | WB | 144.641 | 2016 |

Figure 5-4 Traffic Data File with Volume Data Aggregated to 1 Hour Interval

Figure 5-5 shows an example of speed data averaged over 1-hour interval.

| | A | B | C | D | E | F | G | H | I | J | K | L | M | | | | | |
|----|---------|----------|----------|-----------------------|-------|-------|-------|-------|-------|-------|-------|-------|-------|----------|--------|-----------|----------|------|
| 1 | | | | | 1 | 2 | 3 | 4 | 5 | 6 | 7 | 8 | 9 | | | | | |
| 2 | det_num | date | sum_type | lane_descr | H0100 | H0200 | H0300 | H0400 | H0500 | H0600 | H070 | H080 | H090 | | | | | |
| 3 | 78 | 1/1/2016 | mph | entr from 3rd ave hov | 56 | 67 | 54 | 44 | 49 | 36 | 46 | 58 | 62 | | | | | |
| 4 | 78 | 1/2/2016 | mph | entr from 3rd ave hov | 73 | 42 | 43 | 46 | 29 | 37 | 72 | 65 | 61 | | | | | |
| 5 | 78 | 1/3/2016 | mph | entr from 3rd ave hov | 73 | 70 | 70 | 51 | 48 | 29 | 48 | 50 | 59 | | | | | |
| 6 | 78 | R | S | T | U | V | W | X | Y | Z | AA | AB | AC | AD | AE | AF | AG | |
| 7 | 78 | 1 | 14 | 15 | 16 | 17 | 18 | 19 | 20 | 21 | 22 | 23 | 24 | | | | | |
| 8 | 78 | 2 | H1400 | H1500 | H1600 | H1700 | H1800 | H1900 | H2000 | H2100 | H2200 | H2300 | H2400 | location | route | direction | milepost | year |
| 9 | 78 | 3 | 73 | 74 | 74 | 74 | 72 | 74 | 74 | 72 | 70 | 73 | 69 | I-10 | W I-10 | WB | 144.641 | 2016 |
| 10 | 78 | 4 | 67 | 72 | 71 | 72 | 73 | 71 | 73 | 73 | 60 | 74 | 68 | I-10 | W I-10 | WB | 144.641 | 2016 |
| 11 | 78 | 5 | 72 | 71 | 74 | 74 | 71 | 70 | 64 | 72 | 66 | 67 | 49 | I-10 | W I-10 | WB | 144.641 | 2016 |
| 12 | 78 | 6 | 64 | 66 | 64 | 51 | 51 | 57 | 69 | 67 | 73 | 60 | 65 | I-10 | W I-10 | WB | 144.641 | 2016 |
| 13 | 78 | 7 | 73 | 66 | 51 | 45 | 47 | 54 | 71 | 71 | 72 | 65 | 48 | I-10 | W I-10 | WB | 144.641 | 2016 |
| 14 | 78 | 8 | 74 | 72 | 68 | 63 | 59 | 65 | 73 | 71 | 72 | 72 | 71 | I-10 | W I-10 | WB | 144.641 | 2016 |
| 15 | 78 | 9 | 72 | 70 | 60 | 49 | 42 | 64 | 73 | 72 | 72 | 73 | 75 | I-10 | W I-10 | WB | 144.641 | 2016 |
| | 78 | 10 | 73 | 71 | 65 | 63 | 58 | 65 | 72 | 73 | 73 | 73 | 73 | I-10 | W I-10 | WB | 144.641 | 2016 |
| | | 11 | 73 | 74 | 73 | 71 | 69 | 68 | 73 | 73 | 74 | 74 | 75 | I-10 | W I-10 | WB | 144.641 | 2016 |
| | | 12 | 73 | 75 | 73 | 73 | 73 | 73 | 73 | 66 | 74 | 72 | 74 | I-10 | W I-10 | WB | 144.641 | 2016 |
| | | 13 | 71 | 48 | 23 | 63 | 56 | 70 | 73 | 73 | 70 | 72 | 75 | I-10 | W I-10 | WB | 144.641 | 2016 |
| | | 14 | 73 | 73 | 61 | 54 | 45 | 60 | 70 | 73 | 71 | 73 | 60 | I-10 | W I-10 | WB | 144.641 | 2016 |
| | | 15 | 73 | 70 | 65 | 56 | 53 | 63 | 69 | 74 | 72 | 73 | 61 | I-10 | W I-10 | WB | 144.641 | 2016 |

Figure 5-5 Traffic Data File with Speed Data Averaged over 1 Hour Interval

5.3. Quality Control of Collected Data and General Discussion on Data Aggregation

As it is normally the case with every data set, the collected traffic data had some issues that needed to be addressed before being used in the analysis. Table 5-3 identified some of the problems that were noticed and the actions taken to correct them.

Table 5-3 Summary of Data Checking

| Problems | Number of records | Solutions |
|------------------------|--------------------------|-----------------------|
| Volume and speed data | | Only weekday data are |
| Ramp data include only | 1421 (volume) | Ramps not included in |
| Records with no data | 1 (from Detector 78): | Delete volume records |
| Missing speed data | 53 (from Detector 139): | Delete volume records |
| Volume=0 | 5,229 | Density=0 |
| Weekend numbers not | 2925 | Delete all weekend |

The general rules applied in Table 5-3 can be summarized as follows. Any data not applicable to the research scope, such as weekend data and data from ramps, would be deleted. Also, any bad or missing data would be discarded, as suggested by Bickel et al. (2007). Still, despite these actions, the remaining data cannot be considered accurate since many detector failures and data errors remain undetected (Jacobson et al., 1990). Hence, the accuracy of the results from the analysis would also be affected.

Traffic data collected from detectors needed to be processed before being used in the analysis. Since the scope included only weekday traffic along a freeway corridor, the weekend traffic and ramp traffic data were deleted.

As part of the data aggregation process, the volume and speed data are recorded by the detectors very 5-minute time interval every day of the year. These data were processed to reflect the steady-state conditions needed for the travel time estimation. The 5-minute time interval volume data were aggregated to produce the 1-hour interval volume data and the 5-minute speed data were averaged to generate the 1-hour time interval speed data.

Several studies conducted on traffic state estimation have defined a traffic state as being composed of flow and speed in addition to being in congested or uncongested conditions (Yeon, 2008). However, this research clearly defines the flow and density as the two traffic variables that define a traffic state both in the proposed traffic state estimation and in the proposed travel time estimation method.

5.4. Traffic State Estimation (TSE) Method

Given the scale of the problem, the data used in this proposed method are the 5-minute interval sample data.

5.4.1. Definition of States Using Clustering

A system has to be defined as the traffic states which is analyzed using a measurable characteristic. For the purposes of this research, $m_{x,t}$ is defined as a pair of density and flow. Then, ADOT's data can be used to perform clustering analyses. Now, K-means clustering can be applied to group the traffic state variables. Figure 5-6 shows the state representation using 8 states.

5.4.2. Calibration

Here the method presented in (Dervisoglu et al. 2009) is used to calibrate the parameters in Newell's model. The parameters are displayed in Figure 5-7. It can be observed that there is a capacity drop in the FD, which is an important problem in TSE problem. For simplicity, the problem of a capacity drop is not addressed in this research.

5.4.3. State Prediction

In this case, only the MC model (M1) is considered. Savitzky Golay filter with time-lag 3 hours and 3 orders are used to smooth the estimates. In addition, real-time data is applied to update the estimates. Table 5-4 reports the root-mean-square errors (RMSE) between the estimates and real-time observations with different numbers of states (4, 8, 16, 20, and 30) under both M1 and M2. Generally, after updating the values of RMSE become better (the green numbers imply decreasing RMSE; the red numbers in Table 5-4 mean increasing RMSE).

Although RMSEs are generally decreased with the increase in the number of traffic states, an interesting problem is how many states is needed? Table 5-4 shows that, when only M1 is used, the best prediction appears when the number of states is 20; the best prediction of real-time updating appears when the number of states is 30. Then, in this case study, 30 states might be a good choice. Table 5-5 compares the RMSEs the Markov chain (M1), Bayesian Classifier (M2 when $W=0$), and both of them (M2) are used. The outputs show that M2 can increase the RMSE of density, flow, and speed 2%, 0.7%, 6% respectively. The historical patterns obtained by M1 is also important. The table shows that when W in M2 is set equal to 0, then the RMSE will become very bad.

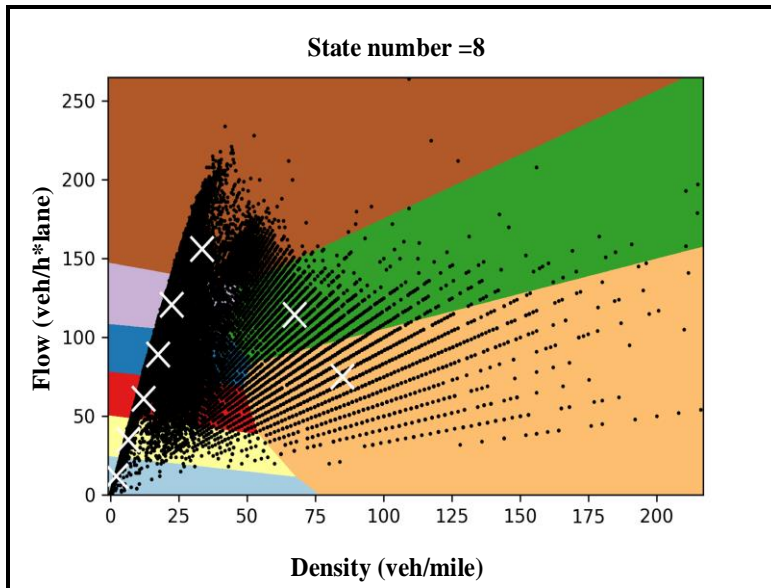


Figure 5-6 Clustering Representation of 8 States

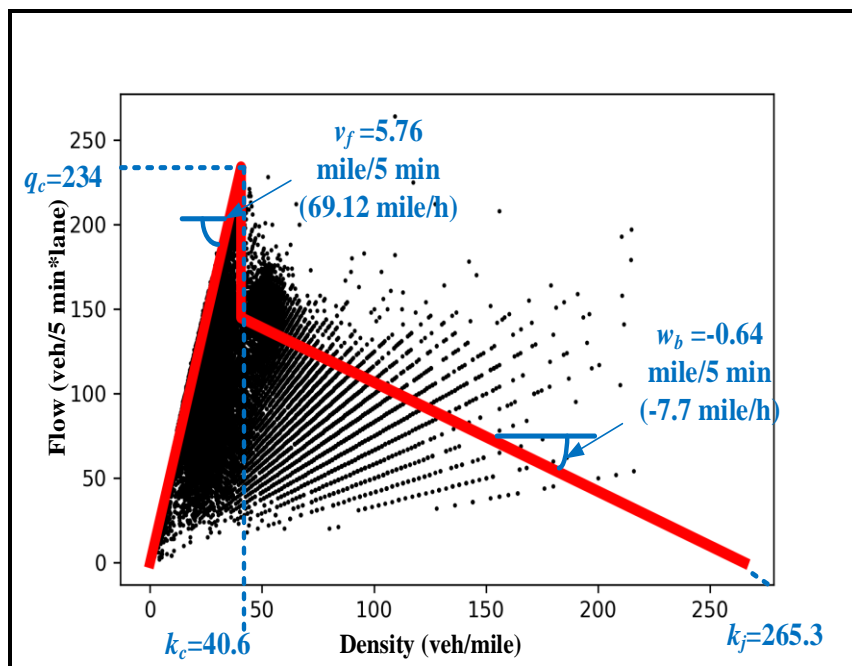


Figure 5-7 Calibration of Basic Parameters Using Collected Data

Table 5-4 RMSE of Estimates Obtained Using M1 and M2 under Different Number of States

| # of states | RMSE (v) | RMSE(k) | RMSE(q) |
|---|--------------|-------------|--------------|
| Only Markov Chain (M1) | | | |
| 4 | 13.28 | 10.92 | 21.57 |
| 8 | 12.88 | 9.82 | 18.32 |
| 16 | 11.7 | 9.23 | 18.06 |
| 20 | 10.07 | 8.95 | 17.83 |
| 30 | 9.19 | 9.04 | 17.88 |
| 40 | 9.22 | 9.13 | 17.9 |
| Markov Chain + Bayesian Classifier (M2) | | | |
| 4 | 12.07 | 9.87 | 20.14 |
| 8 | 11.39 | 9.2 | 17.78 |
| 16 | 9.8 | 9.2 | 17.28 |
| 20 | 9.94 | 9.45 | 16.94 |
| 30 | 9 | 8.97 | 16.69 |
| 40 | 9.05 | 9.31 | 16.61 |

Table 5-5 RMSE Obtained Using M1, M2, and M2 (W=0)

| # of states=30 | RMSE _R (v) | RMSE _R (k) | RMSE _R (q) |
|----------------|-----------------------|-----------------------|-----------------------|
| M1 | 9.19 | 9.04 | 17.88 |
| M2 | 9 | 8.97 | 16.69 |
| M2(W=0) | 15.41 | 20.32 | 50.54 |

Figure 5-8 shows the benchmark of the historical flow, density, and speed. The figure shows the predicted data using M2 (30 states). Figure 5-9 shows the evolution of historical data, real-time data, and the updated estimates of section 84 using M2 (30 states). It is clear that the updated estimates follow closely the observations, though deviations still exist. Figure 5-8 and Figure 5-9 show that the estimates overestimate/ underestimate the density/speed. This is caused by two reasons: (1) real-time updating, and (2) limitation of the K-means clustering. The clustering defines fewer states when the density becomes more congested (Figure 5-6).

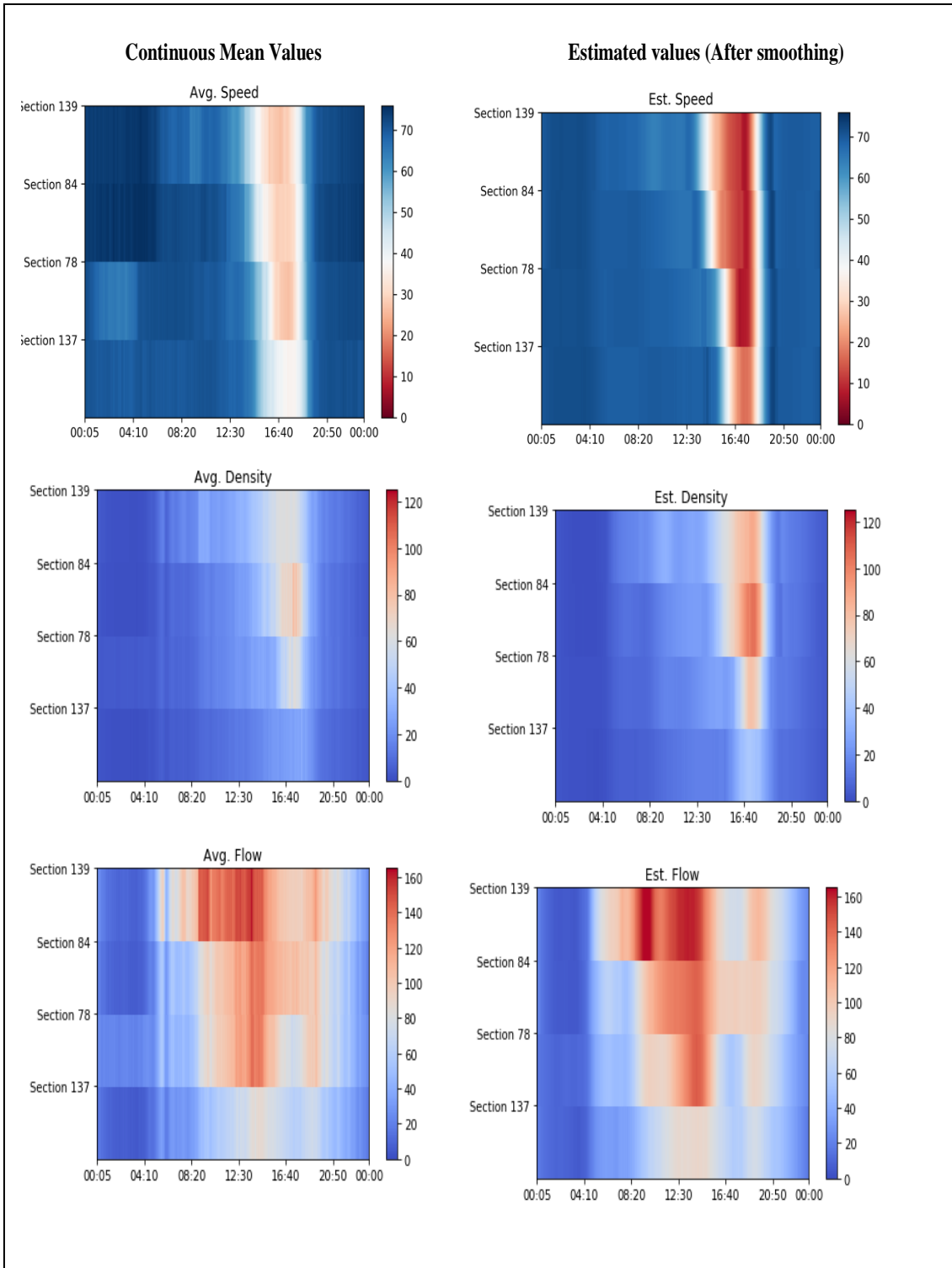


Figure 5-8 Comparison Between State Estimation (Using M2 with 30 States) and Historically Continuous Mean Values

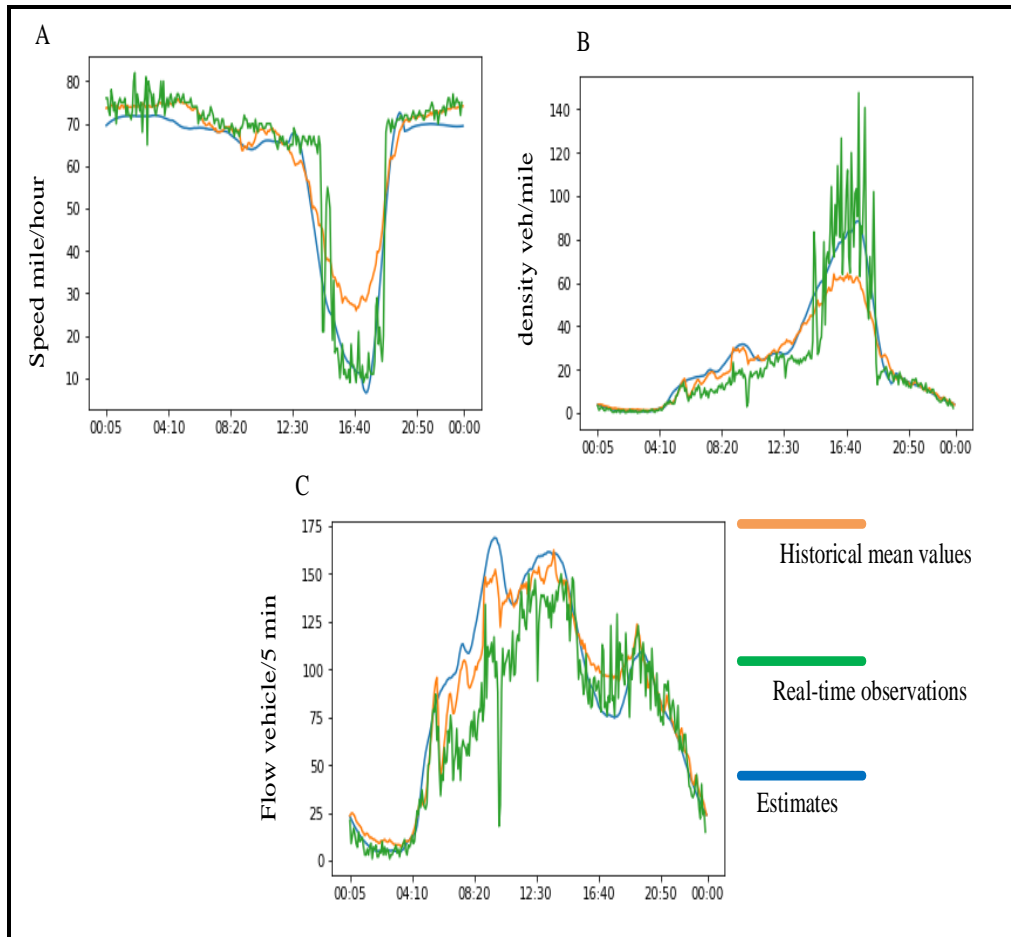


Figure 5-9 Historical, Real-time Observations, and Estimates of Section 84 Updated by Real-time Data (Using M2 with 30 States)

5.5. Average Travel Time Estimation Approach

As already mentioned in the previous section, traffic volume and speed data collected by traffic detectors are recorded and reported at 5-minute time interval. While such a small sampling is appropriate for dynamic traffic analysis (Branston, 1976), it is not for a “steady-state” condition required for the average travel time estimation. A steady-state flow is achieved by increasing the sampling time interval to 60-minutes (Rothrock and Keefer, 1957). However, the 5-minute data will be used whenever the analysis requires it.

5.5.1. Data Visualization Techniques

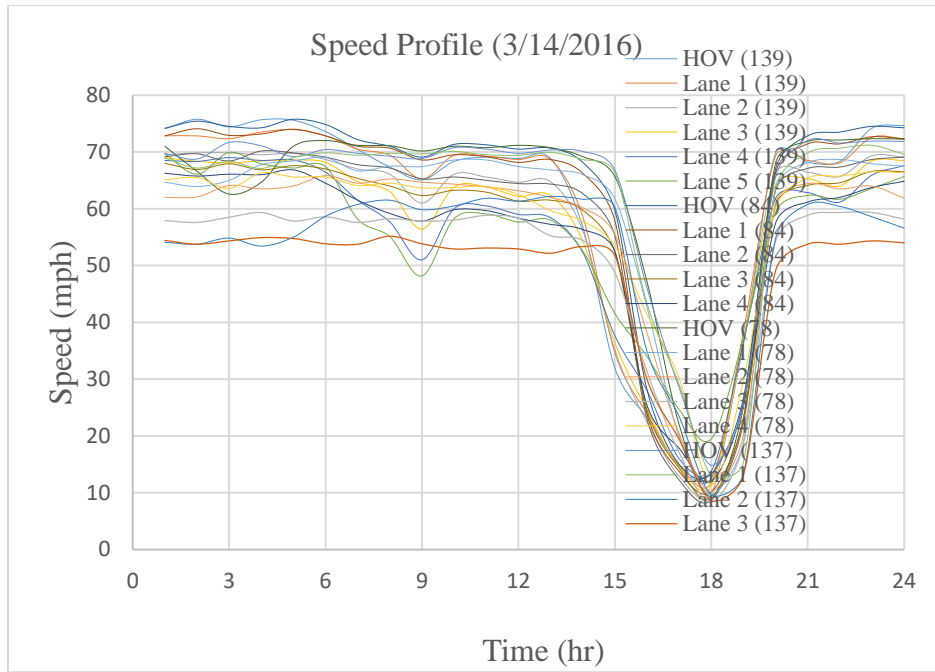
The heat map visualization technique is used to determine the location of the bottleneck on the freeway corridor. Figure 5-10 below captures a typical scenario where bottleneck occurs downstream at detector 137 and as a result, the traffic queue extends to the upstream at detector 139. The red contour represents the congested region where speed is less than 45 mph on all the lanes of the link segments, and the congested period is from 3 PM to 7 PM. The speed heat map can serve as the space-time representation of the bottleneck location, downstream and upstream locations, the congested period, and congested segments

| ID | Date | Speed | Facility | 1 | 2 | 3 | 4 | 5 | 6 | 7 | 8 | 9 | 10 | 11 | 12 | 13 | 14 | 15 | 16 | 17 | 18 | 19 | 20 | 21 | 22 | 23 | 24 | Location | Milepost | |
|-----|-----------|-------|----------|----|----|----|----|----|----|----|----|----|----|----|----|----|----|----|----|----|----|----|----|----|----|----|--------------------------|--------------------------|----------|----|
| 139 | 3/14/2016 | mph | hov | 74 | 76 | 74 | 76 | 76 | 74 | 70 | 67 | 65 | 68 | 69 | 69 | 69 | 57 | 32 | 23 | 15 | 13 | 36 | 70 | 68 | 68 | 74 | 75 | I-10_WB 146.823 16TH ST | 146.823 | 80 |
| 139 | 3/14/2016 | mph | lane1 | 73 | 73 | 72 | 74 | 74 | 73 | 71 | 69 | 65 | 69 | 69 | 69 | 69 | 59 | 35 | 24 | 15 | 12 | 38 | 69 | 69 | 68 | 73 | 72 | I-10_WB 146.823 16TH ST | 146.823 | |
| 139 | 3/14/2016 | mph | lane2 | 70 | 70 | 70 | 70 | 70 | 69 | 67 | 66 | 61 | 66 | 66 | 65 | 65 | 56 | 35 | 22 | 13 | 10 | 37 | 66 | 66 | 66 | 69 | 69 | I-10_WB 146.823 16TH ST | 146.823 | |
| 139 | 3/14/2016 | mph | lane3 | 69 | 68 | 68 | 68 | 69 | 68 | 65 | 63 | 56 | 64 | 64 | 62 | 62 | 54 | 36 | 25 | 15 | 11 | 37 | 64 | 65 | 64 | 68 | 69 | I-10_WB 146.823 16TH ST | 146.823 | |
| 139 | 3/14/2016 | mph | lane4 | 69 | 68 | 69 | 69 | 69 | 66 | 62 | 58 | 51 | 60 | 61 | 59 | 58 | 52 | 38 | 28 | 16 | 14 | 37 | 62 | 63 | 61 | 66 | 68 | I-10_WB 146.823 16TH ST | 146.823 | |
| 139 | 3/14/2016 | mph | lane5 | 70 | 66 | 70 | 68 | 67 | 67 | 58 | 55 | 48 | 58 | 59 | 58 | 58 | 53 | 42 | 34 | 25 | 20 | 37 | 59 | 62 | 62 | 64 | 66 | I-10_WB 146.823 16TH ST | 146.823 | |
| 84 | 3/14/2016 | mph | hov | 74 | 75 | 75 | 74 | 76 | 75 | 72 | 71 | 69 | 71 | 71 | 71 | 71 | 66 | 28 | 15 | 13 | 27 | 67 | 73 | 74 | 75 | 74 | I-10_WB 145.681 7TH ST | 145.681 | | |
| 84 | 3/14/2016 | mph | lane1 | 73 | 74 | 73 | 73 | 74 | 73 | 71 | 71 | 69 | 70 | 69 | 68 | 69 | 66 | 58 | 24 | 14 | 10 | 23 | 66 | 71 | 71 | 73 | 72 | I-10_WB 145.681 7TH ST | 145.681 | |
| 84 | 3/14/2016 | mph | lane2 | 69 | 70 | 68 | 70 | 70 | 69 | 68 | 67 | 65 | 66 | 65 | 64 | 64 | 63 | 55 | 23 | 12 | 9 | 22 | 63 | 67 | 67 | 69 | 69 | I-10_WB 145.681 7TH ST | 145.681 | |
| 84 | 3/14/2016 | mph | lane3 | 68 | 67 | 68 | 67 | 68 | 67 | 65 | 64 | 62 | 63 | 63 | 61 | 62 | 60 | 52 | 25 | 14 | 9 | 23 | 61 | 64 | 65 | 67 | 67 | I-10_WB 145.681 7TH ST | 145.681 | 40 |
| 84 | 3/14/2016 | mph | lane4 | 66 | 66 | 66 | 66 | 67 | 65 | 62 | 59 | 58 | 60 | 60 | 58 | 57 | 56 | 51 | 25 | 18 | 12 | 26 | 57 | 61 | 62 | 64 | 65 | I-10_WB 145.681 7TH ST | 145.681 | |
| 78 | 3/14/2016 | mph | hov | 71 | 67 | 63 | 65 | 71 | 72 | 71 | 70 | 71 | 71 | 71 | 71 | 69 | 66 | 17 | 22 | 9 | 25 | 68 | 72 | 72 | 72 | 72 | I-10_WB 144.641 7TH AVE | 144.641 | | |
| 78 | 3/14/2016 | mph | lane1 | 65 | 64 | 65 | 68 | 68 | 69 | 67 | 68 | 67 | 69 | 69 | 67 | 67 | 66 | 62 | 43 | 20 | 10 | 19 | 64 | 68 | 69 | 68 | 68 | I-10_WB 144.641 7TH AVE | 144.641 | |
| 78 | 3/14/2016 | mph | lane2 | 62 | 62 | 64 | 64 | 64 | 66 | 65 | 65 | 65 | 64 | 64 | 63 | 62 | 60 | 56 | 38 | 20 | 10 | 20 | 61 | 64 | 64 | 64 | 62 | I-10_WB 144.641 7TH AVE | 144.641 | |
| 78 | 3/14/2016 | mph | lane3 | 58 | 58 | 59 | 59 | 58 | 59 | 58 | 58 | 58 | 58 | 58 | 59 | 58 | 54 | 49 | 31 | 17 | 8 | 19 | 54 | 59 | 59 | 59 | 58 | I-10_WB 144.641 7TH AVE | 144.641 | |
| 78 | 3/14/2016 | mph | lane4 | 65 | 66 | 64 | 66 | 66 | 66 | 64 | 65 | 64 | 64 | 64 | 63 | 60 | 58 | 54 | 41 | 30 | 11 | 30 | 60 | 65 | 66 | 67 | 66 | I-10_WB 144.641 7TH AVE | 144.641 | |
| 137 | 3/14/2016 | mph | hov | 70 | 69 | 72 | 71 | 69 | 70 | 70 | 69 | 69 | 71 | 71 | 70 | 70 | 70 | 67 | 46 | 29 | 15 | 25 | 66 | 72 | 72 | 72 | 72 | I-10_WB 143.346 22ND AVE | 143.346 | |
| 137 | 3/14/2016 | mph | lane1 | 69 | 67 | 68 | 67 | 69 | 70 | 69 | 70 | 70 | 70 | 70 | 69 | 70 | 69 | 66 | 43 | 29 | 13 | 15 | 64 | 70 | 71 | 71 | 70 | I-10_WB 143.346 22ND AVE | 143.346 | |
| 137 | 3/14/2016 | mph | lane2 | 54 | 54 | 55 | 53 | 55 | 59 | 61 | 62 | 60 | 61 | 62 | 61 | 62 | 60 | 35 | 23 | 10 | 13 | 55 | 61 | 60 | 59 | 57 | I-10_WB 143.346 22ND AVE | 143.346 | | |
| 137 | 3/14/2016 | mph | lane3 | 54 | 54 | 54 | 55 | 55 | 54 | 54 | 55 | 54 | 53 | 53 | 53 | 52 | 53 | 52 | 30 | 19 | 9 | 13 | 49 | 54 | 54 | 54 | 54 | I-10_WB 143.346 22ND AVE | 143.346 | 0 |

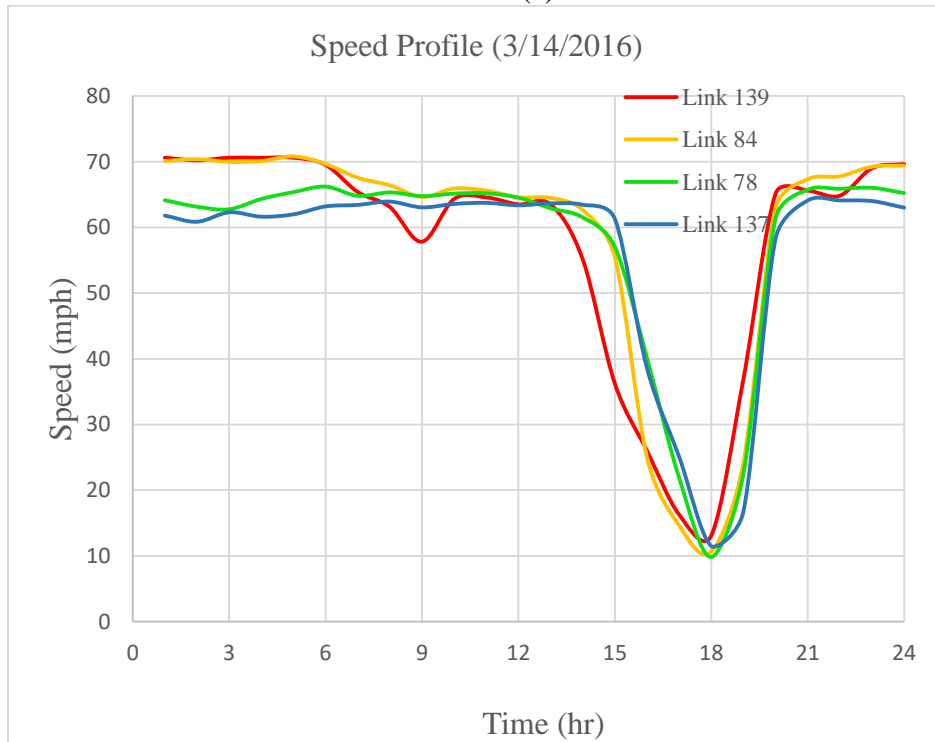
Figure 5-10 Speed Heat Map Showing Bottleneck Location, Congested Segments and Congested Period on a Typical Day

The speed profile is another method that clearly depicts how much the vehicle speeds have been reduced during the congested period. In Figure 5-11, it can be observed that vehicles entering the congested period, both at lane level (Figure 5-11(a)) and at the link level (Figure 5-11(b)), have experienced a speed reduction as slow as 9 mph around 6 PM.

It is particularly important to note that the slow speed experience applies to vehicles on any lane (Figure 5-11(a)) including especially the HOV lane. FHWA classifies any HOV facility as degraded facility if the speed on HOV lane is less than 45 mph for a certain period of time in a year (FHWA, 2020). A HOV Speed Compliance Action Plan must be developed by the transportation agency responsible of managing such a facility to improve the speed conditions on HOV lane.



(a)



(b)

Figure 5-11 Speed Profile Showing Bottleneck and Congested Period at the Lane Level (a) and at the Link Level (b) on a Typical Day

Figure 5-12 shows the speed-density profile that clearly illustrates the relationship between speed and density. Where the speed plot decreases until it reaches the lowest point and start increasing, the density plot increase until it reaches the highest point and starts decreasing. In other words, the same information on the bottleneck can also be obtained from the density data.

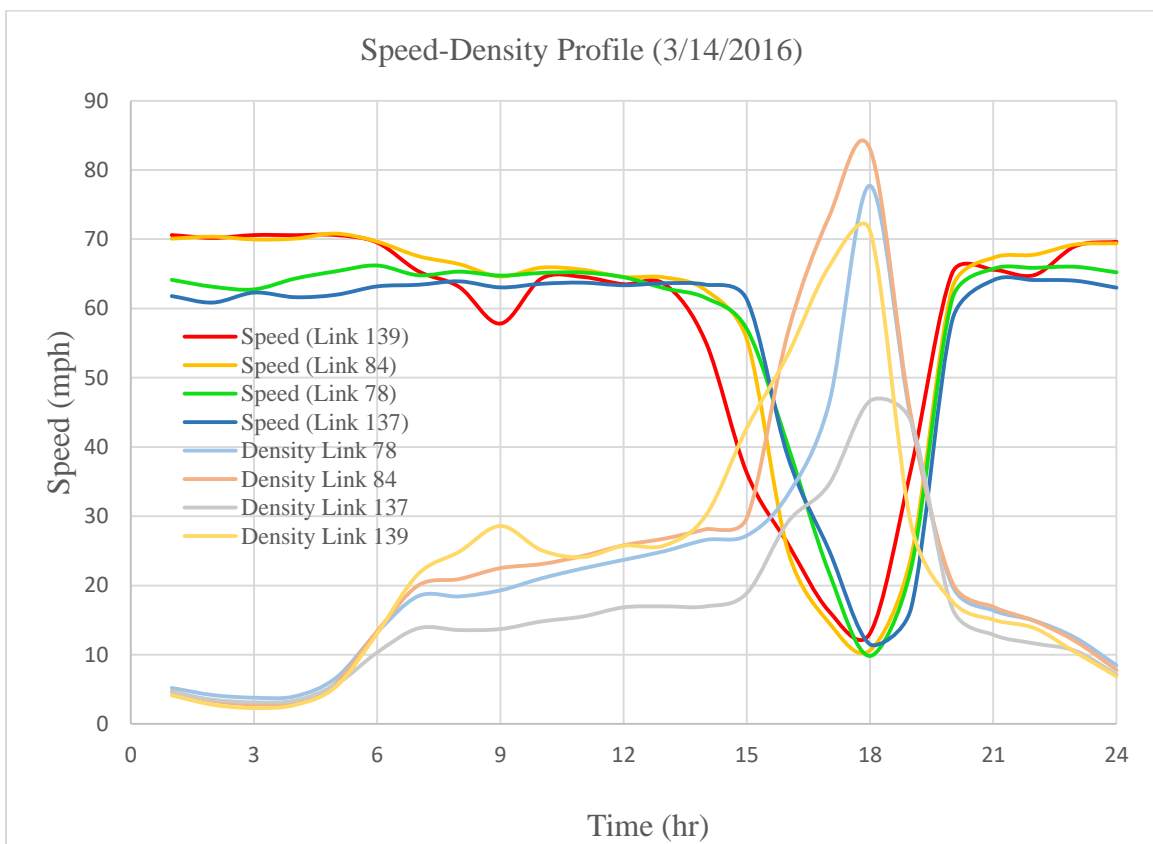


Figure 5-12 Speed-Density Profile Showing Bottleneck and Congested Period at The Link Level on a Typical Day

5.5.2. Maximum Observed Value Method

The maximum observed value method is the easiest method, from a computational perspective, for estimating key traffic variables from empirical data. Following suggestions from Li and Laurence (2015), the maximum observed value method has been used to identify the maximum volume, the free-flow speed, the critical speed, and the critical density from a set of 5-minute interval sample and to a set of 1-hour interval sample data.

The output results are summarized in the plots below. Programming languages such as Python, MathLab, or even GISDK from TransCAD, can be used to process the data and produce statistical results. However, Excel program is selected in this research to process the data and produce the results for several simple reasons. The first reason is that Excel is widely used especially among practitioners. Also, as suggested by Daganzo (1999), in any application, this research will always choose the simplest approach that can produce the expected results. Finally, the traffic data are saved in an Excel spreadsheet and excel can produce statistical results for one day data.

- **5-minute interval data set**

A one day 5-minute interval volume and speed data set from detector 78 is processed using Excel. Figure 5-13 shows the maximum flow and critical speed values from the fundamental flow-speed for both the lanes and the link of detector 78. The link is an aggregation of 5 lanes including high-occupancy vehicle (HOV) lane.

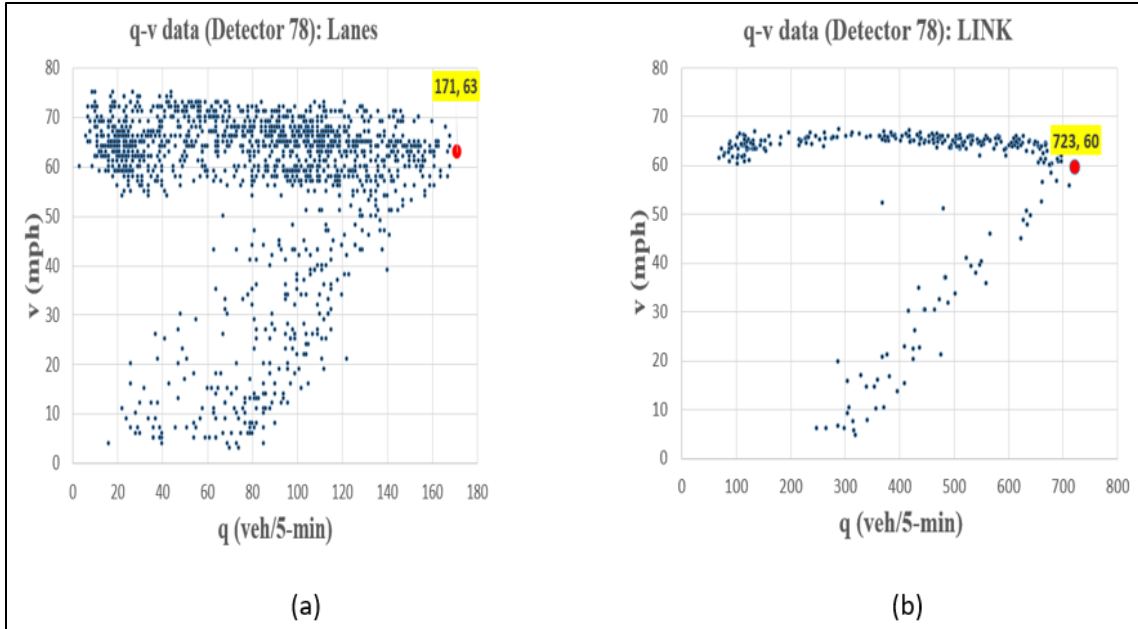


Figure 5-13 Maximum Flow and Critical Speed for All Lanes (a) and for the Link (b) from the Flow-Speed Diagram of Detector 78

In Figure 5-14, the maximum flow and the critical density values are depicted from the fundamental flow-speed for all the lanes and the link of detector 78.

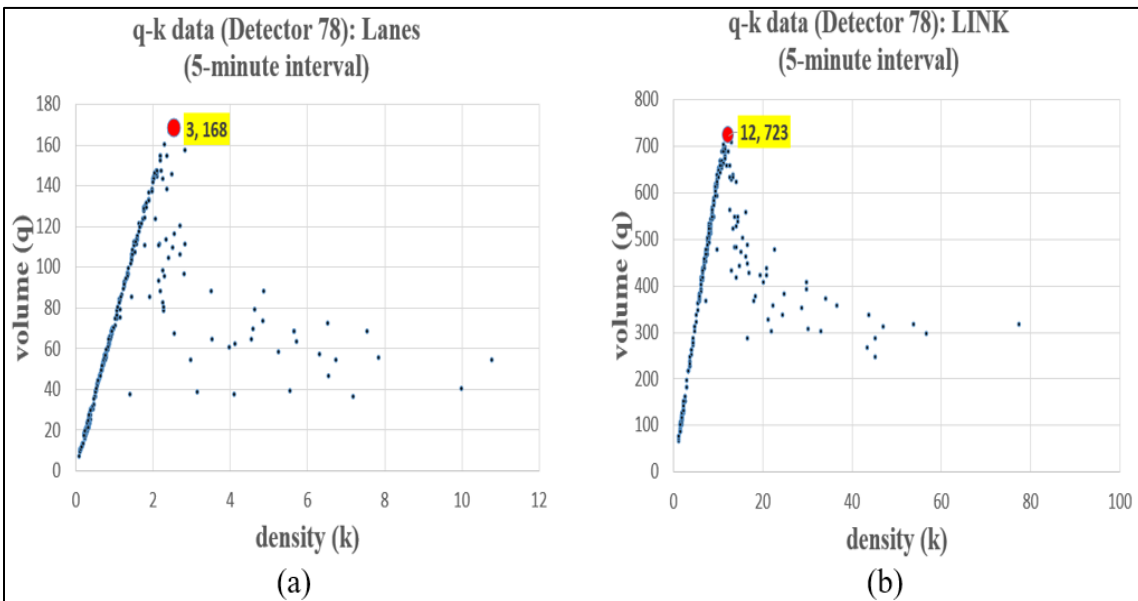


Figure 5-14 Maximum Flow and Critical Density for all Lanes (a) and for the Link (b) from the Flow-Speed Diagram of Detector 78

Among the three main variables for traffic flow theory, ADOT detectors only collect volume and speed data. In practice, detectors generally do not collect density. Instead, they collect vehicle occupancy which can then be converted into density. However, the general rule is that density can be computed from volume and speed. Figure 5-15 shows the computed density data versus the collected volume for all the lanes and the link of detector 78.

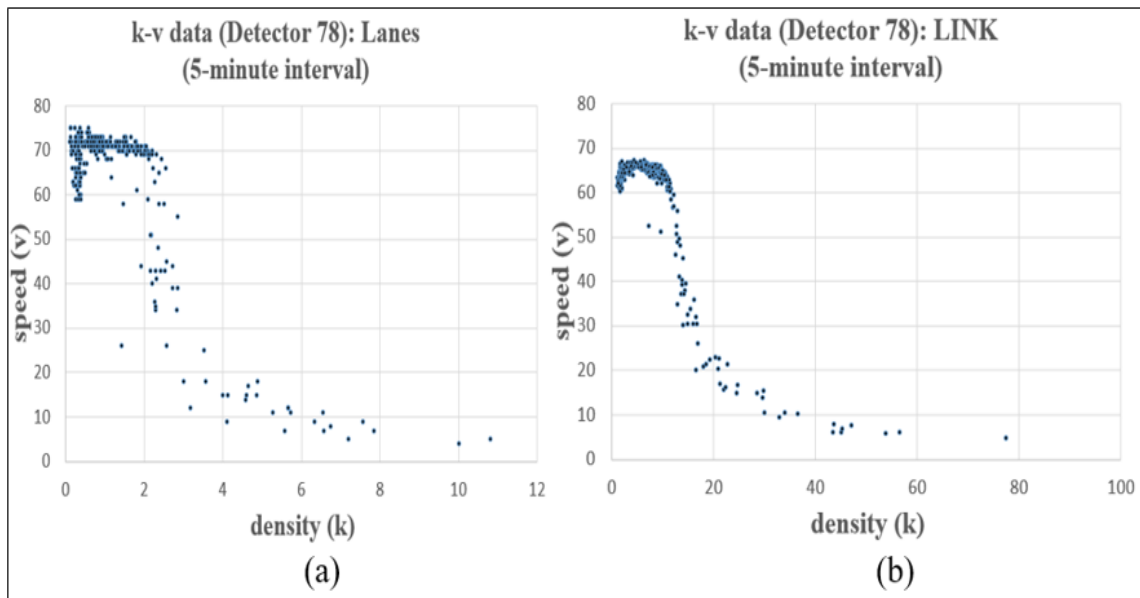
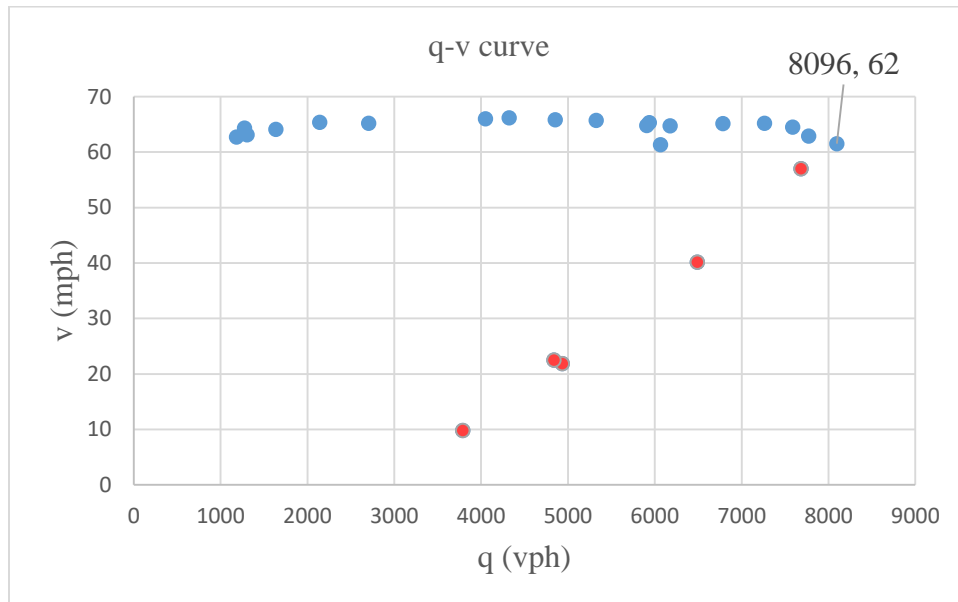


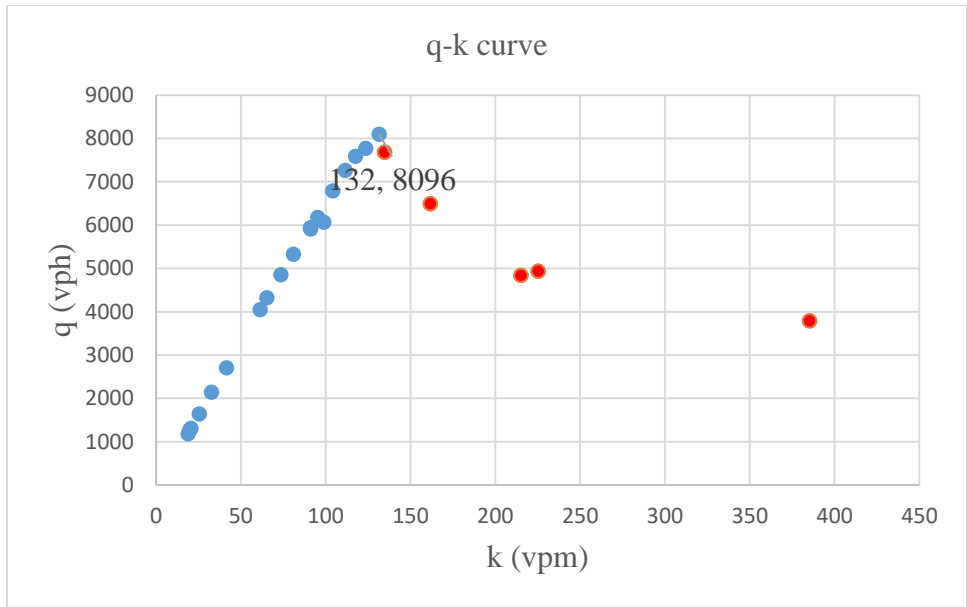
Figure 5-15 Flow-Density Relationship for all Lanes (a) and for the Link (b) of Detector 78

- **1-hour interval data set**

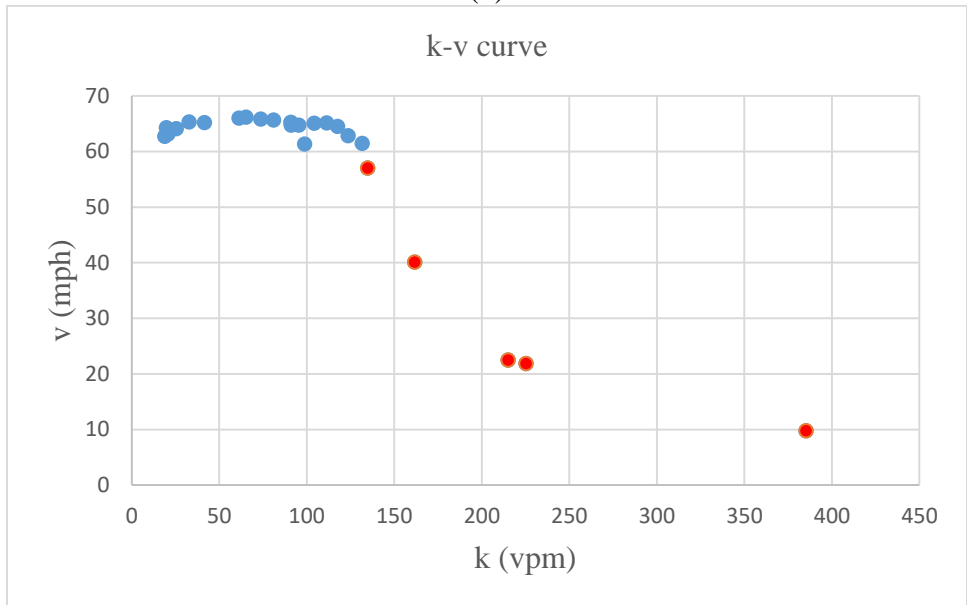
The 5-minute time interval data have been aggregated to 1-hour interval data to reflect the traffic steady-state conditions assumed in the static models (Rothrock and Keefer, 1957). Also, the lanes have been aggregated to links. This aggregation has considerably reduced the number of data to be analyzed. For example, the detector 78 has recorded a set of 288 different vehicle counts in 5-minute time interval in one typical day. After aggregating these vehicle counts to 1-hour time interval, the resulting set will contain only 24 different vehicle counts. The following figures show the fundamental traffic flow relationships between volume, speed, and density variables for 1-hour interval data. The congested data are shown in red to differentiate them from the uncongested ones.



(a)



(b)



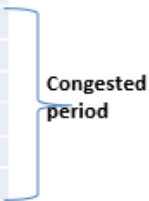
(c)

Figure 5-16 Detector 78 Fundamental Diagrams: Link Maximum Flow and Critical Speed (a), Link Maximum Flow and Critical Density (b), and Speed-Density (c)

Table 5-6 summarizes the traffic data results from detector 78 and also highlights the congested period. It can be observed that all the speed data in the congested period fall below the FHWA (2020) recommended critical speed of 45 mph.

Table 5-6 Traffic Data for Detector 78

| Detector 78 (3/14/2016) | | | | | |
|-------------------------|------|------|-------|---------|--------|
| | Time | Flow | Speed | Density | k-crit |
| | 1 | 1638 | 64 | 26 | 132 |
| | 2 | 1305 | 63 | 21 | 132 |
| | 3 | 1184 | 63 | 19 | 132 |
| | 4 | 1274 | 64 | 20 | 132 |
| | 5 | 2141 | 65 | 33 | 132 |
| | 6 | 4323 | 66 | 65 | 132 |
| | 7 | 5907 | 65 | 91 | 132 |
| | 8 | 5936 | 65 | 91 | 132 |
| | 9 | 6176 | 65 | 95 | 132 |
| | 10 | 6786 | 65 | 104 | 132 |
| | 11 | 7264 | 65 | 111 | 132 |
| | 12 | 7589 | 65 | 118 | 132 |
| | 13 | 7772 | 63 | 124 | 132 |
| t0 | 14 | 8096 | 62 | 132 | 132 |
| | 15 | 7682 | 57 | 135 | 132 |
| | 16 | 6490 | 40 | 162 | 132 |
| t2 | 17 | 4935 | 22 | 225 | 132 |
| | 18 | 3788 | 10 | 385 | 132 |
| t3 | 19 | 4838 | 23 | 215 | 132 |
| | 20 | 6066 | 61 | 99 | 132 |
| | 21 | 5327 | 66 | 81 | 132 |
| | 22 | 4852 | 66 | 74 | 132 |
| | 23 | 4049 | 66 | 61 | 132 |
| | 24 | 2707 | 65 | 42 | 132 |



5.5.3. Cumulative Vehicle Count Method

Now that the congested period have been identified, the cumulative vehicle counts within the congested period can be easily computed by using Eq. 4-1

$$N(t) = N(t - 1) + q(t) \quad \text{for } t_0 \leq t \leq t_3$$

The 5-minute time interval data set for detector 78 will be analyzed first, followed by the 1-hour time interval data set.

- **5-minute interval data set**

Cumulative curve theory can be used to estimate the excess demand experienced during congestion by aggregating arrival vehicles in the queue. Traffic data (including volume, q , speed v , and density k) in Table 5-7 collected from detector 78 in 5-minute time interval during congested period (from 2 PM to 7 PM), are used in the estimation of cumulative count, N , and the queue length, Q . Highlighted in the table is the resulting maximum queue length.

Table 5-7 Cumulative Count, N, and Queue Length, Q
(5-minute Time Interval)

| Detector 78 | | | | | |
|-------------|------|------|------|-------|------|
| t | q(t) | v(t) | k(t) | N(t) | Q(t) |
| 1400 | 670 | 63 | 11 | 670 | 0 |
| 1405 | 664 | 61 | 11 | 1334 | 204 |
| 1410 | 678 | 59 | 12 | 2012 | 423 |
| 1415 | 659 | 61 | 11 | 2671 | 622 |
| 1420 | 660 | 64 | 10 | 3331 | 822 |
| 1425 | 674 | 60 | 11 | 4005 | 1036 |
| 1430 | 689 | 61 | 11 | 4694 | 1266 |
| 1435 | 711 | 56 | 13 | 5405 | 1517 |
| 1440 | 368 | 52 | 7 | 5773 | 1425 |
| 1445 | 623 | 45 | 14 | 6396 | 1588 |
| 1450 | 626 | 49 | 13 | 7022 | 1755 |
| 1455 | 660 | 53 | 13 | 7682 | 1955 |
| ... | ... | ... | ... | ... | ... |
| 1600 | 559 | 36 | 16 | 14731 | 3027 |
| 1605 | 484 | 37 | 14 | 15215 | 3051 |
| 1610 | 409 | 23 | 20 | 15624 | 3001 |
| 1615 | 424 | 22 | 19 | 16048 | 2965 |
| 1620 | 304 | 16 | 22 | 16352 | 2809 |
| 1625 | 356 | 10 | 36 | 16708 | 2705 |
| 1630 | 476 | 21 | 23 | 17184 | 2722 |
| 1635 | 377 | 21 | 18 | 17561 | 2639 |
| 1640 | 329 | 17 | 21 | 17890 | 2508 |
| ... | ... | ... | ... | ... | ... |
| 1800 | 314 | 8 | 47 | 23209 | 471 |
| 1805 | 371 | 11 | 34 | 23580 | 382 |
| 1810 | 359 | 16 | 22 | 23939 | 282 |

| | | | | | |
|------|-----|----|----|-------|-----|
| 1815 | 368 | 21 | 18 | 24307 | 190 |
| 1820 | 338 | 15 | 25 | 24645 | 68 |
| 1825 | 353 | 15 | 29 | 24998 | 0 |
| 1830 | 436 | 23 | 21 | 25434 | 0 |
| 1835 | 435 | 35 | 13 | 25869 | 0 |
| 1840 | 445 | 31 | 15 | 26314 | 0 |
| 1845 | 472 | 33 | 15 | 26786 | 0 |
| 1850 | 446 | 30 | 17 | 27232 | 0 |
| 1855 | 501 | 34 | 15 | 27733 | 0 |
| 1900 | 522 | 41 | 13 | 28255 | 0 |

The cumulative curve and the discharge rate, which is the ratio of the total demand over the congested period, are drawn in the Figure 5-17. The difference between the cumulative curve and the discharge rate represents the queue length.

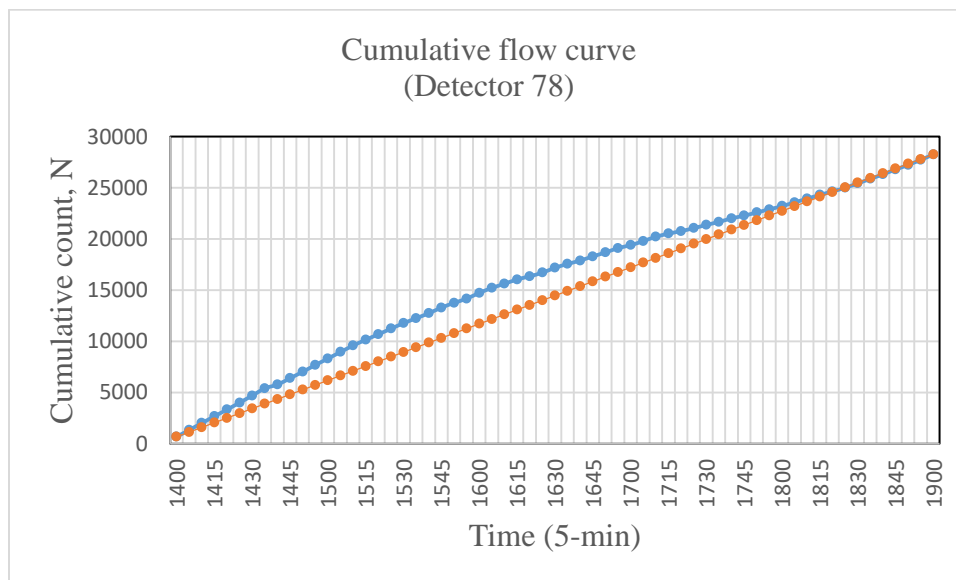


Figure 5-17 Cumulative Flow Curve (in Blue Line) Representing Cumulative Vehicle Count and Discharge Rate (in Orange) within Congested Period for 5-minute Time Interval

Figure 5-18 depicts the queue length curve derived from the cumulative curve plot.

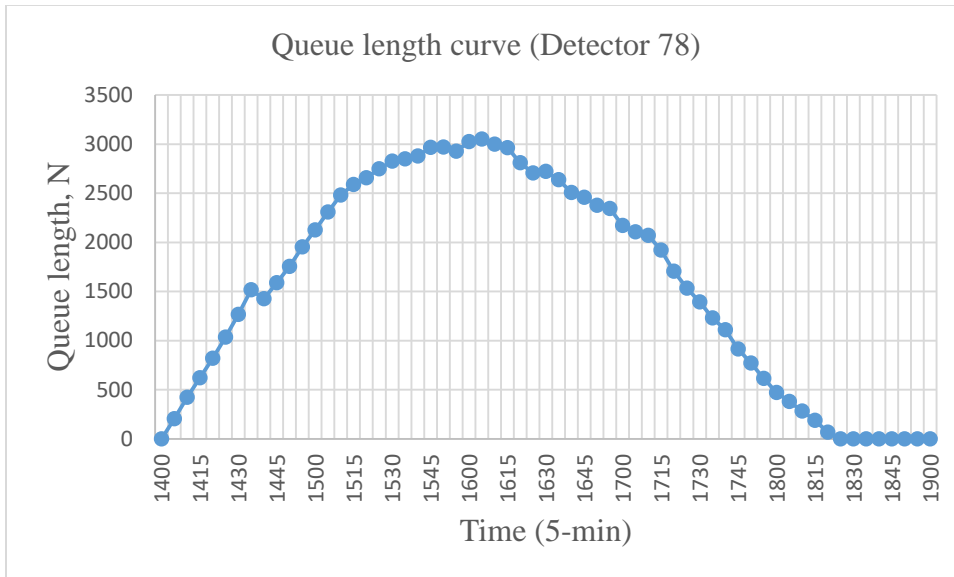


Figure 5-18 Queue Length Curve Derived from Cumulative Curve During Congested Period for 5-minute Time Interval

- **1-hour interval data set**

Traffic data for 1-hour time interval during congested period (from 2PM to 7 PM) is very limited but still enough to produce adequate results. Table 5-8 summarizes the volume, q , the cumulative vehicle arrival count, N , the cumulative vehicle departure count, N' , and the queue length, Q , from detector 78 in 1-hour time interval during congested period. The maximum queue length, $Q(t_2)$, is equal to 3,079. The total demand, $D = N(19) - N(14) = 35,829 - 8,096 = 27,733$

Table 5-8 Cumulative Count, N, and Queue Length, Q
(1-hour Time Interval)

| | Time, t | q(t) | N(t) | N' (t) | Q(t) |
|-----------|---------|------|-------|--------|------|
| t0 | 14 | 8096 | 8096 | 8096 | 0 |
| | 15 | 7682 | 15778 | 13643 | 2135 |
| t2 | 16 | 6490 | 22268 | 19189 | 3079 |
| | 17 | 4935 | 27203 | 24736 | 2467 |
| | 18 | 3788 | 30991 | 30282 | 709 |
| t3 | 19 | 4838 | 35829 | 35829 | 0 |

The cumulative curve and the discharge rate, which is the ratio of the total demand over the congested period, are depicted in the Figure 5-19.

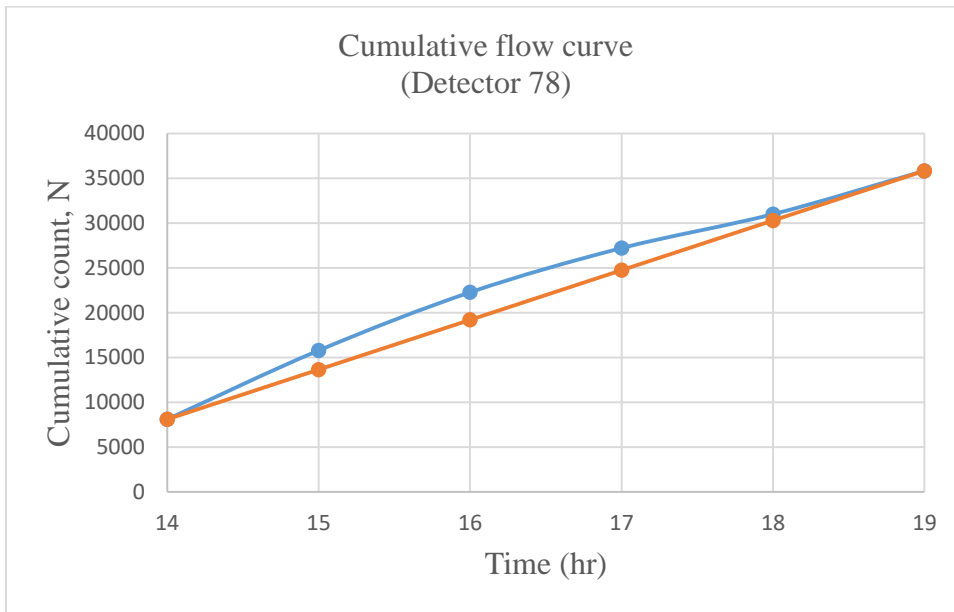


Figure 5-19 Cumulative Flow Curve (in Blue Line) Representing Cumulative Vehicle Count and Discharge Rate (in Orange) within Congested Period for 1-hour Time Interval

The corresponding queue length curve, in Figure 5-20, depicts the difference between the cumulative curve and the discharge rate during the congested period.

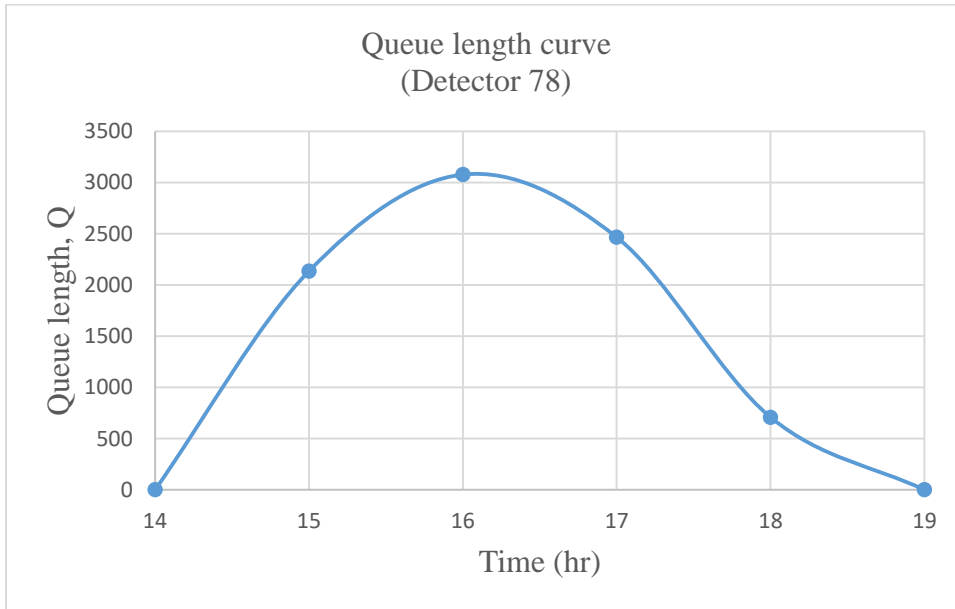


Figure 5-20 Queue Length Curve Derived from Cumulative Curve During Congested Period for 1-hour Time Interval

5.5.4. Calibration of Polynomial Equation Parameters

The polynomial function parameters, including the shape parameter ρ and the discharge rate μ , developed by Newel's method will be estimated using the total demand, D , the congestion period, P , and maximum length, $Q(t_2)$, from the cumulative curve and queue length curve results.

Using Eq. 4-18,

$$\rho = \frac{6Q(t_2)}{(t_2 - t_0)^3} = \frac{6(3079)}{(17-14)^3} = 684.2$$

From Eq. 4-24,

$$\mu = \frac{D}{P} = \frac{27733}{(19-14)} = 5547$$

5.5.5. Travel Time Calibration and Validation

Two data sets from two different days are used for calibration process and for validation process. Considering the traffic data quality of the detectors from the freeway corridor, the traffic data set from 3/14/2016 and from 10/17/2016 are used in the calibration process of the ϕ parameter and for the validation process of the detector 84 for the proposed travel time method.

(1) Calibration

Eqs. 4-27, 4-29, and 4-30 below are used in Table 5-9 below to calibrate ϕ parameter for detector 84 using the traffic data set from 3/14/2016.

$$t_t = t_f + \frac{\rho}{36\mu} \cdot \left(\frac{D}{\mu}\right)^3 = t_f \cdot \left[1 + \frac{\rho}{36\mu t_f} \cdot \left(\frac{D}{\mu}\right)^3\right]$$

$$D(t) = (36(\mu)^4(t_t - t_f)/\rho)^{1/3}$$

$$D(t) = \phi(t) [K(t) L]$$

$$\phi(t) = D(t)/[K(t) L]$$

$$\phi(t) = \left(\frac{36(\mu)^4(t_t - t_f)}{\rho}\right)^{\frac{1}{3}} / [K(t) L]$$

The parameter ϕ is estimated for each time interval during the congested period. The average of these estimated parameters will be used in the link validation of the proposed travel time method.

Table 5-9 Calibration Summary Spreadsheet of ϕ Parameter Using Link Specific Traffic Data from Detector 84 During Congested Period

| Detector 84 (3/14/2016) | | | | | | |
|-------------------------|------|------|------|-----|---------|--|
| Time, t | q(t) | v(t) | K(t) | Kc | K(t)/Kc | |
| 1 | 1623 | 70 | 23 | 140 | 0.17 | |
| 2 | 1153 | 70 | 16 | 140 | 0.12 | |
| 3 | 981 | 70 | 14 | 140 | 0.10 | |
| 4 | 1087 | 70 | 16 | 140 | 0.11 | |
| 5 | 2086 | 71 | 29 | 140 | 0.21 | |
| 6 | 4635 | 70 | 67 | 140 | 0.48 | |
| 7 | 6679 | 68 | 99 | 140 | 0.71 | |
| 8 | 6836 | 66 | 103 | 140 | 0.74 | |
| 9 | 7171 | 65 | 111 | 140 | 0.79 | |
| 10 | 7542 | 66 | 114 | 140 | 0.82 | |
| 11 | 7905 | 66 | 121 | 140 | 0.86 | |
| 12 | 8277 | 65 | 128 | 140 | 0.92 | |
| 13 | 8560 | 64 | 133 | 140 | 0.95 | |
| t0 | 14 | 8758 | 63 | 140 | 1.00 | |
| | 15 | 8251 | 56 | 140 | 1.06 | |
| | 16 | 7052 | 25 | 282 | 2.02 | |
| t2 | 17 | 5335 | 15 | 365 | 2.61 | |
| | 18 | 4461 | 11 | 420 | 3.00 | |
| t3 | 19 | 5355 | 24 | 222 | 1.58 | |

| | |
|-----------|-------|
| qmax | 8758 |
| Kc | 140 |
| Length, L | Speed |
| 1.14 | 71 |

| | |
|----|----|
| t0 | 14 |
| t2 | 17 |
| t3 | 19 |

| | |
|-------|------|
| Q(t2) | 3121 |
|-------|------|

$\phi = 41$

| | |
|-------|------|
| N(t) | Q(t) |
| 8758 | 0 |
| 17009 | 2160 |
| 24061 | 3121 |
| 29396 | 2366 |
| 33857 | 736 |
| 39212 | 0 |

Calibration of parameter ϕ

$$\rho = \frac{6Q(t_2)}{(t_2 - t_0)^3} = 694$$

$$\mu = \frac{D}{P} = 6091$$

$$t_i = t_f + \frac{\rho}{36\mu} \cdot \left(\frac{D}{\mu}\right)^3 = t_f \cdot \left[1 + \frac{\rho}{36\mu t_f} \cdot \left(\frac{D}{\mu}\right)^3\right]$$

$$D(t) = \phi(t) [K(t) L]$$

$$D(t) = (36(\mu)^4 (t_i - t_f) / \rho)^{1/3}$$

$$\phi(t) = D(t) / [K(t) L]$$

| t | v(t) | Q(t2) | ρ | μ | t_i | t_f | D(t) | K(t)*L | $\phi(t)$ | |
|----|------|-------|--------|-------|-------|-------|------|--------|-----------|----|
| t0 | 14 | 8758 | 3121 | 694 | 6091 | 0.02 | 0.02 | 5313 | 159 | 33 |
| | 15 | 17009 | 3121 | 694 | 6091 | 0.02 | 0.02 | 6809 | 169 | 40 |
| | 16 | 24061 | 3121 | 694 | 6091 | 0.05 | 0.02 | 12816 | 321 | 40 |
| t2 | 17 | 29396 | 3121 | 694 | 6091 | 0.08 | 0.02 | 16404 | 416 | 39 |
| | 18 | 33857 | 3121 | 694 | 6091 | 0.11 | 0.02 | 18670 | 478 | 39 |
| t3 | 19 | 39212 | 3121 | 694 | 6091 | 0.05 | 0.02 | 13044 | 253 | 52 |

The calibration process is performed on the remaining detectors for ϕ parameters and the results are shown in Table 5-10.

Table 5-10 ϕ Parameters for Detectors 78, 84, 137, and 139

| | | | | |
|--------|-----------|-----------|------------|------------|
| | 78 | 84 | 137 | 139 |
| ϕ | 42 | 41 | 32 | 48 |

(2) Validation

The validation of the new method uses the calibrated ϕ parameter and the traffic data from the set from 10/17/2016 to estimate the travel time that is compared to the link congested travel time. The standard BPR function (with alpha = 0.15 and beta =4) is used here as a reference. Table 5-11 summarizes travel time from the link/field, from the new method, and from the standard BPR function for detector 84.

Table 5-11 Travel Time Summary Spreadsheet of the New Method Using Calibrated ϕ Parameters and Traffic Data from Detector 84 During Congested Period

| Detector 84 (10/17/2016) | | | | | | | | | |
|--------------------------|------|------|------|-----|---------|-------|-------|------|-------|
| Time,t | q(t) | v(t) | K(t) | Kc | K(t)/Kc | Field | New M | BPR | |
| 1 | 1499 | 70 | 21 | 161 | 0.13 | 0.97 | 0.96 | 0.96 | |
| 2 | 998 | 70 | 14 | 161 | 0.09 | 0.97 | 0.96 | 0.96 | |
| 3 | 894 | 71 | 13 | 161 | 0.08 | 0.97 | 0.96 | 0.96 | |
| 4 | 1071 | 71 | 15 | 161 | 0.09 | 0.96 | 0.96 | 0.96 | |
| 5 | 2311 | 71 | 32 | 161 | 0.20 | 0.96 | 0.96 | 0.96 | |
| 6 | 4709 | 70 | 67 | 161 | 0.42 | 0.97 | 0.99 | 0.97 | |
| 7 | 6625 | 67 | 98 | 161 | 0.61 | 1.01 | 1.04 | 0.98 | |
| 8 | 7246 | 65 | 112 | 161 | 0.69 | 1.05 | 1.07 | 1.00 | |
| 9 | 6430 | 67 | 97 | 161 | 0.60 | 1.03 | 1.04 | 0.98 | |
| 10 | 7097 | 65 | 109 | 161 | 0.68 | 1.05 | 1.07 | 0.99 | |
| 11 | 7258 | 66 | 109 | 161 | 0.68 | 1.03 | 1.07 | 0.99 | |
| 12 | 7454 | 66 | 113 | 161 | 0.70 | 1.04 | 1.08 | 1.00 | |
| 13 | 8380 | 65 | 129 | 161 | 0.80 | 1.05 | 1.14 | 1.02 | |
| t0 | 14 | 8513 | 53 | 161 | 161 | 1.00 | 1.30 | 1.30 | 1.11 |
| | 15 | 7000 | 26 | 266 | 161 | 1.65 | 2.60 | 2.50 | 2.07 |
| | 16 | 5294 | 15 | 351 | 161 | 2.18 | 4.54 | 4.50 | 4.34 |
| t2 | 17 | 4347 | 10 | 450 | 161 | 2.79 | 7.09 | 8.43 | 10.10 |
| | 18 | 4166 | 9 | 452 | 161 | 2.80 | 7.42 | 8.50 | 10.23 |
| t3 | 19 | 5600 | 30 | 189 | 161 | 1.17 | 2.30 | 1.51 | 1.24 |

In Figure 5-21, the travel time data from the field/link, BPR, and the new method from detector 84 during the congested period are plotted. It can be observed that the curves remain constant in the uncongested region where $K/K_c < 1$ and then they scatter after the congestion has been reached at $K/K_c=1.0$

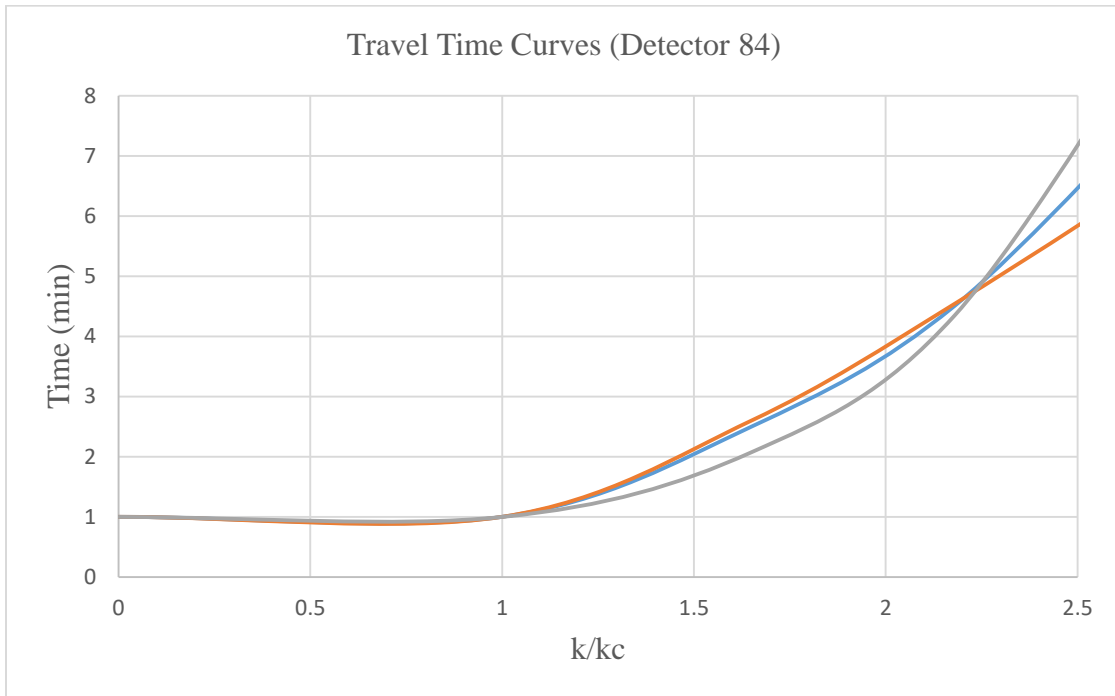


Figure 5-21 Link/Field, BPR, and New Method Travel Time Curves from Detector 84
All Curves Display an Increase in Steepness after the Congestion Occurs at $K/K_c=1.0$

The validation process is performed on all the remaining detectors and the statistical results are shown in Table 5-12. The detectors show very high R-squared numbers.

Table 5-12 Statistical Results (R-Squared) of the New Method and BPR Validation with Field Data

| | 78 | 84 | 137 | 139 |
|-------------------|------------------|--------|--------|--------|
| | R-squared | | | |
| New Method | 0.9716 | 0.985 | 0.8041 | 0.9942 |
| BPR | 0.9461 | 0.9606 | 0.8361 | 0.9882 |

5.6. Discussions of the Results

This dissertation focuses on traffic congested conditions since traffic variables behave differently under congested conditions. Selecting density as one variable for traffic state, in addition to the flow variable, ensures that congested traffic conditions necessary for planning purposes are captured in the analysis. This section compiles the comments and observations from the results from the previous sections. The comments are gathered under a heading similar to their section titles.

- Cumulative Flow Curve and Queue Length Curve

The visual difference between 5-minute time interval and 1-hour time interval data was obvious in the diagrams especially queue length curve diagram. Because of dynamic traffic conditions, there were several irregularities in the 5-minute time interval queue length curve. However, the 1-hour time interval queue length curve was smooth, reflecting the steady-state conditions of traffic. Despite a few discrepancies in the shapes of curves, the 5-minute time interval data and the 1-hour time interval data displayed similar patterns and

produced the almost same maximum queue length. Only congested volume data are needed to produce the cumulative flow curve and the queue length curve.

Even though the data was collected from individual lanes, the final analysis was based on link data. The main reason for this decision is that travel demand models represent roadway system as a series of links with number of lanes as an attribute of these links. So, the volume data from lanes were aggregated to produce link volume data and the speed data from lanes were averaged to generate link speed data.

- Average Delay and Travel Time Estimation

In Newell's method, the queue length estimate during the congested period is central because it serves as the transition from cumulative flow curve to the quadratic polynomial function. The shape parameter of the function can be computed using the maximum queue length and the congested time parameters. The average delay can then be estimated using the shape parameter and the congested time parameters.

The proposed travel time method transforms the average delay formula by including the congested volume and the discharge rate (capacity) in the equation.

- Travel Time Calibration and Validation

The proposed travel time function satisfies the two most important requirements for a well behaved congestion function (Spiess, 1989). The function is a convex and an increasing function, which ensures that an assignment will converge to a unique solution. The function's exponent is an indication of the congestion effect when the capacity limit is reached.

The validation results show very high statistical results in R^2 values between the proposed method and the field results. This indicates that the proposed model can relatively predict the field data accurately.

The possible future implementation of the proposed travel time function in a travel demand model will demonstrate any possible reduction in the computing runtime from the proposed function when compared to the BPR function.

- Future Considerations

The possible future implementation of the proposed travel time function in a travel demand model will demonstrate any possible reduction in the computing runtime from the proposed function when compared to the BPR function.

The proposed method is time-dependent and can compute travel time in 5-minute time interval during congestion period provided the 5-minute time interval volume data and speed data are used as input. This important option can transform a static assignment model into a dynamic assignment model, pending further detailed research.

In the conclusion chapter, the concept applied in this research is referred to as the BPR-x method. It consists in calculating the time-dependent queue length based on cumulative arrival and departure curves, assuming the queue length distribution curve is equivalent to a polynomial function (in this research, a quadratic function), calculating the average delay with the integral of queue length function, and obtaining the analytical form of the average travel time function during the oversaturated period.

CHAPTER 6

CONCLUSIONS

This dissertation proposes a TSE framework that is updated by real-time traffic data considering spatiotemporal correlations based on Newell's KW model. Using STPG, the framework combines the local MC model and Bayesian classifiers to update the online estimation. A case study, based on the traffic data from ADOT, is implemented to validate the method and to determine the traffic state with a good estimation/prediction. It is also found that both the historical patterns and real-time updating are important for a better on-line estimation system.

Link travel time performance functions (or volume-delay functions) have been widely used in static traffic assignment (STA) for transport planning. Among a variety of link performance functions, the BPR function, created by the US Bureau of Public Roads in 1964, is recognized as an analytical building block for system-wide performance evaluation. Focusing on the traffic volume and delay, relationship, the BPR function in its polynomial form is computationally efficient and simple for implementation in the transport planning software.

As shown in Figure 6-1, the derivative process for the proposed BPR-x can be summarized as the following: 1) assume the inflow rate function follows a polynomial form and determine the order of the polynomial inflow rate function; 2) establish the equivalent factor form of the polynomial inflow rate function; 3) calculate the time-dependent queue length based on cumulative arrival and departure curves; 4) calculate the total delay and

average delay with the integral of queue length function; 5) obtain the analytical form of the average travel time function during the oversaturated period.

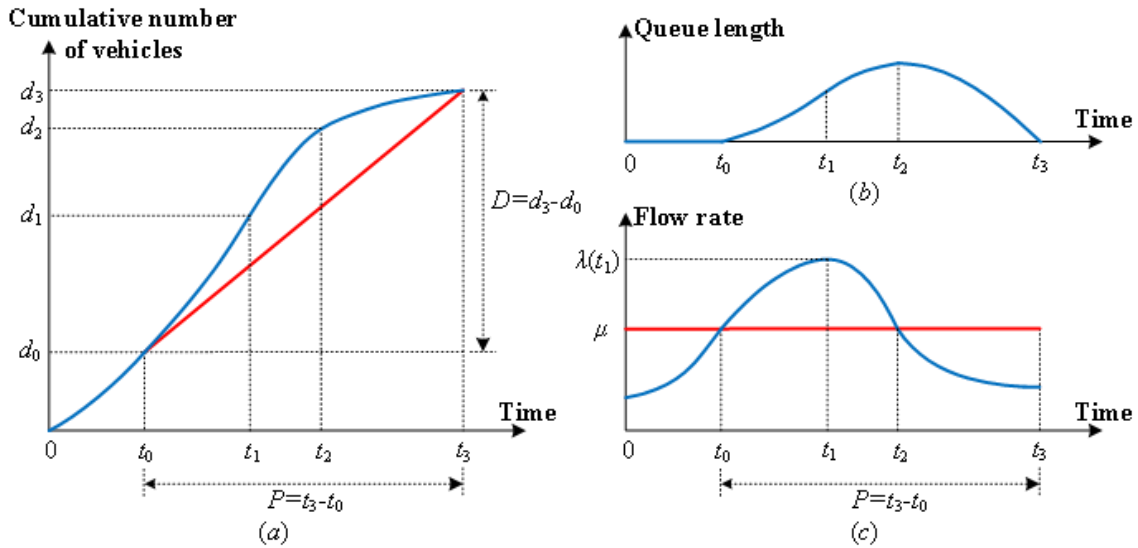


Figure 6-1 General Graphical Illustration of Queue Evolution for a Single Oversaturated Bottleneck

The proposed BPR-x function has four advantages compared with existing models. Firstly, it has a similar structure with BPR function, but with more intuitional meanings for the coefficients (including the coefficient of the highest order term in the polynomial inflow rate function, the capacity or practical discharge rate, and the peak duration) compared to the original BPR function. With the assumption of constant capacity, the peak duration (i.e., degree of peakness) equals to the peak period demand over capacity, thus describing how inflow coverage and capacity parameters influence the average travel time. Secondly, it establishes the equivalence between the analytical BPR average performance functional form and the corresponding queue evolution form. Thirdly, a new type of calibration process from the point queue bottleneck perspective is proposed, and it is very simple to

fully utilize the sensor data (e.g., flow, speed, density) to calibrate the coefficients based on the three-detector model. Lastly, with well-posed assumptions, the BPR-x function can be smoothly transferred for a simplified approximation of the full-scale DTA model. It also has broad applications in the transport system management (e.g., dynamic signal control, traffic system evaluation and optimization, bus and metro demand management), as long as we can obtain the system's cumulative arrival and departure curves.

The BPR-x function opens a window for the performance evaluation of a single oversaturated freeway bottleneck. However, it still has many challenges in the future research. As the freeway has different facility types with merge and diverge ramps, so how to model the BPR-x with merging and diverging is still an open question. To extend the BPR-x from freeway to arterial streets, one of the inevitable problems is how to consider the travel time functions with oversaturated signals and how to optimize the signal control with BPR-x. Many theoretical issues also arise in the BPR-x. Which order should we choose to best represent the traffic system performance? The higher order may have a better fitness, but the structure may be tedious and result in a slow convergence for equilibrium traffic assignment; so how to make a tradeoff between the fitness and parsimonious structure is worthy of deep consideration. In the proposed BPR-x functions, the derivative process is based on point queue model. It is widely recognized that the point queue model cannot capture the spatial dynamics of traffic flows, so how to establish the analytical form of BPR-x from point queue model to spatial queue and kinematic wave models should be investigated. In addition, when multi-bottlenecks are considered, the impact of queue spillbacks should be studied seriously.

REFERENCES

- Akcelik, R., 1991. Travel time functions for transport planning purposes: Davidson's function, its time dependent form and alternative travel time function, *Australian Road Research*, vol. 21, no. 3.
- Antoniou, C., Koutsopoulos, H. N., & Yannis, G., 2013. Dynamic data-driven local traffic state estimation and prediction. *Transportation Research Part C: Emerging Technologies*, 34, 89-107.
- Ben-Naim, E., & Krapivsky, P. L., 1998. Steady-state properties of traffic flows. *Journal of Physics A: Mathematical and General*, 31(40), 8073–8080.
<https://doi.org/10.1088/0305-4470/31/40/004>
- Bickel, P. J., Chen, C., Kwon, J., Rice, J., Van Zwet, E., and Varaiya, P., 2007. Measuring traffic. *Statistical Science*, 22(4), 581– 597
- Branston, D., 1976. Link capacity functions: a review. *Transportation Research*, vol. 10, no. 4, pp. 223 – 236.
- Brilon, W., Geistefeldt, J., Zurlinden, H., 2007. Implementing the concept of reliability for highway capacity analysis. *Transportation Research Record*, No. 2027, pp. 1 - 8
- Bureau of Public Roads, 1964. *Traffic Assignment Manual*, Department of Commerce, Urban Planning Division, Washington, DC, USA.
- Cetin, M., Foytik, P., Son, S., Khattak, A., Robinson, M., Lee, J., 2012. Calibration of volume-delay functions for traffic assignment in travel demand models. 91st Annual Meeting of the Transportation Research Board, Transportation Research Board, Washington, DC
- Choe, T., Skabardonis, A., Varaiya, P., 2002. Freeway Performance Measurement System (PeMS): an operational analysis tool. *Transportation Research Board 81st Annual Meeting*, Washington DC.
- Chu, L., 2005. Adaptive Kalman filter based freeway travel time estimation. *Transportation Research Board 84th Annual Meeting*, Washington DC.
- Coifman, B., 2015. Empirical flow-density and speed-spacing relationships: evidence of vehicle length dependency. *Transportation Research Part B: Methodological*, vol. 78, pp. 54 – 65.
- Coifman, B., Ergueta, E., 2003. Improved vehicle reidentification and travel time measurement on congested freeways. *Journal of Transportation Engineering* 129 (5), 475–483.

Daganzo, C. F., 2002. A behavioral theory of multi-lane traffic flow. Part I: long homogeneous freeway sections. *Transportation Research Part B: Methodological*, vol. 36, no. 2, pp. 131 - 158.

Daganzo, C.F., 1999. Remarks on traffic flow modeling and its applications in Traffic and Mobility. *Proc. Traffic and Mobility - Simulation, Economics and Environment Conference*, Aachen, Germany, Springer. , pp. 105-115

Daganzo, C. F., 1994. The cell transmission model: A dynamic representation of highway traffic consistent with the hydrodynamic theory. *Transportation Research Part B: Methodological*, 28(4), 269-287.

Daganzo, C.F., Geroliminis, N., 2008. An analytical approximation for the macroscopic fundamental diagram of urban traffic. *Transportation Research Part B: Methodological*, vol. 42, no. 9, pp. 771 - 781.

Davidson, K. B., 1966. A flow travel time relationship for use in transportation planning. *Proceedings of the 3rd Australian Road Research Board (ARRB '66) Conference*, vol. 3, no. 1, Sydney, Australia.

De Laski, A., Parsonson, P., and Brisbin, G., 1985. *Traffic Detectors*. FHWA, U.S. Department of Transportation.

Del Castillo, J.M., 2001. Propagation perturbation in dense traffic flow: a model and its implications. *Transportation Research Part B* 35 (4), 367–389.

Deng, W., Lei, H., & Zhou, X., 2013. Traffic state estimation and uncertainty quantification based on heterogeneous data sources: A three detector approach. *Transportation Research Part B: Methodological*, 57, 132-157.

Dervisoglu, G., Gomes, G., Kwon, J., Horowitz, R., Varaiya, P., 2009. Automatic calibration of the fundamental diagram and empirical observations on capacity. In *Transportation Research Board 88th Annual Meeting (Vol. 15)*.

Donnelly, R. , Erhardt, G.D. , Moeckel, R. , and Davidson, W. A., 2010. *NCHRP Synthesis of Highway Practice 406: Advanced Practices in Travel Forecasting*, Transportation Research Board of the National Academies, Washington, D.C.

Dowling, R., Ryus, P., Schroeder, B., Kyte, M., Creasey, F. T., Roupail, N., Rhoades, D., 2016. *NCHRP Report 825: Planning and Preliminary Engineering Applications Guide to the Highway Capacity Manual*, Transportation Research Board, Washington, D.C.

Dowling, R., Kittelson, W., Skabardonis, A., Zegeer, J., 1997. *NCHRP Report 387: Techniques for Estimating Speed and Service Volumes for Planning Applications*. TRB, National Research Council, Washington, D.C.

Dowling, R., Skabardonis, A., 1993. Improving average travel speeds estimated by planning models. *Transportation Research Record*, vol. 1366, pp. 68 - 74.

Duncan, N. C., 1979. A further look at speed/flow/concentration. *Traffic Engineering & Control*, vol. 20, no. 10, pp. 482 - 483.

Elefteriadou L., Lertworawanich P., 2003. Defining, measuring and estimating freeway capacity. Paper presented at the 82nd TRB Annual Conference, Washington DC

Elefteriadou, L., Roess, R.P., Mcshane, W.R., 1995. Probabilistic nature of breakdown at freeway merge junction. *Transportation Research Record* 1484, 80–89.

Evans, J., Elefteriadou, L., Natarajan, G., 2001. Determination of the probability of breakdown on a freeway based on zonal merging probabilities. *Transportation Research Part B* 35 (3), 237–254.

Federal Highway Administration, 2005. 21st century operations using 21st century technologies. Federal Highway Administration, US. Dept. of Transportation, Washington, D.C. <http://www.ops.fhwa.dot.gov/aboutus/opstory.htm>

Frank, M., Wolfe, P., 1956. An algorithm for quadratic programming. *Naval Research Logistics Quarterly*, vol. 3, no. 1-2, pp. 95 - 110.

Friedman, N., Geiger, D., & Goldszmidt, M., 1997. Bayesian network classifiers. *Machine learning*, 29 (2-3), 131-163.

Fukushima, M., 1984. A modified Frank-Wolfe algorithm for solving the traffic assignment problem. *Transportation Research. Part B. Methodological. An International Journal*, vol. 18, no. 2, pp. 169 - 177.

Gartner, N.H., Messer, C.J., Rathi, A. K., 1997. *Monograph on Traffic Flow Theory*, Federal Highway Administration (FHWA)

Gentile, G., Meschini, L., Papola N., 2005. Macroscopic arc performance models with capacity constraints for within-day dynamic traffic assignment. *Transportation Research Part B: Methodological*, vol. 39, no. 4, pp. 319 - 338.

Gentile, G., Noekel, K., 2009. Linear user cost equilibrium: the new algorithm for traffic assignment in VISUM. In *Proceedings of the European Transport Conference*, Noordwijkerhout, The Netherlands.

Ghahramani, Z., 2001. An introduction to hidden Markov models and Bayesian networks. In *Hidden Markov models: applications in computer vision* (9-41).

Heidemann, D., 2001. A queueing theory model of nonstationary traffic flow. *Transportation Science* 35 (4), 405–412.

Helbing, D., 2009. Derivation of a fundamental diagram for urban traffic flow. *European Physical Journal B*, vol. 70, no. 2, pp. 229 – 241.

Horowitz, A. J. Delay–Volume Relations for Travel Forecasting: Based upon the 1985 Highway Capacity Manual. FHWA, U.S. Department of Transportation, March 1, 1991. <http://tmip.fhwa.dot.gov/resources/clearinghouse/docs/general/dvrt/dvrt.pdf>. Accessed June 2009

Hurdle, V. F., & Son, B., 2000. Road test of a freeway model. *Transportation Research Part A: Policy and Practice*, 34(7), 537-564.

Immers, L. H., & Logghe, S., 2002. Traffic flow theory. Faculty of Engineering, Department of Civil Engineering, Section Traffic and Infrastructure, Kasteelpark Arenberg, 40, 21.

Jacobson, L., Nihan, N., and Bender, J., 1990. Detecting Erroneous Loop Detector Data in a Freeway Traffic Management System. *Transportation Research Record* 1287, Transportation Research Board, Washington, D.C., 151-166.

Jastrzebski, W., 2000. Volume delay functions. Proceedings of the 15th International EMME/2 Users Group Conference, Vancouver, Canada.

Kharoufeh, J.P., Gautam, N., 2004. Deriving link travel time distributions via stochastic speed processes. *Transportation Science* 38 (1), 97–106.

Kurth, D. L., A. van den Hout, and B. Ives, 1996. Implementation of “Highway Capacity Manual”-Based Volume–Delay Functions in Regional Traffic Assignment Process. In *Transportation Research Record* 1556, TRB, National Research Council, Washington, D.C., pp. 27–36.

Li, Z. C., Huang, H. J., & Yang, H., 2020. Fifty years of the bottleneck model: A bibliometric review and future research directions. *Transportation research part B: methodological*, 139, 311-342. :

<https://www.sciencedirect.com/science/article/pii/S0191261520303490>

Li, Z., Laurence, R., 2015. An analysis of four methodologies for estimating highway capacity from ITS data. *J. Modern Transportation* 23(2), 107-118.

Lorenz, M., Elefteriadou, L., 2000. A probabilistic approach to defining freeway capacity and breakdown. Fourth International Symposium on Highway Capacity, Hawaii.

Lv, Y., Duan, Y., Kang, W., Li, Z., & Wang, F. Y., 2015. Traffic flow prediction with big data: a deep learning approach. *IEEE Transactions on Intelligent Transportation Systems*, 16(2), 865-873.

Moses, R., Mtoi, E., Ruegg, S., McBean, H., 2013. Development of speed models for improving travel forecasting and highway performance evaluation. Final Report, Florida Department of Transportation (FDOT).

Muñoz, L., Sun, X., Horowitz, R., & Alvarez, L., 2003. Traffic density estimation with the cell transmission model. In *Proceedings of the 2003 American Control Conference*, 2003. 5, 3750-3755. IEEE.

Nam, D. H., Drew, D. R., 1998. Analyzing Freeway Traffic under Congestion: Traffic Dynamics Approach. *Journal of Transportation Engineering*, 124(3), 208–212. [https://doi.org/10.1061/\(asce\)0733-947x\(1998\)124:3\(208\)](https://doi.org/10.1061/(asce)0733-947x(1998)124:3(208))

Newell, G. F., 1993. A simplified theory of kinematic waves in highway traffic, part II: Queueing at freeway bottlenecks. *Transportation Research Part B: Methodological*, 27(4), 289-303.

Oh, J., Jayakrishnan, R., Recker, W., 2003. Section travel time estimation from point detection data. *Transportation Research Board 81st Annual Meeting*, Washington DC.

Olszewski, P., Fan, H.S.L., Tan, Y.W., 1995. Area-wide traffic speed-flow model for the Singapore CBD. *Transportation Research Part A: Policy and Practice*, vol. 29, no. 4, pp. 273 - 281.

Omar, S., Mallikarjuna, C., 2016. Analysis of the macroscopic relations for no-lane based heterogeneous traffic stream. *Procedia Engineering*, vol. 142, pp. 243 - 250.

Pai, M., and P. Weinberger. Hot Topics: Speed Flow Curves. *TMIPConnection*, Issue 21, Fall 2004. <http://tmip.fhwa.dot.gov/resources/clearinghouse/docs/tmip/newsletter/>

Persaud, B., Yagar, S., Tsui, D., Look, H., 2001. Breakdown-related capacity for freeway with ramp metering. *Transportation Research Record* 1748, 110–115.

Ramezani, M., & Geroliminis, N., 2012. On the estimation of arterial route travel time distribution with Markov chains. *Transportation Research Part B: Methodological*, 46(10), 1576-1590.

Research Council, Washington, D.C., 1985.

Rickert, M., Nagel, K., Schreckenberg, M., Latour, A., 1996. Two lane traffic simulations using cellular automata. *Physica A: Statistical Mechanics and its Applications*, vol. 231, no.4, pp. 534 - 550.

- Ross, S., 1996. Stochastic Processes, second ed. John Wiley and Sons.
- Sau, J., Monteil, J., Billot, R., El Faouzi, N.-E., 2019. Steady-state analysis of second-order traffic models and application to traffic flow control. *Transportmetrica B: Transport Dynamics*, 7(1), 1444–1466. <https://doi.org/10.1080/21680566.2019.1630690>
- Seo, T., Bayen, A. M., Kusakabe, T., & Asakura, Y., 2017. Traffic state estimation on highway: A comprehensive survey. *Annual Reviews in Control*, 43, 128-151.
- Shaw, T., 2002. Reliability Measures for Highway Systems and Segments. TRANSYSTEMS Corporation.
- Singh, R., Dowling, R., 2002. Improved speed-flow relationships: application to transportation planning models. Proceedings of the 7th TRB Conference on the application of Transportation Planning Methods.
- Skabardonis, A., Dowling, R., 1997. Improved speed-flow relationships for planning applications. *Transportation Research Record*, no. 1572, pp. 18 - 23.
- Special Report 87: Highway Capacity Manual, 2nd ed. HRB, National Research Council, Washington, D.C., 1965.
- Spiess, H., 1990. Conical Volume-Delay Functions. *Transportation Science*, Vol. 24, No. 2, pp. 153–158.
- Travel Model Improvement Program, FHWA, U.S. Department of Transportation. Technical Synthesis: Speed Adjustments. http://tmip.fhwa.dot.gov/resources/clearinghouse/docs/tmip/technical_syntheses/2009/january.pdf. Accessed June 2009.
- Treiber, M., & Helbing, D., 2002. Reconstructing the spatio-temporal traffic dynamics from stationary detector data. *Cooperative Transportation Dynamics*, 1(3), 3-1.
- Treiber, M., Kesting, A., 2013. *Traffic Flow Dynamics: Data, Models and Simulation*, Springer, Berlin, Germany.
- Treiber, M., Kesting, A., Helbing, D., 2010. Three-phase traffic theory and two-phase models with a fundamental diagram in the light of empirical stylized facts. *Transportation Research Part B: Methodological*, vol. 44, no. 8-9, pp. 983 - 1000.
- Turner, S., Margiotta, R., Lomax, T., 2004. Lessons learned: monitoring highway congestion and reliability using archived traffic detector data, FHWA-OP-05-003.

Turner, S.M., 1996. Advanced techniques for travel time data collection. Transportation Research Board 75th Annual Meeting, Washington DC.

VanLint, J.W.C., van Zuylen, H.J., 2005. Monitoring and predicting freeway travel time reliability using width and skew of the day-to-day travel time distribution. Transportation Research Board 84th Annual Meeting, Washington DC.

Wang, Y., Papageorgiou, M., Messmer, A., 2007. Real-time freeway traffic state estimation based on extended Kalman filter. *Transportation Science* 41 (2), 167–181.

Wardrop, J. G., 1952. Some theoretical aspects of road traffic research.

Wong, W., Wong, S. C., 2016. Network topological effects on the macroscopic Bureau of Public Roads function. *Transportmetrica A: Transport Science*, vol. 12, no. 3, pp. 272 – 296.

Yang, H., Lo, H.K., Tang, W.H., 1999. Travel time versus capacity reliability of a road network. Bell, M.G.H., Cassir, C. (Eds.), *Reliability of Transport Networks*. Research Studies Press, Baldock, pp. 119–138.

Yeon, J., Elefteriadou, L., & Lawphongpanich, S., 2008. Travel time estimation on a freeway using Discrete Time Markov Chains. *Transportation Research Part B: Methodological*, 42(4), 325-338.

Zhang, X., Rice, J., 2003. Short-term travel time prediction. *Transportation Research Part C* 11 (3–4), 187–210.